SPLIT RING RESONATORS IN MICROWAVE REGIME FOR SENSING OF REAGENTS IN AQUEOUS SOLUTIONS

by

Berk Çamlı

B.S., Electrical and Electronics Engineering, Bogazici University, 2010

M.S., Electrical and Electronics Engineering, Bogazici University, 2013

Submitted to the Institute for Graduate Studies in
Science and Engineering in partial fulfillment of
the requirements for the degree of
Doctor of Philosophy

Graduate Program in Electrical and Electronics Engineering
Boğaziçi University
2020

ACKNOWLEDGEMENTS

I would like to express my gratitude to my supervisor Arda D. Yalçınkaya first and foremost for his mentorship, help, and guidance throughout the years that I had the privilege to work with him. Likewise, thank the members of the thesis jury Günhan Dündar, Sema Dumanlı Oktar, Onur Ferhanoğlu, and Mehmet R. Yüce. This work could not have become what it is without their invaluable contribution.

My Ph.D. journey, as any other, owes a great deal to many other figures of inspiration, guidance, and support. I have had the luck to have work together with and learn from Hamdi Torun and Cansu Canbek Özdil through my thesis process. I am in debt of Seyhan Salman, Hüseyin Kızıl, and Şükrü Kocabaş for their academic contributions to this thesis. I also want to thank Yasemin Kahya, Şenol Mutlu, Faik Başkaya, Ali Pusane, Yağmur Denizhan, and Ömer Cerid for their efforts in my education.

One of the things that increases one's quality of life significantly is when one has the opportunity to have colleagues that one can actually enjoy working together with and learn a lot from. For their help in the completion of the thesis work, I would like to extend my gratitude to Sevil Özer, Emre Kuşakçı, Berkan Lafcı, Emre Altınağaç, Ida Sadeghzadeh, Shahrzad Zahertar, Aybüke Çalıkoğlu, Semih Sevim, Sinem Solak, Onur Ateş, Deniz Özen, Ozan Ertop, Naci Pekçokgüler, Berk Omuz, and Elif Gençtürk. I also would like to thank my dear colleagues at GlakoLens, fellow teaching assistants who I worked with in harmony and joy, the administration of the Department of Electrical and Electronics Engineering, and the Clean Room Facilities in Center for Life Sciences and Technologies.

On a similar note, every member of the BETA family I have come to know and learn from over generations have their impression on me and this work. It was a pleasure to be there together with Dağhan Gökdel, Baykal Sarıoğlu, Okan Batur, Melih Akçakaya, İskender Haydaroğlu, Gürkan Sönmez, Engin Afacan, İsmail Kara, Artun Oyman, Murat Tümer, Kemal Ozanoğlu, İhsan Çiçek, Betül Küçükakarsu Usta,

Hossein Mazaheri Kouhani, Hikmet Çeliker, Gönenç Berkol, Emre İşeri, Mustafa Becermiş, Ertaç Kızılca, Zeynep Sütgöl, Mustafa Öz, Mohammad Ahmadlou, Barış Can Efe, Mustafa İçel, Oğuz Erden, Semih Ramazanoğlu, Erdem Çil, Berk As, Baran Demirer, and many others.

For their invaluable friendship through and through, I also thank Rıza Akdeniz, Güray Güner, Burak Özdemir, Çağdaş Yaman, Alp Türedi, Nur Sevindik Özdemir, Özlem Hür, Nurcan Aydın Şahan, Fulya Ersoy Güzeltürk, Simge Ay Polat, Barış Gedik, Barış Görmez, Oktay Koçak, Özkan Yıldırım, Özlem Kahveci, Hannah Alongi, Uraz Çakacı, Can Kırbaç, Oğuz Karaduman, Ceyhun Coşkun, Aram Canan, Can Doğan, Doğan Er, Buket Vidinlisan, Özlem Kaplan, Volkan Saraçoğlu, Umut İnetaş, Ayşenur Şayakçı, Derya Güntekin Sönmez, Lorraine Turner Akçakaya, Gözde Çetinkaya Ertop, Selin Uysal Afacan, Zeynep Gülöz Bakır, Burcu Tepekule, Martin Müller, Alper Bayram, Kaan Oktay, Gizem Ekinci, Kerem Kaya, Müge Uysal Kaya, Birses Debir, Mert Ergen, Olcayto Külünkoğlu, Dorukhan Salepçi, Sinan Kara, Alican Kartal, Aycan Suyabatmaz, Mete Oğuz and all dear Stormlings, Luying Feng, Onur Tatar, Metehan Zorluğlu, Orhan Buğur, Ferit Büyükkeçeci, Gökhan Köroğlu, Çeşminaz Eser, Mesut Gökdai and everyone whom I had the pleasure to meet via the University Promotion Office. Thank you for supporting me at my best and worst.

Last but most definitely not the least, my deepest gratitude is to the family members who were always supportive and encouraging throughout my life, particularly my dearest grandmothers and my parents. Thank you for helping me become who I am today.

ABSTRACT

SPLIT RING RESONATORS IN MICROWAVE REGIME FOR SENSING OF REAGENTS IN AQUEOUS SOLUTIONS

In this thesis, design, fabrication, and characterization of different microwave band split ring resonator-based sensors used for sensing of glucose in aqueous solutions are presented. Following an introduction to metamaterials and split ring resonators, a literature survey of their applications in sensing is given. After this, an analytical model that describes the operation of a single loop SRR is demonstrated along with additional theoretical considerations. Exploratory work in which simulated and measured electromagnetic interaction of different split ring resonator geometries with dielectric loads is reported. Change of resonance characteristics of the split ring resonator is shown to be correlated with different dielectric loads, such as aqueous glucose solutions of different concentrations. After the exploratory work, a biosensor application incorporating a glucose specific element glucose oxidase immobilized in a PEDOT:PSS matrix is discussed. The biosensor application had a sensitivity of 0.107 $\mathrm{MHz/mg\,mL^{-1}}$ to glucose. Its specificity was demonstrated by comparison of its response to other reagents, such as sucrose, fructose, and NaCl. Precision, linearity, and repeatability improvements to this design was done by adoption of conceptual developments by switching to a differential measurement scheme, use of loop antennas instead of monopole antennas, and incorporation of microfluidic elements to the system. An improved iteration of the original sensor system was presented at the end, fabricated from materials highly compatible with relevant biosensor applications.

ÖZET

SULU ÇÖZELTİ İÇİNDEKİ MADDELERİN ALGILANMASINA YÖNELİK MİKRODALGA FREKANSLI YARIK HALKA TINLAYICILAR

Bu tezde, sulu çözeltilerde glukoz derişimi ölçmek için kullanılan mikrodalga bandında yarık halka tınlayıcılar tabanlı farklı algıçların tasarım, üretim ve belirlemesi sunulmuştur. Metamalzemeler ve yarık halka tınlayıcılara bir girişi takiben, bunların algılama uygulamaları üzerine bir literatür taraması verilmiştir. Bundan sonra, tek halkalı yarık halka tınlayıcının çalışmasını betimleyen bir analitik model başka bazı teorik meselelerin yanında anlatılmıştır. Farklı yarık halka tınlayıcı biçimlerinin dielektrik yükler ile etkileşiminin benzetimsel ve ölçümsel sonuçları bildirilmiştir. Yarık halka tınlayıcının tınlaşım karakteristiğinin değişiminin değişen glukoz derişimleri gibi dielektrik yükte meydana gelen farklılaşmalarla ilişkili olduğu gösterilmiştir. Keşfi çalışmaların ardından PEDOT:PSS anamadde içine sabitlenmiş glukoza biyoözgül glukoz oksidaz enzimi barındıran bir biyoalgıç uygulaması tartışılmıştır. Biyoalgıç uygulamasının glukoza hassasiyeti 0.107 MHz/mg mL^{-1} kadardır. Biyoözgüllüğü, algıcın sukroz, fruktoz ve NaCl gibi başka maddelere verdiği cevap ile karşılaştırılarak gösterilmiştir. Bu tasarımın kesinlik, doğrusallık ve tekrarlanabilirlik iyileştirmeleri farksal ölçüm tasarısına geçiş, halka antenen kullanımı ve mikroakışkan unsurların sisteme dahil edilmesi ile yapılmıştır. Son olarak, başlangıçtaki tasarımın bu şekilde geliştirilmiş ve biyoalgıç uygulamaları ile yüksek derecede uyumlu malzemeler kullanılarak üretilmiş bir versiyonu sunulmuştur.

TABLE OF CONTENTS

LIST OF FIGURES

LIST OF SYMBOLS

$\mathbf{B}$	Magnetic Flux Density
C	Capacitance
C_{gap}	Gap Capacitance
C_{sur}	Surface Capacitance
$\mathbf{D}$	Electric Flux Density
d	Thickness of SRR Substrate
$\mathbf{E}$	Electric Field Strength
f	Frequency
f_0	Resonance Frequency
f_{0p}	Resonance Frequency of a Parallel RLC Network
f_{0s}	Resonance Frequency of a Series RLC Network
$[G]$	Glucose Concentration
g	Gap Width of SRR
$\mathbf{H}$	Magnetic Field Strength
$\mathbf{J}$	Current Density
k	Reaction Constant
$\mathbf{k}$	Wave vector
L	Inductance
Q	Quality Factor
Q_p	Quality Factor of a Parallel RLC Network
Q_s	Quality Factor of a Series RLC Network
R	Resistance
r	Inner Radius of SRR Conductor
r_m	SRR Modeling Parameter Related to Conductor Radius
S	Sensitivity Constant
S_{11}	Reflection Scattering Parameter of Port 1
S_{22}	Reflection Scattering Parameter of Port 2
S_{21}	Transmission Scattering Parameter

t	Thickness of SRR Conductor
w	Width of SRR Conductor
ε	Permittivity
ε_0	Permittivity of Free Space
ε_1	Real Part of Complex Permittivity
ε_2	Imaginary Part of Complex Permittivity
ε_{eff}	Effective Permittivity
ε_r	Relative Permittivity
ε_s	Permittivity under Static Field
ε_∞	Permittivity at Very High Frequencies
μ	Permeability
μ_0	Permeability of Free Space
ρ	Charge Density
σ	Conductivity
τ	Time
τ_r	Relaxation Time
ω	Angular Frequency

LIST OF ACRONYMS/ABBREVIATIONS

2D	Two Dimensional
3D	Three Dimensional
ASRR	Asymmetric Split Ring Resonator
CMOS	Complementary Metal-Oxide Semiconductor
CSRR	Complementary Split Ring Resonator
DI	Deionized
DSRR	Double Loop Split Ring Resonator
ELCR	Electrical LC Resonator
FEA	Finite Element Analysis
FEM	Finite Element Method
FOM	Figure of Merit
GOx	Glucose Oxidase
LOC	Lab-on-Chip
MEMS	Microelectromechanical Systems
PCB	Printed Circuit Board
PDMS	Polydimethylsiloxane
PEDOT:PSS	Poly(3,4-ethylenedioxythiophene) poly(styrenesulfonate)
PMMA	Polymethyl methacrylate
SIW	Substrate Integrated Waveguide
SNR	Signal to Noise Ratio
SRR	Split Ring Resonator
SSRR	Single Loop Split Ring Resonator
TSRR	Triple Loop Split Ring Resonator
UV	Ultraviolet
VNA	Vector Network Analyzer

1. INTRODUCTION

1.1. Metamaterials and SRR Variants

1.1.1. Metamaterials Overview

Metamaterials are artificial electromagnetic structures formed of periodically arranged unit elements smaller than the incident electromagnetic waves. These are interesting in that they behave in unusual ways to demonstrate seemingly unnatural responses to electromagnetic actuation, such as backward propagation, reverse Doppler effect, negative refraction, and cloaking [1]. Many singular properties associated with metamaterials are related to the ability to engineer constitutive parameters of permittivity and permeability [2].

These structures are observed to have shared resonance characteristics, which are determined by their simple geometric designs. Their power thus lies in the fact that they can be designed for a variety of applications within a broad spectrum of electromagnetic frequencies. Examples as absorbers, [3], electromagnetic cloaks [4], and lenses [5, 6] have been demonstrate in the literature.

Roots of metamaterial research can be traced back to 1898 when J. C. Bose showed the possibility of existence of artificial materials by conducting microwave experiments on twisted structures [7]. Theoretical investigation was supplied by Victor Veselago in 1968 [8] and in 1999 Pendry demonstrated negative permeability magnetic plasma using split ring resonators [9]. The first practical demonstration came in 2000 [10], followed by the experimental observation of negative refraction [11] and backward wave radiation [12]. With these initial steps, metamaterials attracted intensive research interest from various fields and found applications in diverse fields.

Operation of metamaterials can be understood via Maxwell's equations:

$$\nabla \times \mathbf{E} = -j\omega\mu\mathbf{H} \tag{1.1}$$

$$\nabla \times \mathbf{H} = \mathbf{J} + j\omega\varepsilon\mathbf{E} \tag{1.2}$$

$$\nabla.\mathbf{D} = \rho \tag{1.3}$$

$$\nabla.\mathbf{B} = 0 \tag{1.4}$$

where, $\mathbf{E}$, ω, μ, $\mathbf{H}$, $\mathbf{J}$, ε, $\mathbf{D}$, ρ, and $\mathbf{B}$ represent electric field, angular frequency, permeability, magnetic field, current density, permittivity, electric flux density, charge density, and magnetic flux density, respectively. Permittivity is a measure by which a medium can undergo polarization when subjected to an external electric field. Permeability, on the other hand, is a measure of resistance of a medium to formation of magnetic fields. Both parameters together define the electromagnetic properties of a given material. As a general rule, naturally occurring materials have positive values for these parameters.

For a plane wave, the Equations (1.1)-(1.4) can be reduced to following forms [13]:

$$\mathbf{k} \times \mathbf{E} = \omega\mu\mathbf{H} \tag{1.5}$$

$$\mathbf{k} \times \mathbf{H} = -\omega\varepsilon\mathbf{E} \tag{1.6}$$

where $\mathbf{k}$ denotes the wave vector.

This implies that, for a positive ε and μ, $\mathbf{E}$, $\mathbf{H}$ and $\mathbf{k}$ form a right-handed orthogonal system, as is the case for natural materials. On the other hand, for negative ε and μ, a left-handed orthogonal system should exist theoretically, as demonstrated in Figure 1.1. Here, the refraction index will be negative, but the electromagnetic wave propagation is still the case, since the product of permittivity and permeability remains positive. It is in fact these interesting properties of negative index of refraction, reverse Doppler effect, and backward propagation [8] of such a material that gives it its name.

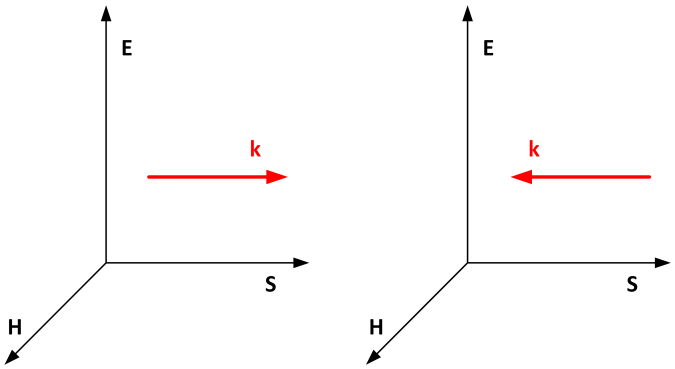

Figure 1.1. Poynting vectors of electromagnetic waves for right-handed systems (left) and for left-handed systems (right).

In more detail, four possible ways exist to classify materials based on the signs of their ε and μ values, which is demonstrated in Figure 1.2. Even though some materials such as cold plasma and silver exhibit negative permittivities at microwave and optical frequencies and ferromagnetic materials exhibit negative permeability behavior in high frequency regimes, double negative materials to this date are not naturally observed [13].

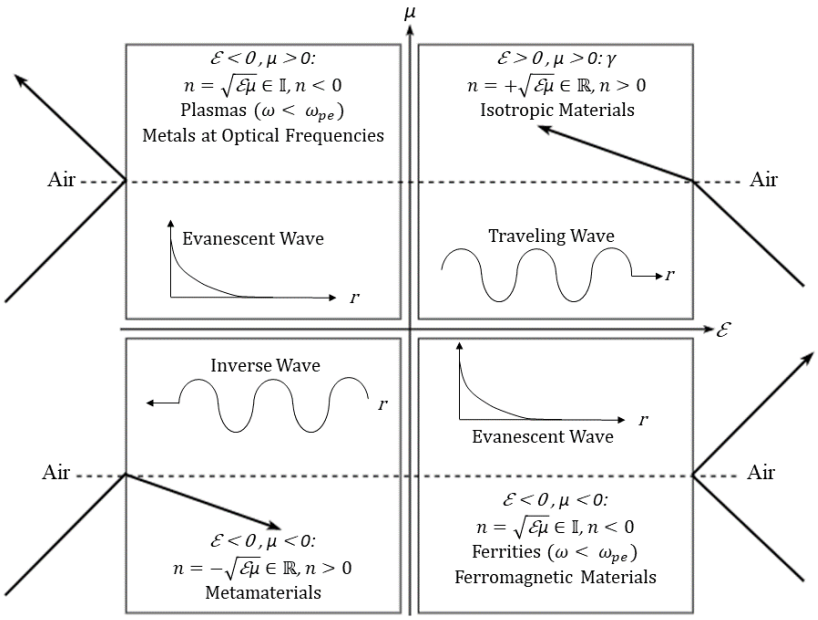

Figure 1.2. Possible domains of electromagnetic materials and the resultant wave refraction.

Realization of a left-handed system can be done with the use of artificial materials. This usually involves periodic arrangement of subparticles, or inclusions or

structures of dielectric or metallic materials. It is possible to use a combination of two different structures, one of which providing a negative permittivity ($\varepsilon < 0$) and the other satisfying the negative permeability ($\mu < 0$) condition. Traditionally, the former is a mesh made of thin wires and the latter is a split ring resonator as shown in Figure 1.3.

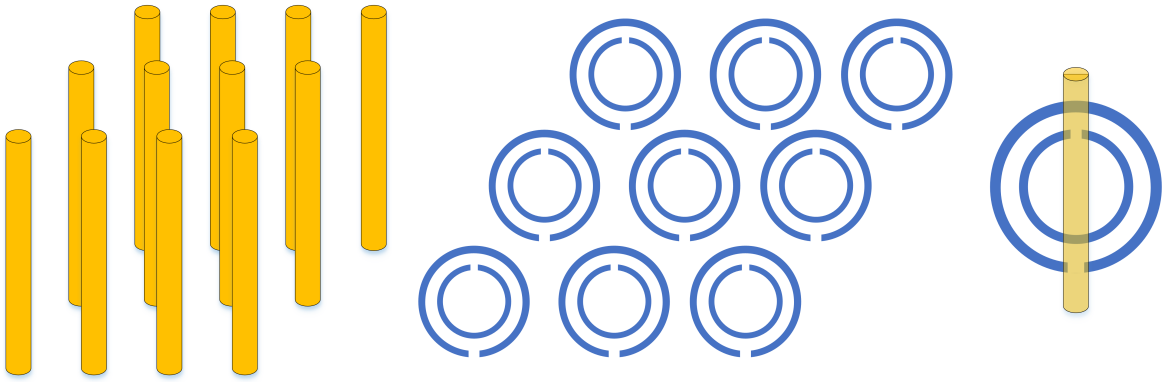

Figure 1.3. Negative permittivity material (left), negative permeability material (middle), and composite double negative material (right).

Until now, metamaterials of different forms and sizes were studied with resonant frequencies covering a large band spanning radio, terahertz, infrared, and optical frequencies [14–22].

1.1.2. Split Ring Resonators

A variety of metamaterial designs are studied in the literature as the negative permeability component, such as spiral, v-shaped, s-shaped, and Ω-shaped resonators [23–26]. The most popular negative permeability structure is formed of a single or multiple concentric split rings and their complementary versions as shown in Figure 1.4. The shape is formed of concentric split rings. Variants of these structures are called split ring resonators (SRR) in the literature. SRRs are and complementary SRRs (CSRR) are examples of most widely used and studied metamaterial structures. Figure 1.5 shows fundamental geometric parameters of the most basic SRR. The parameters of resonator radius r, gap width g, conductor width w, conductor thickness t, and substrate thickness d play an important role in how an SRR interacts with electromagnetic waves. This is because, standalone, they act as electromagnetic

resonators [27], due to inherent inductance and capacitances brought about by their geometric compositions. Relationship between the geometry and the values of these inherent parameters will be explained in more detail in the next chapter of this thesis.

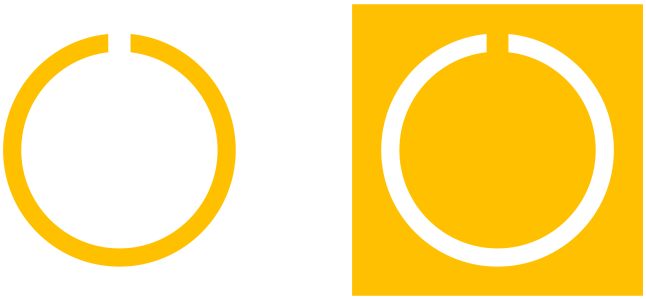

Figure 1.4. SRR (left) and CSRR (right), where colored regions show the metallization regions.

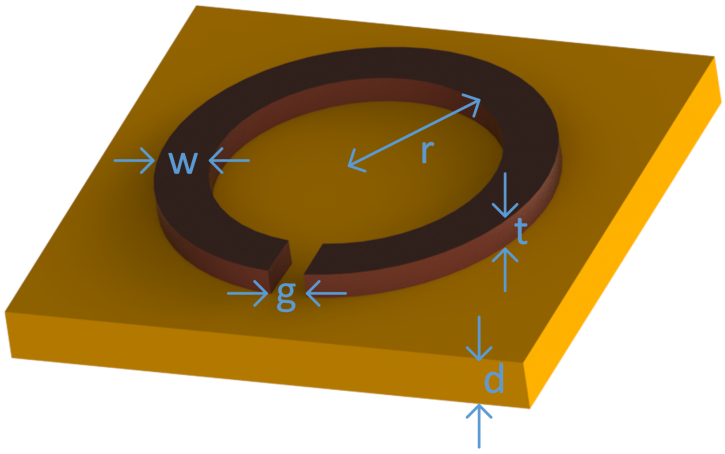

Figure 1.5. Dimensions of a single loop SRR.

SRRs of different sizes and gap arrangements were investigated in the literature [28–31]. Number of rings, gaps, and their arrangement can vary as can be seen in Figure 1.6. All possible different arrangements result in different effective capacitance and inductance values. It is therefore possible to engineer these structures at a desired of frequency, depending on the application. In Figure 1.7, effect of unit SRR size and number of series gaps on resonance frequency is shown [32].

Value of the resonance frequency will be determined by the values of these inherent capacitances and inductances. Small gaps existing along the conductive paths provide high capacitances causing the resonance to occur at relatively low frequencies. Moreover, loop structures allow larger inductances to be realized in a small area. As a

Figure 1.6. Different geometries of SRRs.

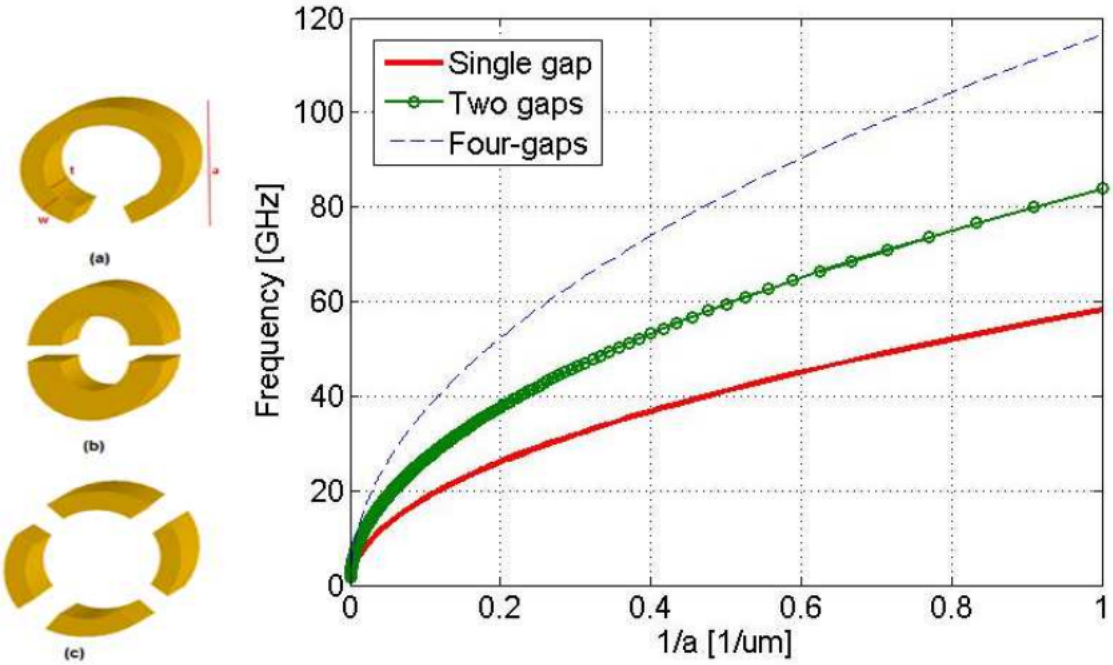

Figure 1.7. Single loop SRR structures with (a) single, (b) double, and (c) quadruple gaps and their resonance frequencies based on unit dimension denoted as a in the graph, as presented in [32].

result, SRRs can be realized as electrically small units [9]. Resonance itself is achieved by opposing or constructive effects of magnetically induced electric currents due to Faraday's Law. Their unique properties allow realization of SRRs with low radiating losses and thus achieving higher quality factors. Above the resonance frequency, the structures have negative real permeabilities, allowing their use in construction of double negative media.

As a general approach, SRRs can be modeled as RLC networks, since the conductive paths introduce resistance and inductances, whereas the gaps between the strips and slits create capacitances [33, 34] (Figure 1.8).

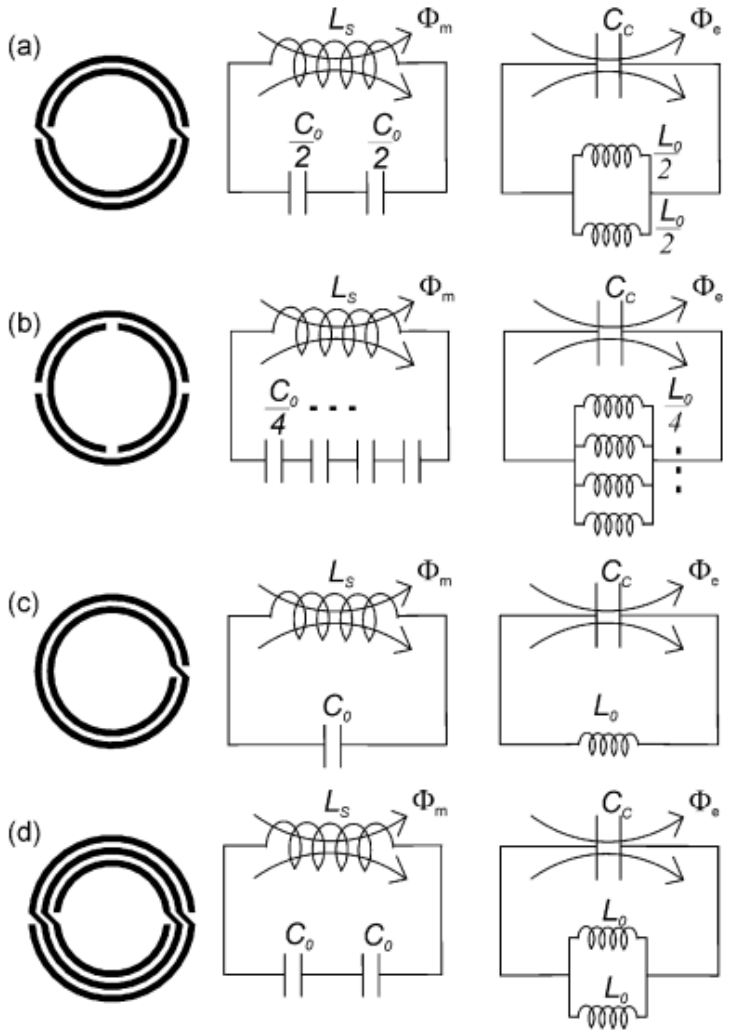

Figure 1.8. Equivalent RLC circuit models for single and double loop SRR structures, from [34].

The RLC network of the single ring SRR structure has a resonance frequency f_0 and a quality factor Q, defined by the effective resistance, capacitance and inductances, which depend on the structure geometry as well as the materials involved as shown in the following equations:

$$f_0 = \frac{1}{2\,\pi\,\sqrt{L\,C}} \tag{1.7}$$

$$Q = \frac{1}{R}\sqrt{\frac{L}{C}} \tag{1.8}$$

1.2. SRRs as Sensors

Many of present applications and technologies of today requires the utilization of cost-effective, fast, sensitive, and label-free sensors. A sensor, in general terms, is a device that is designed to detect changes in its environment and quantifies this change into a measurable signal. Mechanism of sensing itself relies on the interaction between the sensor and any physical characteristic of the material under test. Permittivity and permeability of a material, as an example, can be used in sensing via utilization of electromagnetic principles and approaches. SRRs have many advantages that make them popular in a variety of sensing applications [1].

Electrically small characteristics of the SRRs bring about the fact that electromagnetic fields can be focused within a small, confined area [35–37]. This causes SRRs to be particularly sensitive to changes in their close vicinity. As a result, they are frequently used in sensing applications of metamaterials. Disturbing of these focused electromagnetic fields with physical changes or introduction of different materials alters the resonance characteristics can be altered and sensing can be performed. Different SRR structures were thus studied in the literature for a variety of sensor applications [34, 38–40].

Sensing with SRRs is usually done by tracking of the resonance frequency of the structure. In majority of the cases, this stems from a change in the capacitive

components, but alternatives based on inductive changes, related to SRR/transmission line coupling efficiency, are also present [41]. For an application that can alter the resistance of the conductive path or coupling efficiency of the SRR, it is possible to perform sensing on amplitude tracking. For the capacitive sensing approaches, depending on the application, it may be preferable to confine and condense the electric field within a focused spot with an SRR with few gaps or distribute it by using multiple and extensive capacitive features, or a CSRR, or even an array of resonators [42, 43]. When not being the actual sensors themselves, SRRs can also be used as tools to increase the sensitivity of an existing sensor technology [44, 45]. This shows that use of SRRs in sensing opens up new possibilities in sensor applications in general.

SRRs also offer some advantages that are desirable in many sensing applications. A desirable property of a sensor is the possibility of reduction in size. This is especially true in biosensing and health monitoring sinceit allows management of chronic diseases in real time can be done easily [46]. SRRs offer reduced sizes due to their electrically small characteristics and their two dimensional (2D) nature. It should be noted that, as discussed before, size of an SRR can be reduced even further at a given resonance frequency via the introduction of additional capacitive features. This makes them good candidates for implantable devices, since their electromagnetic nature also allows contanctles measurements [30, 47].

This geometric flexibility is what makes it possible that SRRs can be easily engineered to operate at a wide range of frequencies, making them powerful and versatile tools [48]. They can be scaled down to operate at THz frequencies, where they offer to contribute significantly to THz science and research, bridging the gap between electrical and optical ranges of the electromagnetic spectrum [49–51]. SRR sensors are quite popular in microwave applications as well. In this range, it is easier to couple SRR sensors with electronic readout blocks, offering less complex and more cost-effective measurement schemes compared to THz alternatives. Microwave frequencies also have higher penetration into dielectric media, allowing a larger sensing or communication range for the sensor. In other words, at this regime, it is possible to perform noninvasive sensing within high volume samples or bodies without sample destruction or

need of prior treatment or labeling of the material [52]. Another advantage is that in microwave frequencies, trace molecules in water can be sensed better since water absorption is particularly high in THz frequencies. This is particularly interesting in lab-on-chip and implantable biomedical applications [53].

SRRs are also very easy and cost-effective to fabricate, owing to their simpler geometries and material requirements. For most applications, conventional in-house printed circuit board (PCB) fabrication methods will suffice [54,55]. Nevertheless, they are also compatible with conventional cleanroom fabrication techniques for production of miniaturized versions [56, 57]. Examples of downscaled metamaterials and SRRs, microfabricated in standard complementary metal-oxide semiconductor (CMOS) compatible technology [58–60] or custom processes on various rigid substrates [55, 61–63] are present in the literature. CMOS approaches offer easier integration with any electronic circuitry. In [60], CMOS on-chip integration of SRR modulators and surface plasmon polariton interconnects are shown. These structures can be realized with metal layers of a standard CMOS process as shown in Figure 1.9.

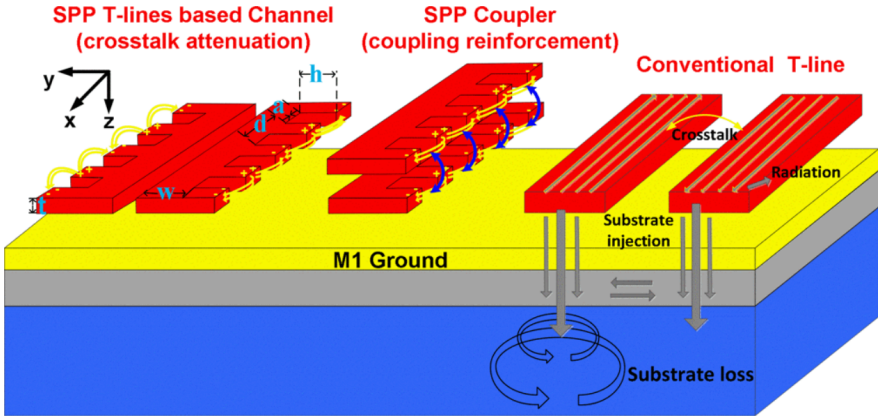

Figure 1.9. CMOS on-chip integration of the surface plasmon polariton structure presented in [60].

Custom fabrication trades complexity for increased flexibility in sensor design. In [61] an interdigital (IDT) capacitive architecture was applied as shown in Figure 1.10. Here, it was possible to realize a resonance frequency as low as 2.5 GHz with a structure fabricated on 400 μm GaAs substrate in an area of 700 μm $\times$ 900 μm [61]. An important advantage of such custom fabrication approaches is the ability to work

with a larger variety of materials. This allows the designer to incorporate materials that are inert, biocompatible, or agreeable to surface functionalization, which might be necessary in biosensor designs in particular.

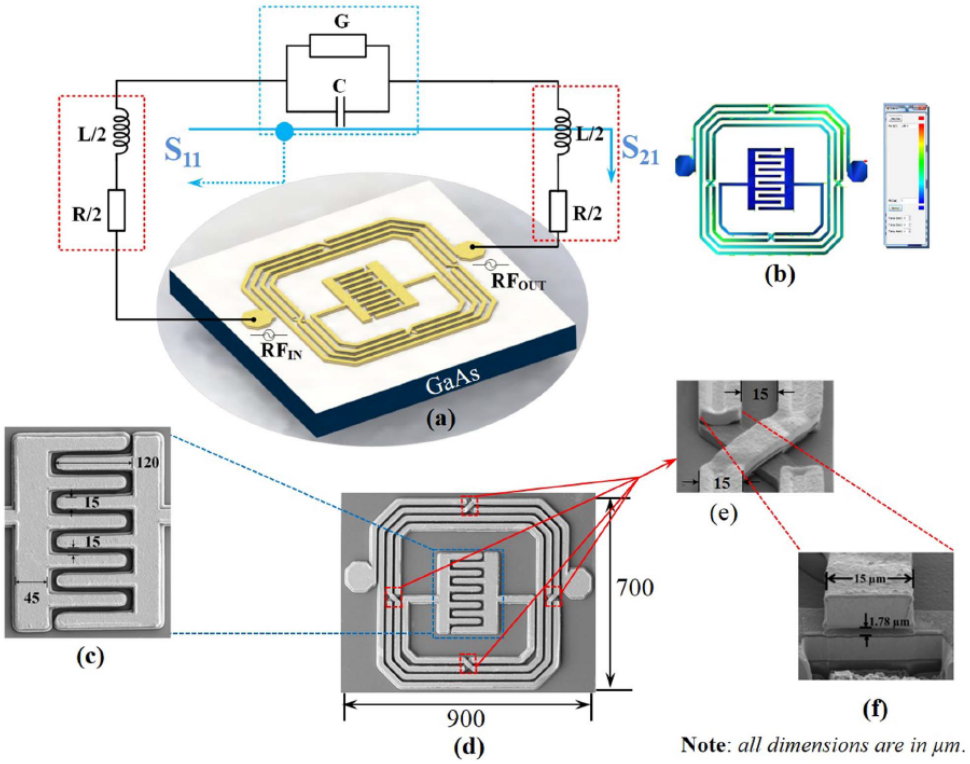

Figure 1.10. IDT capacitive structure used in integration of the metamaterial with a resonance frequency around 2.5 GHz presented in [61].

SRRs fabricated on flexible and soft substrates were also demonstrated, which shows they have the potential to be geometrically conformable and suitable for wearable applications [64–66]. Techniques such as shadow mask deposition, inkjet printing or imprint lithography are often applied to account for the potential involvement of polymer materials and three-dimensional (3D) or curved surfaces. In [64], The substrate material was polyimide tape with a 0.1 μm thick Au layer and a 0.1 μm thick Si_3N_4 as a dielectric deposited on top with standard metallization techniques and plasma enhanced chemical vapor deposition, respectively. Finally, 0.1 μm thick Au layer was applied with standard lithography, metal evaporation and lift off techniques to form the resonator structures. The fabrication steps and the fabricated samples are shown in Figure 1.11. SRR structures fabricated via embroidering with conductive thread on fabric were also shown [67].

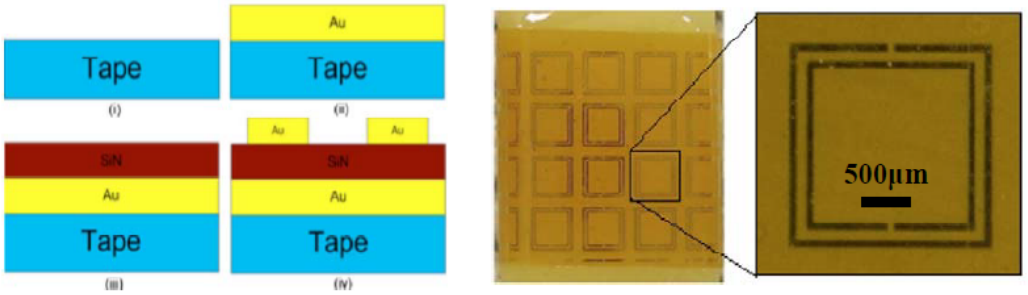

Figure 1.11. SRR fabricated on a flexible surface presented in [64].

Owing to all the advantages mentioned above, SRR/metamaterial sensing drew significant attention and did attain a certain degree of sophistication [1], although being a relatively new area of research. Sensing with SRR and CSRR variants have been shown in the literature in a wide range of applications. Again, majority of these sensors rely on capacitive changes within or around the SRR structure. There are two main driving factors that bring about this: geometric changes and permittivity/material changes. Via geometric changes in the SRR structure itself, it is possible to perform sensing of physical quantities such as strain, pressure, and rotation. Sensing of dielectric changes, on the other hand, are useful in thin film sensing, food quality monitoring, liquid characterization, pH measurement, gas sensing, reagent sensing, and biosensing, among other fields. In the following subsections, a summary of recent developments in SRR sensors are presented, based on the method of sensing.

1.2.1. SRR Sensing Based on Geometric Changes

SRRs of different shapes and arrangements are shown for position, angular displacement and alignment sensing [68–71]. Here the sensing can be done via tracking of the coupling efficiency between the SRR shapes and a waveguide structure exciting them. Depending on the resonator type used, the output can be based on changes in amplitude or frequency of the scattering parameters. In [71], rotation and displacement is tracked with a CSRR perfectly aligned with co-planar waveguides. As the alignment is broken with rotation or displacement, an increase in resonance excitation occurs. The system presented in [69] is based on rotation sensing only, with the waveguide designed and coupled to an electric LC resonator (ELCR) accordingly, as

shown in Figure 1.12. A rotation sensor relying on capacitive changes in addition is also possible, as demonstrated in [70, 72]. An application for tracking eye movements is shown in [73].

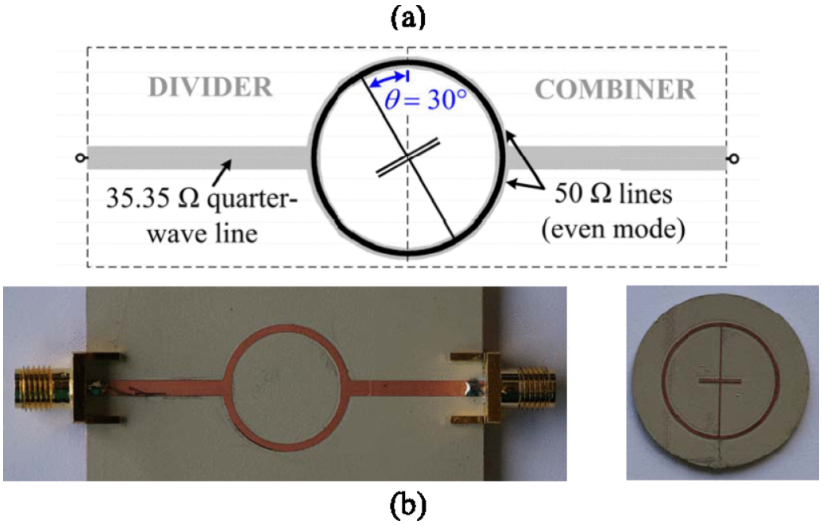

Figure 1.12. Layout (a) and image (b) of the fabricated electrical-LC based rotation sensor presented in [69].

Measurement of strain and pressure is important in different fields in daily life, including the assessment of structural integrity in buildings, flexural rigidity of aircraft, and the monitoring of the healing process of fractured long bones. In many of these applications, it is desirable to perform the sensing in a wireless manner. This is especially crucial in the endeavor of the realization of an implantable biological sensor used in real-time monitoring. Many SRR strain sensors operate wirelessly since they can be activated passively with the application of electromagnetic fields [64, 74–80]. Sensing is based on changing gap sizes and distances between rings, since this affects the overall capacitance and thus the resonance frequency. Depending on the application area, a single structure or an array can be used.

Kirigami-based [75, 76] approaches fabricate sensors on substrates with slits so that these slits are aligned with the SRR gaps. Strain causing a separation in substrate slits alter the resonance frequency of the sensing element. An array of RF MEMS resonators are fabricated on flexible substrates in [64]. Number of rings were kept high here to increase the overall capacitance, thereby increasing sensitivity to capacitive

changes. Pressure sensor developed in [77] demonstrate a double SRR adaptable to harsh environments. A standalone SRR with increased gap capacitance was demonstrated in [78] for wireless monitoring of glaucoma. A similar sensor system embedded in a polymer matrix was also presented later for the same purpose in [79], as shown in Figure 1.13.

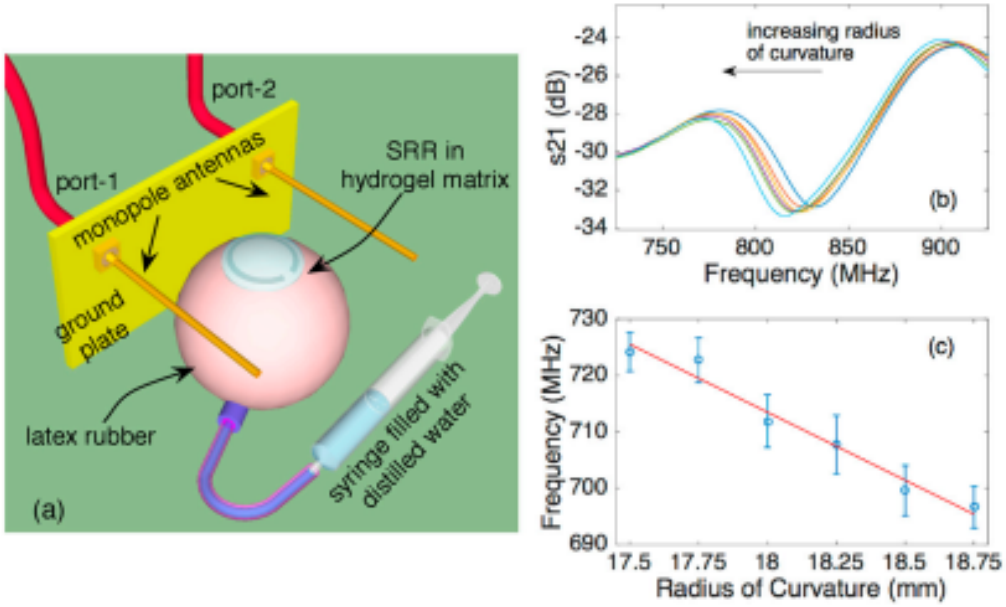

Figure 1.13. Experimental setup (a), read out spectra with increased intra-ocular pressure (translated into radius of curvature) (b), and change of resonance frequency vs. radius of curvature (c), as presented in [79].

1.2.2. SRR Sensing Based on Dielectric Changes

SRR structures are known to respond to temperature changes, making them suitable for temperature sensing applications [81–83]. Approaches to temperature sensing with SRRs can include stacked structures in broadside direction. This brings about considerable increase in overall capacitances since 2D conductor paths are now in overlapping arrangement. These approaches focus on the change of permittivity of the dielectric medium between the stacked resonators. In [81], stacked SRRs of different shapes were investigated as temperature sensors in simulation environment as shown in Figure 1.14, where permittivity was changed to account for the change in temperature. A shift to lower frequencies with increased temperatures was observed.

The author of thesis work believes temperature sensing can be performed also relying on the thermal expansion and thereby geometric changes in the sensor. This can be viable since SRRs are often made of conductive materials with high thermal expansion coefficients.

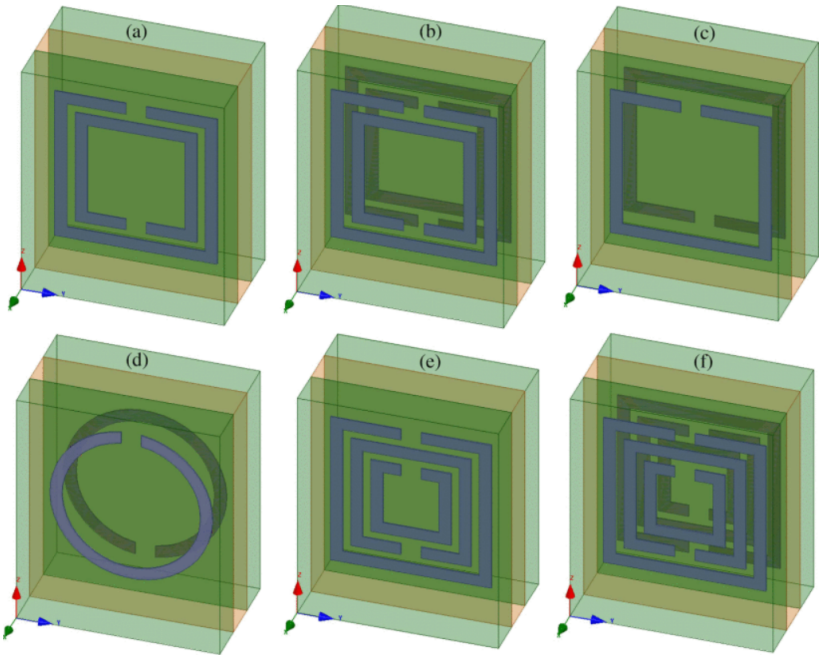

Figure 1.14. Temperature sensor units arranged in stacks around a dielectric, as shown in [81].

SRR sensing technology can be used as a sample preserving way of determining fruit and vegetable ripeness [84]. Using such sensing systems, the consumer or producer potentially can decide easier which item to buy or offer to the market [85]. Composition of the material properties will yield different permittivities at these different stages, causing a shift in the resonance frequency of the SRR. This of course, requires accurate characterization of material property for each type of food item at different stages of organic growth and decay. Examples exist in the literature for monitoring of meat quality [86], characterization and classification of beverages and foodstuffs [87, 88], quality monitoring [89].

The fact that resonance frequency of an SRR is directly related to the dielectric loading paved the way of them being used related scenarios. This approach is arguably the most popular and extensively studied area of SRR sensing. In the broader sense,

the applications include, but not are limited to, humidity/moisture sensing [90–93], characterization of dielectrics/liquids/gasses, pH sensing [94], reagent/molecule detection, and biosensing.

Dielectric sensing of SRR structures can be applied to sensing of volumetric bodies, thin films/surfaces, microfluidic samples and droplets, or individual particles. The basic principle remains the same: The overall capacitance of the SRR will be affected by the effective permittivity of the material composition around it. For volumetric analysis, high frequencies of resonance are avoided for increased penetration. Thin film and surface inspection points to a case where the sample volume or thickness is smaller. Volumetric or surface level inspection can be done to perform material characterization, surface quality inspection, or structural monitoring [52, 95–103]. This is possible due to fringing fields occurring at surface imperfections causing changes in resonance frequencies of SRR structures in vicinity, as shown in Figure 1.15. Use of CSRR or an array of sensors is common in applications requiring the monitoring of larger areas.

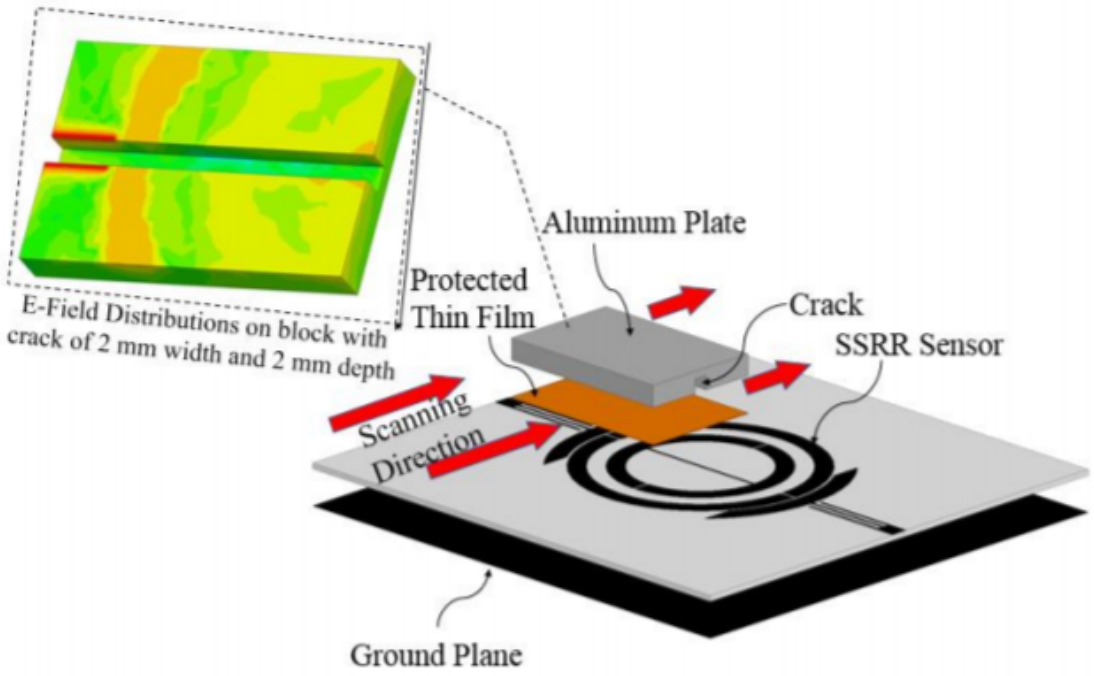

Figure 1.15. Enhanced symmetrical SRR and its detection of surface imperfections, as presented in [99].

Microfluidic sensing with SRR resonators were proposed to address certain limitations associated with microfluidic sensors using different methods of sensing [95, 104–107]. While microfluidic sensing with SRRs, the microfluidic platform is usually designed so that the sample remains in close vicinity in one of the more sensitive regions of the SRR. This corresponds to areas where electric field confinement is the highest. SRRs are often preferred over their complementary versions due to this, since gaps between conductive paths constitute smaller areas in non-complementary SRRs, where the fields can be focused to a greater degree. However, it is possible to design microfluidics along the slots of a CSRR [106]. As a result, microfluidic platforms were integrated with SRR structures in different ways, for different approaches. Microchannels fabricated with low-cost methods such as mechanical carving, 3D printing, or laser cutting are also suitable for these applications [104, 108–116].

In [108], a gold-coated copper, rectangular SRR-based sensor coupled to a microstrip line was fabricated on an RT/duroid 6010.2LM laminate, with a ground plane on the back side. A polymer film was placed and fixed on the resonator with a water-proof adhesive to characterize the sensor under water and ethanol loadings. Microfluidic platforms were integrated with CSRRs were fabricated on a patch [112] and a quarter mode substrate integrated waveguide (SIW) [110], and eighth mode SIW [111]. A laser-cut polydimethylsiloxane (PDMS) microfluidic channel was bonded with adhesive on a double-ring CSRR fabricated on a patch fed by a microstrip line was presented in [112] for detection of ethanol. A triple ring CSRR was presented with a microchannel perpendicular to sensor plane as well [113]. To increase capacitive sensitivity, different SRR gap shapes were studied in [114] as shown in Figure 1.16. Rectangular resonators capacitively coupled to input/output ports were shown for contactless microfluidic flow [115] and escherichia coli concentration sensors [116]. SRR arrays have also been proposed for microchannel applications to increase efficiency in use of multiple resonators per channel [117], and with trapezoidal structures fabricated to increase fluid resistivity [118].

Dielectric sensing with SRRs were used to detect and analyze organic and inorganic molecules and reagents of a large variety, such as biotin and streptavidin

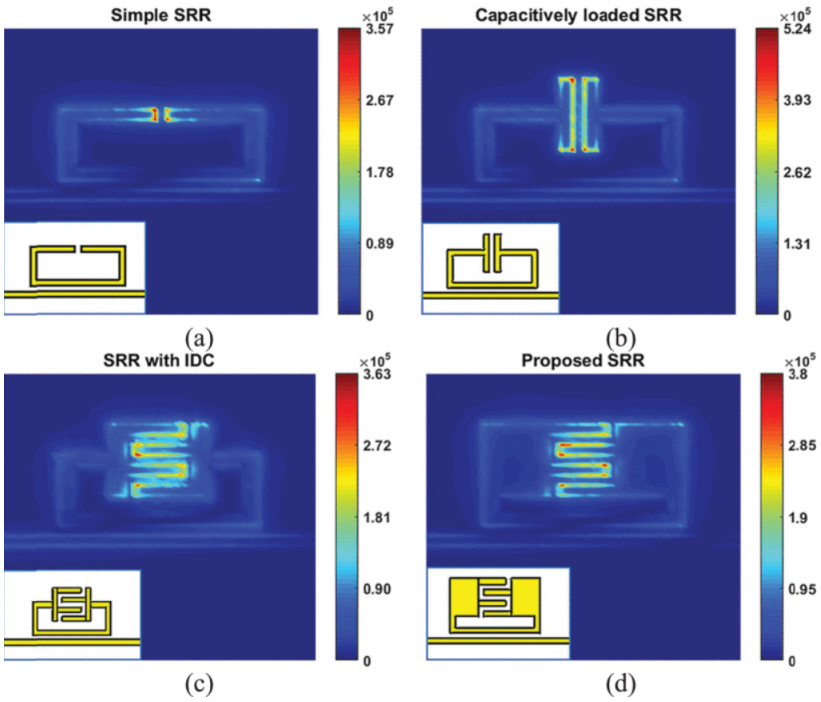

Figure 1.16. Electric field confinement capabilities of SRRs with different gap shapes, as presented in [114].

[43],DNA [54], organic tissues [119], cortisol [120], heparin [121], viruses, cells [122], [123], cancerous tissue [124,125], and proteins [126]. Sensing of reagents and biomolecules are sometimes reported as concentration detection in aqueous solutions. On the other hand, biosensing applications require incorporation of reagent or biomolecule specific sensing elements onto the surface to ensure specificity.

Biosensors are biochemical sensing devices used to perform bioanalytical measurements. Their broad application spectrum spans fields from medical diagnostics to food safety, from process control to environmental monitoring. User-friendly and simple medical devices for home use comprise a significant portion of the overall demand for biosensors [127]. They are mainly formed of a biological sensing element exploiting the high selectivity available in genuine biological systems and a transducer element that actually performs the measurement. Electrochemical [128], optical [129], acoustic [130], thermometric [131], and magnetic [132] transducers are proposed in the literature for biosensing. As an alternative, SRR structures can also be used as transducers in a biosensor system, owing to their many advantages mentioned so

far [1, 43, 121, 133]. This is done by incorporation of the biospecific element onto the SRR transducer. The region of interest is often where the electromagnetic fields are focused by the resonator. Binding or enzymatic activity related to the presence of the biospecific element result in a change of electrical permittivity. Such a change can be capacitively sensed by the SRR as demonstrated in Figure 1.17 from [121]. In THz frequencies, biospecific detection of some molecules can be done following the fact that these frequencies are close to vibrational frequencies of some biomolecules [106]. In [134], single gap and two gap symmetric SRR structures were designed in THz frequencies for detection of cancer biomarkers in accordance, as shown in Figure 1.18. One very interesting application is the use of SRRs in sensing of glucose.

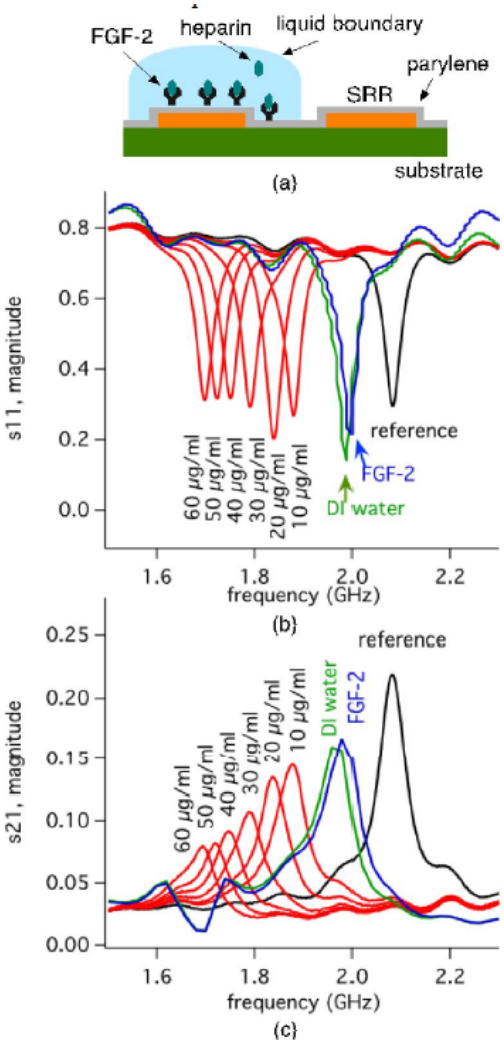

Figure 1.17. Working principle of an SRR used as biosensor, as demonstrated in [121].

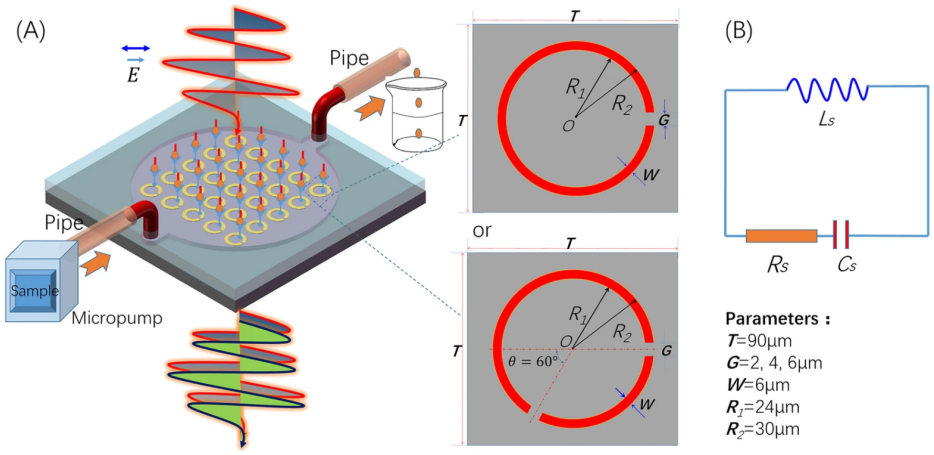

Figure 1.18. Single gap and two gap asymmetrical SRR structures and the integrated microfluidic chip studied in, as presented in [134].

1.3. Challenges and Motivation

In recent years, sensing applications of SRRs provided novel opportunities for development a new generation of sensors. SRRs can be used to improve properties of existing sensors, or can be used themselves as sensors of high sensitivity or transducing elements. This renders sensing even with small samples practical, providing a way to realize downscaled, high throughput sensors much needed especially in biological applications. Integration of microfluidic platforms can increase measurement repeatability and bring the better of both worlds together [106]. With the advances in materials and fabrication technologies, realization of low-cost microfluidic platforms with wireless, noninvasive, efficient, and versatile sensing capabilities is now even more attainable a goal than ever. SRR sensors in different frequency ranges can be fabricated on rigid and flexible substrates, standalone or in array formation, and can be used in sensing of many different physical and chemical quantities.

One of the main challenges the metamaterial inspired sensors face is that they their performance is limited by the fluctuations caused by internal and external mechanisms. Interference of these effects manifests itself as the noise in readout and lower precision in readings [135]. External noise sources include shot noise and noise introduced by the readout circuitry as well as fluctuations caused by environmental effects,

such as temperature changes [136]. The internal effects, related to adsorption and desorption of analyte particles on the metamaterial can also occur [137]. It is reported that this noise remains the main limiting factor of the ultimate performance of all such devices, because each structure must be interfaced to some kind of environment and thus the adsorption and desorption noise will influence to a certain degree the performance of any metamaterial structure [1]. Scaling of metamaterials may be an issue where chemical solutions are used, which may render the use of conventional photolithography microfabrication impossible. For such cases, obtaining metamaterial structures of high resolution and small feature sizes require the application of more involved fabrication techniques.

Aiming to contribute to this fast-developing field of research, an SRR based sensor for detection of glucose in aqueous solutions is presented in this work. Wireless and low-cost monitoring of blood glucose is in high demand, since 85 % of the marketed biosensors are blood glucose biosensors, dedicated to the management of diabetes. Some of the goals and challenges associated in realization of the proposed design are as follows:

(i) While designing sensors, maintaining a strong and linear signal at a practical resolution is of the essence. Therefore, a sharp peak with a good quality factor is desired in the context of SRRs. This requires a careful design of measurement mechanism as much as using the most suitable sensor structure.

(ii) For biosensor applications, sensor selectivity is also a crucial consideration. This refers to the ability to provide an output only for the change of the traced parameter. Integrability of the biospecific regent and the design would be one of the most serious challenges that has to be overcome in design of a metamaterial based biosensor.

(iii) Changes caused by secondary physical parameters or in case of a biosensor, presence of secondary regents should interfere with the sensor response as little as possible. The sensor should be able to suppress the external effects negatively affecting sensor operation.

(iv) Demonstration that fabrication of the sensor is possible with the use of materials compatible with biosensor applications is important. Materials that are biocompatible, inert, and having limited toxicity should be preferred. Such a sensor will have a potential for future applications to be used in vicinity of human body or may be improved as an implantable device.

The rest of this document is organized as follows: In Chapter 2, relevant literature review, modeling of SRR structures, and some additional theoretical considerations are given. In Chapter 3, the set of preliminary and exploratory work done in development of an SRR based sensor is presented. In Chapter 4, design, fabrication, and operation of a glucose selective SRR sensor is demonstrated. In Chapter 5, strategies to improve sensor design and its integration with conventional microfluidics are shown, followed by the demonstration of an improved microfluidic sensor design fabricated of biological sensor compatible materials. In the final chapter, state of the art and the future potential of SRR based glucose sensors are discussed.

2. RELEVANT LITERATURE REVIEW AND THEORY

2.1. Monitoring of Blood Glucose

Application of SRRs for sensing of glucose constitutes one of the most interesting and promising ideas related to their use. Sensing of glucose has relevant applications in food industry and especially in healthcare. This is mainly in relation to monitoring of blood glucose levels and management of diabetes [138]. Diabetes is a metabolical disease necessitating artificial regulation of blood glucose levels at human average levels of 80-120 $\mathrm{mg\,dL^{-1}}$ (4.4-6.6 mM) [139]. It is categorized in two main types [140]. Type 1 diabetes is characterized by insufficient levels of insulin produced by the pancreas. Type 2, comprising more than 90 % of the cases, is indicated by the body showing an abnormal sensitivity to insulin. Without a cure at present, this is a serious condition, since blood glucose levels have to be maintained within acceptable levels. Excessive levels of blood glucose can cause damage in blood vessels in vital organs. On the other hand, insufficient blood glucose levels can similarly threaten the life of the affected individual. Pataphysiological levels of blood glucose can reportedly vary between 36-540 $\mathrm{mg\,dL^{-1}}$ (2-30 mM) [141].

Prevalence of diabetes has only been increasing according to the World Health Organization, with the number of the diagnosed is more than 422 million worldwide [138]. Management of diabetes thus is a considerable global economic toll, especially since the patients need to monitor their glucose levels several times a day. It is reported that around 11.6 % of the overall worldwide healthcare spending was dedicated to diabetes in 2010 and more than half of the biosensors produced are used for glucose monitoring [141]. This economical potential has been an important driving factor in biosensor research since home-use point-of-care sensors were needed for conventional management of diabetes. The first patent for a point-of-care blood glucose sensor for diabetes monitoring was filed in 1971 in the USA by Arthur Clemens [142]. Since then, a wide variety of sensors, majority of them being optical or electrochemical, dedicated to detection of glucose in blood has been presented in the literature.

Optical transducing methods exploit the properties of the interaction between light and glucose molecules. These bear the advantage of offering real time and noninvasive monitoring and use methods such as near infrared spectroscopy, photoacoustic spectroscopy, and optical coherence tomography. These applications come at the cost of sizable and expensive equipment [139]. Moreover, trained personnel is often needed to operate them and interpret the output. In contrast, many of the more conventional techniques use electrochemical methods. These rely on potentiometric, amperometric, and conductometric measurement of changes in a liquid due to electrochemical reactions. For glucose sensing, widely used approach is to use the enzymatic reaction occurring between glucose and glucose oxidase (GOx) enzyme. The reaction produces gluconolactone (lactone of gluconic acid) and hydrogen peroxide (H_2O_2) as shown in the following:

$$\text{Glucose} + \text{GOx}_{(\text{oxd})} \rightarrow \text{Gluconolactone} + \text{GOx}_{(\text{red})} \tag{2.1}$$

$$\text{GOx}_{(\text{red})} + \text{O}_2 \rightarrow \text{GOx}_{(\text{oxd})} + \text{H}_2\text{O}_2 \tag{2.2}$$

Other enzyme alternatives are glucose dehydrogenase and isoenzyme 2 of hexokinase [128], while non-enzymatic electrochemical detection methods are also available [143].

Conventional electrochemical testing devices necessitate drawing of a blood sample from the patient. To achieve this, the patient has to prick their own skin, which is uncomfortable and not desirable, while bearing risk of infection on the side [138]. Since via this technique, it is only possible to measure the blood glucose level at a specific time, this operation has to be performed several times throughout the day. This is pushing the industry and research into finding alternative methods of blood glucose sensing, which will offer noninvasive, low-cost, easy to use, portable, and simple alternatives. As a result, some alternative noninvasive or minimally invasive glucose sensors based on various technologies are offered in the market. These methods may use samples other than such as urine [144, 145], saliva [146–148], sweat [149, 150], or

tear [151, 152] for sensing. Breathalyzers based on measurement of acetone in breath, which is correlated to blood glucose levels, poses an alternative that does not require a fluid sample [153]. Measurement of propagation characteristics of ultrasound [154] and mm-wave/microwave band electromagnetic waves are among other proposed approaches to noninvasive blood glucose detection methods.

Use of electromagnetic waves for glucose sensing is based on the principle that changes in blood glucose concentrations alters the permittivity of the tissue, particularly in the interstitial fluid. A decrease in permittivity is observed with increased concentrations of glucose concentrations in a fluid [155, 156]. As opposed to optical frequency signals, signals in mm-wave and microwave frequency have the advantage of higher penetration into the tissue due to lower absorption and tissue conductivity, offering more reliable readings. There are four main approaches to sensing with mm-wave/microwave frequencies. These are radar, reflection, transmission, and resonant methods, the latter three of which are based on similar principles [157].

Radar approach is different from the other three in that it is based on operation in the far field. With this approach, an electromagnetic wave is sent to the sample and the reflected signal is measured. Reflected signal contains information about the material composition of the sample as well as other parameters such as location and speed [158, 159]. Reflection and transmission approaches are based on scattering parameter measurements performed with the sample located in near field. With reflection methods, reflection scattering parameter S_{11} is measured over a wide frequency band with a vector network analyzer (VNA) through a single port. Transmission approach is very similar to this, with the measured parameter changing to the transmission scattering parameter S_{21} and the use of two ports [160–165]. The scattering parameters will respond to electric permittivity of the medium around them during the measurement and thus will be able to measure changes in levels of glucose concentrations. Resonant approach can be considered a subset of measurements based on this method often operate on a narrower range of frequency. Here, a resonator with a high quality factor is used. Resonance frequency, quality factor, and the bandwidth of the resonator, being affected by electrical permittivity, can be used in determi-

nation of glucose levels in a sample. With high quality factors available, sensors of this type offer significantly improved sensitivity and performance [138]. Many examples of resonant sensing of glucose were presented in the literature, based on cavity resonators [166, 167], dielectric resonators [168], co-planar waveguides [161, 169, 170], filters [171,172], antennas [156,173], and metamaterial inspired resonators such as the SRR, which will be explained in greater detail below.

2.1.1. A Review of SRRs and Microwave Resonators as Glucose Sensors

SRRs and similar microwave resonators have been widely applied for sensing of glucose in the literature due to many advantages discussed previously. Single loop SRR is the most basic geometry studied for sensing of glucose. It appears in its rectangular and circular shapes, and is often coupled to a co-planar waveguide for performing of transmission type measurement. In its most cost-effective form, this arrangement can be fabricated via conventional PCB production techniques. The sample is often applied to the most sensitive region of the SRR, which is its capacitive regions (corresponding to the gap region for a single loop SRR). A small reservoir or liquid container can be added to hold a small volume sample together at a designated spot to increase measurement repeatability. In [174], all this was applied for the demonstration of sensing not only for glucose, but also for fructose, sucrose, and sorbitol. The sensitivity measurements were based on amplitude of S_{21} parameters.

There are various alternatives to this basic approach. Alternative transmission measurement schemes can be performed in a way where the SRR is loading two separate probes instead of a transmission line [175, 176]. It is also possible to load the transmission line with modified SRR geometries. An asymmetric SRR such as the one demonstrated in [177] is shown to achieve higher quality factors and sensitivities compared to its symmetrical counterpart. Here, the asymmetrical SRR experienced a resonance frequency shift of 170 MHz as opposed to 110 MHz achieved by the symmetrical version when a glucose sample of 0.25 % concentration was applied. SRRs with inward extensions were demonstrated in [178], aligned in different orientations with respect to the coupled probes. These extensions offered higher gap capacitances,

promising higher sensitivity for detection of the reagent. Simulation results suggest a frequency shift-based sensitivity increase of up to 20 % at a load permittivity increase of about 30. [114] similarly worked with gaps utilizing extensions, but also added IDT shapes to increase gap capacitance further. Increased gap capacitance shifted the nominal resonance frequency of a single loop SRR of similar dimensions to 4.18 GHz from 6.54 GHz according to simulations. Fabricated design achieved a resonance frequency shift of 26 kHz per mg dL^{-1} within the concentration range of 0-5000 mg dL^{-1} with a good linearity.

Other resonator shapes that can focus strong electric fields at one spot also exist. ELCR is one of these, as studied in [179]. A co-planar waveguide-coupled ELCR at 3.41 GHz nominal frequency with a sample container was fabricated here and was tested with glucose solutions in deionized (DI) water and phosphate buffer saline solutions. As opposed to focusing electric field at a confined space, it may be desirable to distribute it over an area with multiple capacitive components. This will be useful in a scheme where the sample will be in contact with the sensor over a larger area. Spiral shape resonators, or multiple loop SRRs are possible solutions to such a case [180].

A pair of rectangular SRRs coupled to each other were proposed as a wearable, noninvasive, real-time glucose monitoring system in [181]. One of the SRR structures acting as a passive tag, designed at 4 GHz nominal frequency, is to remain on the skin. A second resonator coupled co-planarly to readout ports act as the measurement device in the system. Measured resonance frequency shifts based on the changes in glucose concentrations in the interstitial fluid. Experiments conducted with glucose in saline solutions measured behind a layer of 300 μm shaved mouse skin yielded a sensitivity of 2.1 kHz per mg dL^{-1} over a concentration range of 0-1.67 mg mg dL^{-1}.

2.1.1.1. Advanced Fabrication Methods and Sensor Concepts. Microwave resonators employed for glucose sensing are not limited to be macro-scale fabrication methods used in PCB production. As scalable, planar elements, they are well compatible with

more advanced fabrication processes. As potential candidates for wearable sensor applications, particularly being in contact with skin and eye, fabrication of glucose sensors on flexible substrates are noteworthy. Metamaterial inspired frequency selective surfaces were fabricated by deposition of gold through a 500 nm thick silicon nitride film on 280 μm thick paper substrates via shadow mask patterning in [66]. Unit cells were of sub-mm dimensions with minimum feature sizes less than 10 μm with resultant nominal frequencies occurring between 0.5-1.1 THz. A frequency shift-based sensitivity of 0.79 GHz per mg dL^{-1} concentration with a limit of detection at 19 μg dL^{-1} was attained when the surface is coated with glucose solutions.

A high quality factor of 160 was achieved in [182], where a circularly folded T-shaped uniform impedance resonator was screen-printed as silver on polyethylene substrate. The resonator has a nominal resonance frequency of 11.8 GHz, while covering an area of 16 mm $\times$ 12.3 mm. A sensitivity of 710 kHz per mg dL^{-1} concentration was achieved at a concentration range of 100-500 mg dL^{-1}. Another paper-based glucose sensor with integrated microfluidics is presented in [183]. Microchannel is printed on paper by a wax printer. Following this, the rectangular SRR structures made of gold were deposited on the paper substrate via magnetron sputtering through a laser-cut SUS304 shadow mask. After cutting, sensor units were assembled with a PVC support preventing the deformation of the structure, along with a sample pad and an absorbent pad. A transmission measurement method was applied with waveguides. A sensitivity of 564 kHz per mg dL^{-1} glucose concentration was obtained over a concentration range of 0-1.67 mg dL^{-1}.

Fabrication of sensors in smaller scales allow them to be integrated with electronics easily and is particularly attractive for implantable or point-of care applications. Scaling down while remaining in microwave frequencies require incorporation of a high number of capacitive features. A microwave resonator of long, intertwined pair of looping conductive paths forming an interdigital capacitive gap at the center was proposed as a glucose sensor in [61]. It was possible to realize a resonance frequency as low as 2.5 GHz on fabricated on a 400 μm GaAs substrate in an area of 700 μm $\times$ 900 μm. Thanks to the high capacitance realized, it was possible to obtain a relatively high sen-

sitivity of 1.13 MHz mg dL^{-1} glucose in human blood serum. Nevertheless, fabrication process demonstrated here is a costly one requiring multiple layers of metallization and formation of air bridges, as is the case for [55, 184].

2.2. Modeling of SRR

Modeling of SRRs can be done efficiently with finite element analysis (FEA), using finite element methods (FEMs). FEM is nowadays arguably the most widespread method used for solving of engineering problems requiring solving of differential equations. The method is based on the division of the problem into smaller divisions giving the method its name. FEM connects equations related to discrete sub-divisions to approximate the solution to a more complex model [85]. For electromagnetic FEA, this includes the solution of Maxwell's equations for given boundary conditions in iteration, minimizing the residual error at each step. Application of FEA in electromagnetics research has the advantages of easily representing complex geometries and inclusion of different materials. Downside is the necessity to transform near field solutions to far field solutions as well as the large matrix.

Various FEA software alternatives are present for the simulation of resonance characteristics of SRRs today. However, it is important to have analytical models at hand derived from the geometry and physics, which are useful at the initial design steps and at providing an insight to the operation of SRRs. Studies modeling SRR variants using different approaches are present in the literature, including spiral, double/multiple ring structures [23, 34, 37, 185–190], broadband coupled SRR pair [39], and a three dimensional array [191].

A SRR is a resonant structure that responds to external electromagnetic effects. Magnetic fields coupled to the ring structure excites a circulating current along the conductor due to inherent inductance of the structure. This current creates a voltage at the gaps, which act similar to parallel plate capacitors. Presence of the capacitance and inductance creates resonances at certain frequencies. Taking into account the ohmic losses, a lumped component model for a single loop SRR will be a basic series

RLC circuit [33, 192, 193] as shown in Figure 2.1. This simple model is useful in that it provides an intuitive understanding of the operation and resonance of the SRR.

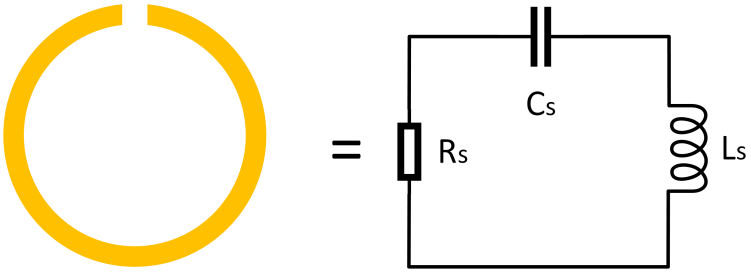

Figure 2.1. Series RLC circuit equivalent of SRR.

According to this approach, resonance frequency f_{0s} and quality factor Q_{0s} of an SRR modeled by a series lumped component model are [194]:

$$f_{0s} = \frac{1}{2\pi\sqrt{L_s\,C_s}} \tag{2.3}$$

$$Q_s = \frac{1}{R}\sqrt{\frac{L_s}{C_s}} \tag{2.4}$$

Derivation of circuit parameters appearing in the expressions above are presented below [33, 195]. The analysis is based on an SRR with inner radius r, conductor width w, gap width g, and conductor thickness t as shown in Figure 1.5.

The resistance component R is related to ohmic losses along the conductor. Provided that g is small compared to the loop radius, the loop inductance L_s can be taken as:

$$L_s = \mu_0\, r_m \left(\log \frac{8r_m}{t+w} - \frac{1}{2} \right) \tag{2.5}$$

where

$$r_m = r + \frac{w}{2} \tag{2.6}$$

and μ_0 is the permeability of free space.

The capacitance C_s has two different contributors from the gap (C_{gap}) and the surface (C_{sur}) capacitance due to loop structure. For a sufficiently narrow gap, C_{gap} can be written as:

$$C_{gap} = \varepsilon_0 \frac{t\,w}{g} + \varepsilon_0 (t + w + g) \tag{2.7}$$

where ε_0 is the permittivity of free space. First term in the sum accounts for parallel plate capacitance associated with the gap, and the second term is a correction term added to represent the effect of fringing fields [33]. The surface capacitance for a loop with gap with sufficiently small gap size can be modeled as:

$$C_{sur} = \frac{2\varepsilon_0 (t + w)}{\pi} \log \frac{4r}{g} \tag{2.8}$$

Thus, the total capacitance is:

$$C_s = C_{gap} + C_{sur} \tag{2.9}$$

We see that both capacitive components are directly proportional to dielectric permittivity of the medium, which is described as the free space for the model described in [33]. An SRR, on the other hand, will be fabricated on a dielectric substrate with an electric permittivity ε different than that of the free space as described as:

$$\varepsilon = \varepsilon_r \varepsilon_0 \tag{2.10}$$

where ε_r is a material specific constant, greater than 1, that relates the permittivity of free space to permittivity of the said medium. A more accurate approach would be to use an effective permittivity that approximates the interfacing substrate-air dielectric compound as a single dielectric block as shown in Figure 2.2 [196] .

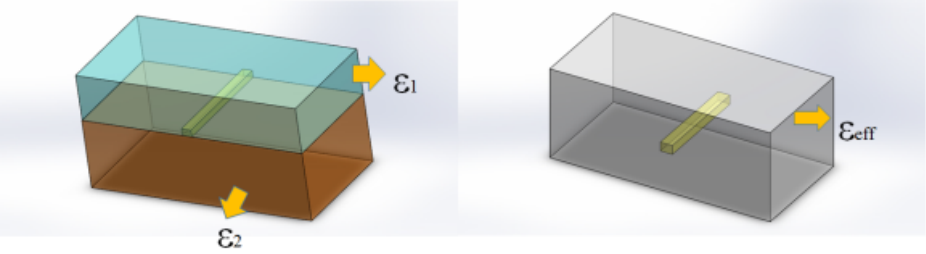

Figure 2.2. Approach to use an effective relative dielectric permittivity ε_{eff} in analytical modeling [196].

Effective relative permittivity ε_{eff} in this case can be calculated as follows [196, 197]:

$$\varepsilon_{eff} = \frac{\varepsilon_r + 1}{2} + \frac{\varepsilon_r - 1}{2 \times \sqrt{1 + 12\, w/d}} \tag{2.11}$$

where d is the thickness of the substrate on which the SRR is fabricated.

A CSRR, on the other hand, can be modeled as a parallel RLC network as shown in Figure 2.3 [193]. Resonance frequency f_{0p} and quality factor Q_p values associated with such a network is [194]:

$$f_{0p} = \frac{1}{2\pi \sqrt{L_p\, C_p}} \tag{2.12}$$

$$Q_p = R\sqrt{\frac{C_p}{L_p}} \tag{2.13}$$

where the circuit parameters can be separately calculated. We see that the SRR and CSRR have the same expressions for the resonance frequency f_0 but an inverse relationship for the quality factor Q. The dielectric sensing of glucose with SRR/CSRR structures rely on the change of C through a change in ε_0 of the medium. Increased sensitivity to such a change is theoretically possible with structures engineered to have large C values. A large C results in a low Q for SRR, whereas it has the opposite effect with CSRR, which is an advantage for the latter. On the other hand, for applications where it is desirable to concentrate electric field lines in confined spots, SRRs with $C_{gap} > C_{sur}$ do a better job while maintaining a high sensitivity compared to CSRRs.

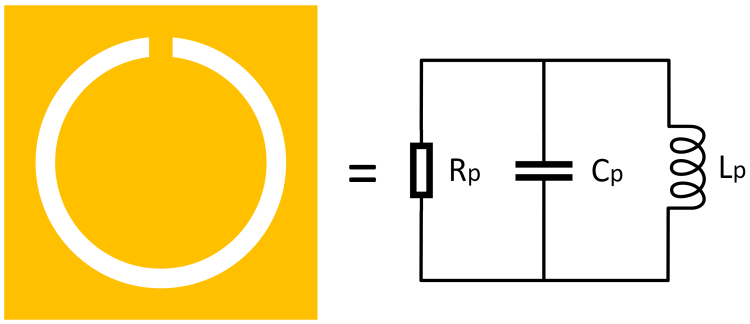

Figure 2.3. Parallel RLC circuit equivalent of SRR.

2.3. Dielectric Properties of Materials

Dielectric properties of materials were first observed due to change they create in capacity of storing electrical energy in a parallel plate system. This capacity is expressed by the ε of the material [198]. Said capacity owes to the polarization capability of the material, and is related to it having few free charge carriers that can contribute to electrical conduction.

This polarization can occur in different ways [199]. All dielectric materials are subject to electronic polarization, related to the distortion of the electron clouds of the atomic nuclei within the material due to the electric field. Oftentimes, it is a weak polarization and it is the only polarization mechanism valid for hydrocarbons. Ionic polarization is caused by the displacement of ions in materials made up of molecules bonded by ionic forces, such as crystalline solids. Essentially distorting the bonds that make up the material, this creates a stronger polarization. Orientation polarization is observed in polar materials, whose molecules are permanent dipoles, such as water. With the applied electric field, the molecules are aligned according to the direction of the field, potentially storing a large amount of electrical energy.

Permittivity ε is modeled as a complex quantity. To see this, we can start from the Equation (1.2), which is given below once more:

$$\nabla \times \mathbf{H} = \mathbf{J} + j\omega\varepsilon_0\,\varepsilon_r\mathbf{E} \tag{2.14}$$

The current density is related to electric field as:

$$\mathbf{J} = \sigma\,\mathbf{E} \tag{2.15}$$

where σ denotes material conductivity. This expression can then be substituted in in Equation (2.14) to obtain:

$$\nabla \times \mathbf{H} = \sigma\,\mathbf{E} + j\omega\varepsilon_0\,\varepsilon_r\mathbf{E} = j\omega\left(\varepsilon_0\,\varepsilon_r - j\frac{\sigma}{\omega}\right)\mathbf{E} \tag{2.16}$$

Using this, the permittivity can thus be expressed as a complex quantity:

$$\varepsilon = \varepsilon_0\,\varepsilon_r - j\frac{\sigma}{\omega} = \varepsilon_1 - j\varepsilon_2 \tag{2.17}$$

so that ε_1 denotes the real part and ε_2 denotes the imaginary part.

This is particularly relevant under fast alternating electric field applications. Particle motions due to polarization attempts to follow the variations in field and can do so at low frequencies. On the other hand, at high frequencies a phase delay of polarization will occur. Such phenomena involving phase shifts are often modeled with the use of complex quantities.

Typical dependence of ε_1 and ε_2 to frequency in a hypothetical dielectric is similar to what is shown in Figure 2.4 [199]. As can be seen here, at low frequencies ε_2 has no significance since the polarization motion can follow the rate at which the field alternates. Variation observed in microwave band is related mainly to dipole relaxation. Atomic and electronic polarizations cause the subsequent variations in permittivity at higher frequencies.

Dipole relaxation has significance for SRR based sensing applications since many of these sensors are designed at microwave frequencies and interact with an aqueous solution. Water, being a polar liquid, is subject to dipole relaxation and related phe-

nomena. For polar liquids, dipole relaxation is often described by the Debye relaxation model [198], provided as follows:

$$\varepsilon(f) = \varepsilon_\infty + \frac{\varepsilon_s - \varepsilon_\infty}{1 + j2\pi f \tau_r} \tag{2.18}$$

where f denotes frequency, ε_∞ is the value of permittivity at high frequencies, ε_s is the permittivity under static field, and τ_r is the relaxation time, a constant describing the rate at which dipole relaxation for that material occurs.

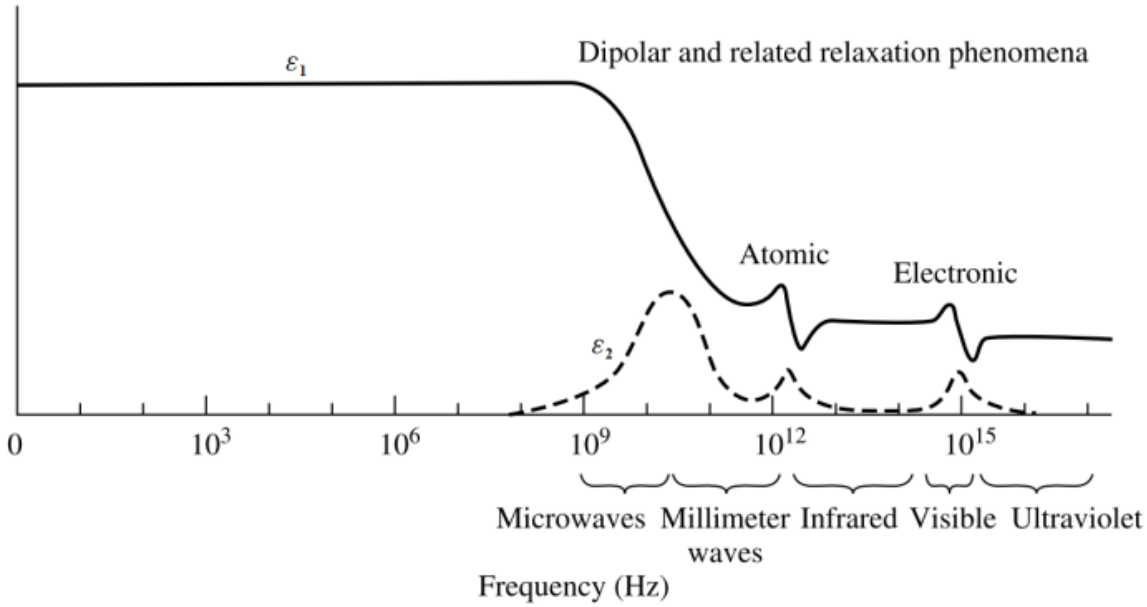

Figure 2.4. Change of real and imaginary parts of electric permittivity with respect to frequency for a hypothetical dielectric, from [199].

According to the Debye model, permittivity behavior has variations over three frequency bands [198], namely low frequency, relaxation frequency, and high frequency. At low frequencies, the dipoles can align themselves with the fields fast enough, as mentioned above. This way, electrical energy can be more efficiently stored via polarization of particles, giving the ε_1 its highest value, where ε_2 remains low. At frequencies around the relaxation frequency, where $\omega\,\tau_r \approx 1$, it is hard for dipoles to keep in phase with the electric field. Relaxation motions are significant, and so is the additional dissipation of power associated with these motions. ε_1 is in decrease and ε_2 reaches

at a maximum. At higher frequencies, polarization approximates to a 90° phase delay with electric field. Here, ε_1 and ε_2 are both small, amount of power dissipation is reduced.

It should be noted that polarization mechanisms are affected by temperature. As a result, ε has significant dependence on temperature. Another point to note is that the shape of the dielectric material can also affect its polarization behavior. In the case of a dielectric material having a long and thin cylinder shape, internal electric field approximates to a maximum when the external field is applied along the direction of the cylinder axis. When the field applied in a direction perpendicular to cylinder axis, internal electric field approximates to zero [199]. This can be significant in design of sensors incorporating microchannels.

3. EXPLORATORY WORK

Exploratory work regarding the basic interactions of SRRs with dielectrics has been conducted as part of the first step. Since SRRs are the prevalent metamaterial components used in sensing applications, primary focus has been on these structures. Research began with the investigation of some basic SRR geometries in simulation environment, followed by the fabrication and characterization of the said structures.

3.1. Simulation of Different Designs

Design of the SRR structures begins with the analytical models presented in the literature such as the one presented in the previous chapter, where available. For the most part of the preliminary work, we used the basic single loop SRR architecture for simple analysis and design. After the geometric parameters are defined via analytical models, the design can be fine-tuned and studied in more detail using CST Microwave Studio solver tool performing FEA. Chosen designs are modeled in the tool with parametric inputs, allowing easier tuning of the resonators.

Conductor was chosen as copper, and substrate material was set to represent FR4. A f_0 of 2 GHz were targeted for the designs, fitting in an area of 3 cm $\times$ 3 cm. To model the presence of a liquid load along with the resonator, a semi-spherical dielectric with relevant permittivity is added to the location of interest in simulation environment. For free-standing resonator simulations, the boundary conditions were set so that magnetic field coincides perpendicularly with the resonator plane, allowing for optimal excitation. Via simulations, the designs were fine-tuned to desired frequencies. Simulation results confirm that electric fields are highly confined in gap regions of SRR structures. Figure 3.1 shows the transmission spectra for a single loop SRR design in its unloaded and 1 μL DI water droplet loaded cases as obtained from the simulations. As expected, with the addition of the droplet, the resonance frequency shifts from 1.85 GHz to 1.65 GHz, due to increased permittivity of the water material.

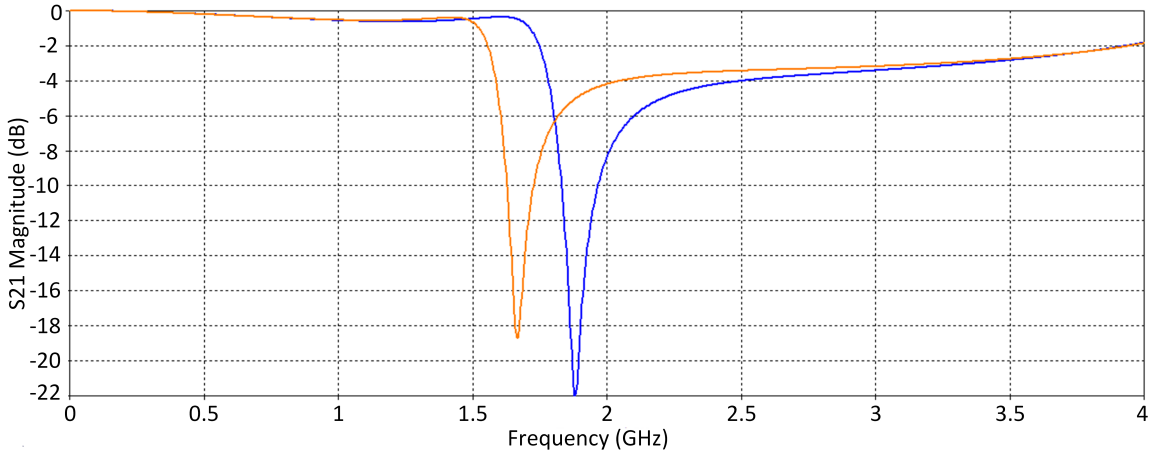

Figure 3.1. Simulation results of the S_{21} parameters for the nominal state of a resonator and when 1.0 μL water droplet is added.

3.1.1. SRR Structures and Their Dielectric Sensitivity

In order to obtain a high measurement performance, different resonator structures were simulated under similar conditions to see how sensitive they are to dielectric loading. Sensitivity in this case is understood as the amount of f_0 shift in response to a given dielectric loading. Sensitivity to dielectric changes is desirable since it gives an idea about how well a sensor can potentially resolve between minute differences of changes caused by alterations in glucose concentrations. It is also desirable that the sensor geometry remains at a size that is easy to handle, bulky at the target frequency of operation. A bonus will be the ability to operate well with sample volumes as small as possible.

Structures presented in the SRR sensing literature are investigated for this purpose [61, 69, 200–202] in simulation environment. Namely, these are single loop SRR (SSRR), double loop SRR (DSRR), triple loop SRR (TSRR), asymmetric SRR (ASRR), and ELCR structure. Variants designed at a fundamental nominal f_0 at around 2 GHz were investigated. Resonators were simulated in air, excited by free standing waveguide ports unless otherwise specified. The dielectric is modeled as placement of a semi-spherical volume of 1.5 mm radius of variable ε_r. On some select cases, loading schemes including placement of multiple semi-sphere shapes or a semi-cylinder shape

were also applied. Shift in transmission spectra were shown for varying ε_r values ranging from 1 to 80 were investigated. The maximum value of 80 was chosen as being a value close to that of water. A sensitivity figure of merit (FOM) was defined as follows for sensitivity comparison:

$$FOM = \frac{f_0(1) - f_0(80)}{f_0(1)} \tag{3.1}$$

where $f_0(\varepsilon_r)$ denotes the f_0 of a resonator obtained with a dielectric load having relative permittivity value ε_r.

3.1.1.1. SSRR, DSRR and TSRR. Single, double, triple, and multiple loop ring resonators have been used widely in sensing applications. Number of the loops may be increased to increase the capacitance, allowing for lower resonant frequencies while keeping the structure relatively small. It should be noted that this distributes the field confinement, rather than focusing it. That is why the sample contact area is often dispersed over these regions as well. A trio of structures, designed at a f_0 of 2 GHz were simulated. As can be inferred from the increased capacitances for TSRR, largest structure ended up being the SSRR, with a total radius of 10.25 mm. All three structures have the same gap width of 2 mm and can be seen in Figure 3.2.

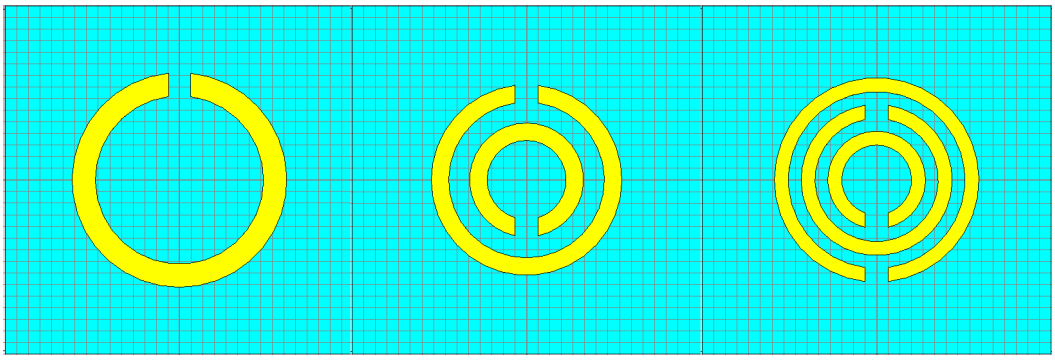

Figure 3.2. SSRR (left), DSRR (middle), and TSRR (right) designs. Not to scale.

Figures 3.3, 3.4, and 3.5 show the resonance frequency shift for the SSRR, DSRR, and TSRR, respectively when semi-spherical dielectric drops of various ε_r were applied to the outer-most gap region.

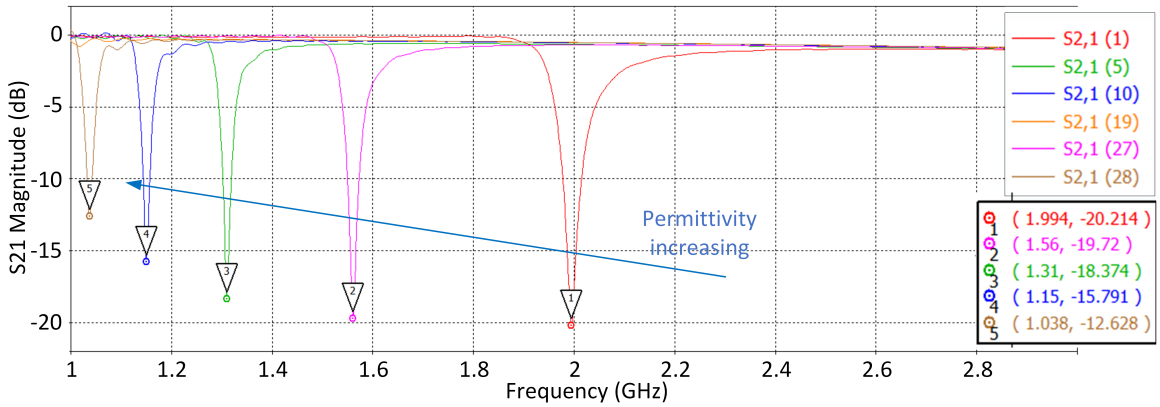

Figure 3.3. Resonance frequency shift of SSRR when the semi-spherical dielectric loads of 1.5 mm radius having relative permittivities of 1, 20, 40, 60, 80 were applied.

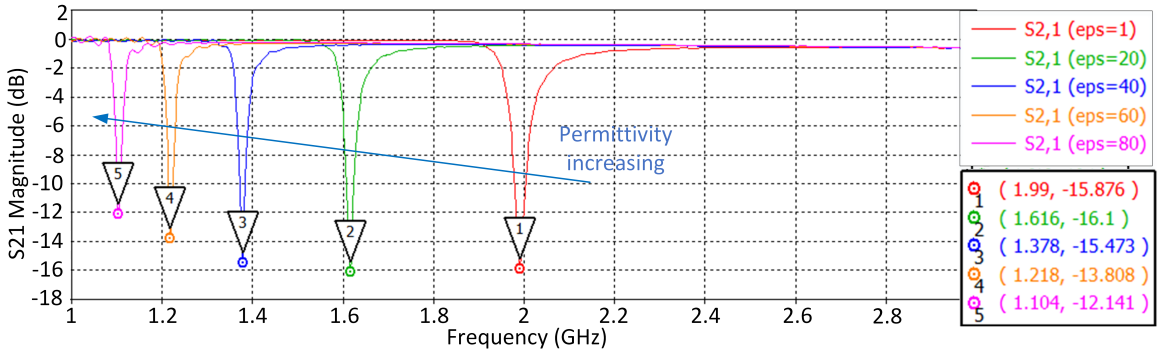

Figure 3.4. Resonance frequency shift of DSRR when the semi-spherical dielectric loads of 1.5 mm radius having relative permittivities of 1, 20, 40, 60, 80 were applied.

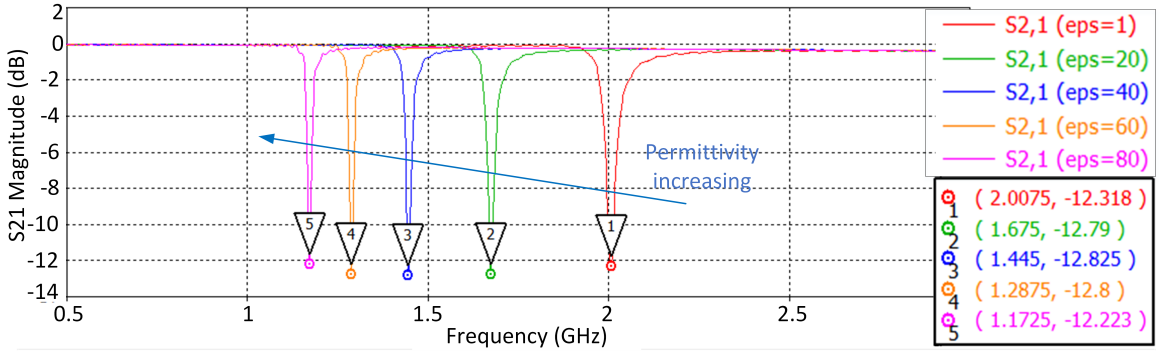

Figure 3.5. Resonance frequency shift of TSRR when the semi-spherical dielectric loads of 1.5 mm radius having relative permittivities of 1, 20, 40, 60, 80 were applied.

FOM associated with SSRR, DSRR, and TSRR geometries are 0.48, 0.44, and 0.42, respectively. A decrease in f_0 as well as Q are observed. Decrease in sensitivity with increased number of rings can be explained by the fact that only one of the multiple high field concentration regions available in the structure were used. What seems to be promising is that there seems to be a slight improvement in the quality factor as the number of the loops are increased. Sharper transmission response could be helpful for increased resolution.

In order to test the view that the decrease in FOM is related to unused gap capacitances, two additional loading schemes were applied to TSRR. In one of these, all three gaps of the TSRR were loaded with the semi-spherical dielectric, whereas in the other one, a semi-cylindrical load running through all three gaps were defined, imitating a microchannel. All three loading schemes are shown in Figure 3.6 and the results associated with the second an third loading scheme are demonstrated in Figures 3.7 and 3.8, respectively.

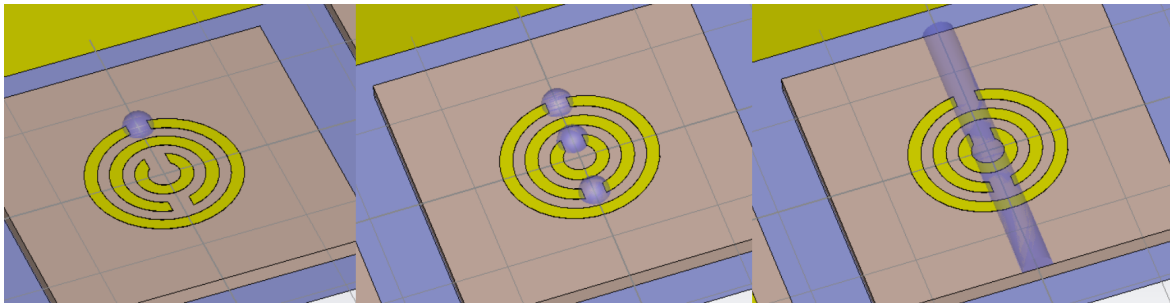

Figure 3.6. Single drop (left), three drops (middle), and channel dielectric (right) load cases for the TSRR structure.

For TSRR, FOM obtained with the additional loading schemes are 0.45 and 0.51, respectively, according to the simulation results. These indicate an increase in f_0 sensitivity. TSRR having increased number of capacitive components due to multiple gaps and regions between loops can perform better only when the material under test is interacting with these as a whole. Depending on the application, this may be an advantage or a disadvantage. As seen in Figure 3.8, there is also an additional risk of higher order resonances starting to shift close to fundamental nominal resonance frequency in the case of high shifts, which may lead to readout ambivalence problems.

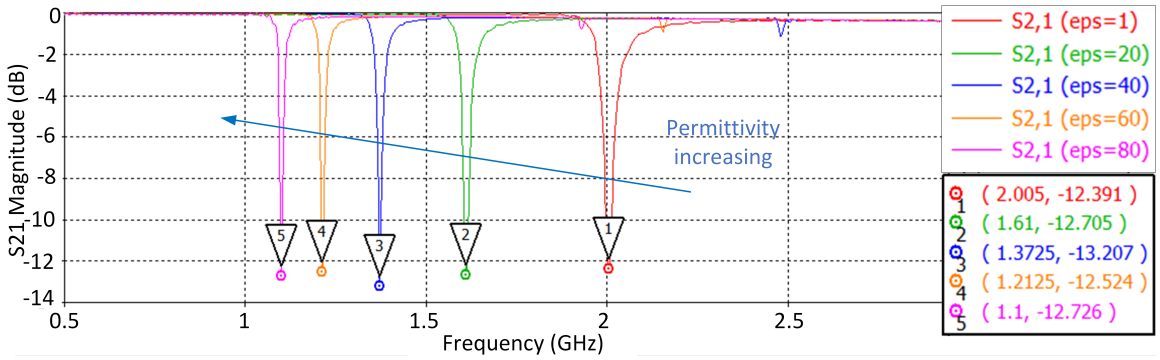

Figure 3.7. Resonance frequency shift of TSRR when the semi-spherical dielectric loads of 1.5 mm radius having relative permittivities of 1, 20, 40, 60, 80 were applied to all three gaps.

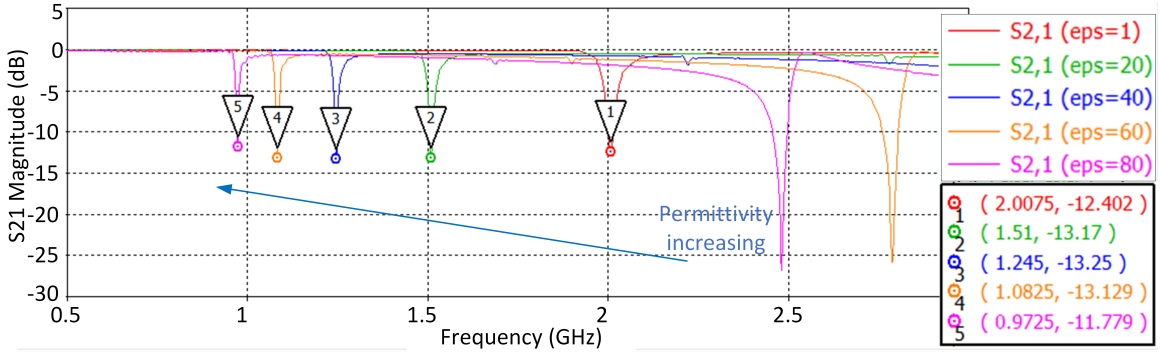

Figure 3.8. Resonance frequency shift of TSRR when the semi-cylinder dielectric loads of 1.5 mm radius having different relative permittivities of 1, 20, 40, 60, 80 were applied across all three gaps.

3.1.1.2. ASRR and ELCR. ASRR is a single ring having two slits, which are offset from the axis of symmetry. It is essentially formed of two unequal arcs. Since the resonator frequency is related to arc lengths, the structure can be used to obtain higher resonant frequencies for the same given structure radius, thanks to the presence of the short arc. It is therefore used in more high frequency applications and is reported to have a high sensitivity. ELCR structures consist of two loops connected to a capacitive gap positioned in the middle of the structure. They are reported in the literature to have high linearity, which is a desirable sensor quality. The structure can be electrically driven with electric fields perpendicular to the capacitive 'plates'. Magnetic actuation is possible only when the fields passing through the individual loops are of reverse directions, hence the name. This may make them difficult to excite in certain arrangements. Both these structures need to be larger compared to the resonators of the previous category at a given frequency. Both ASRR and ELCR structures are shown in Figure 3.9.

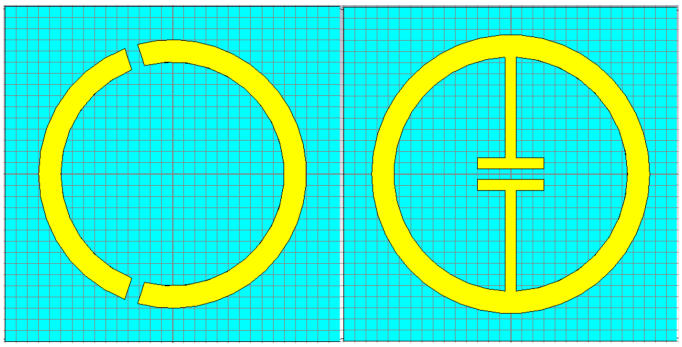

Figure 3.9. ASRR structure with 18° gap offset (left) and ELCR structure (right). Not to scale.

Two structures designed for a f_0 of about 2 GHz are simulated in a manner similar to previously done. ASRR structure, having multiple gaps and motivated from the results described above was loaded with a semi-cylindrical dielectric load instead of a semi-spherical one. The resonance frequency shift behaviors for ASRR and ELCR are shown shown in Figures 3.10 and 3.11, respectively.

FOM value obtained from the ASRR and ELCR structures are 0.62 and 0.48, respectively. It is observed that the ASRR by itself presents a better FOM compared to TSRR, while still maintaining a high Q factor, when both of the structures are

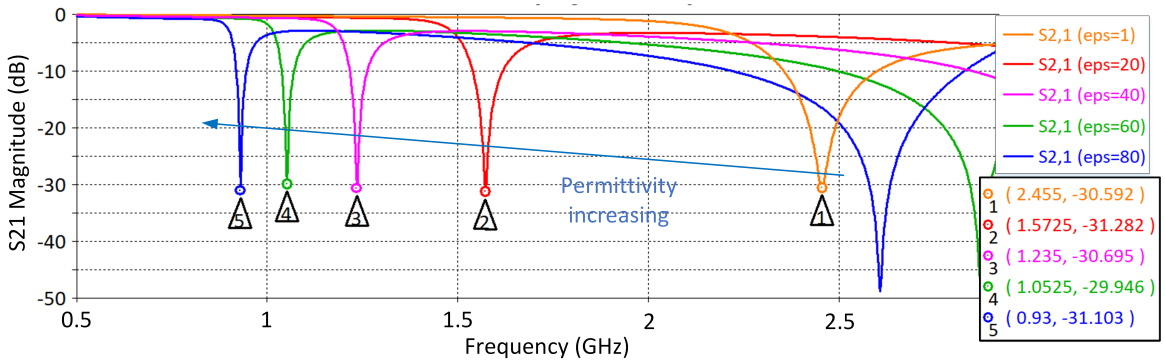

Figure 3.10. Resonance frequency shift of ASRR when the semi-cylindrical dielectric loads of 1.5 mm radius having relative permittivities of 1, 20, 40, 60, 80 were applied across the gaps.

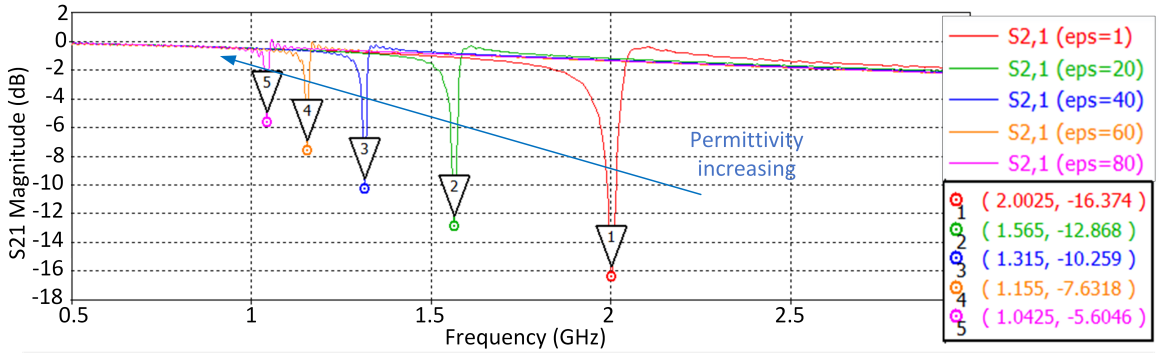

Figure 3.11. Resonance frequency shift of ELCR when the semi-spherical dielectric loads of 1.5 mm radius having relative permittivities of 1, 20, 40, 60, 80 were applied to the gap.

loaded with a semi-cylinder. Again, it is worth considering is the appearance of higher frequency resonances in the spectrum of interest with great amount of f_0 shift. For ELCR, FOM is the same as the simpler SSRR, whereas Q deterioration is considerably higher, which is undesirable.

3.1.1.3. Tip Shaped Gaps. Simulation results confirm that much of the sensitivity to dielectric changes is related to the capacitive components associated with gap regions, where electric field confinement is higher. Sensitivity can possibly be increased further by modifications around the gap regions. Tip shaped gaps were demonstrated in SRRs to increase sensitivity [201]. Such a shape can contribute to high confinement of electric fields. This approach was applied to SSRR and ASRR models in simulation environment, as seen in Figure 3.12.

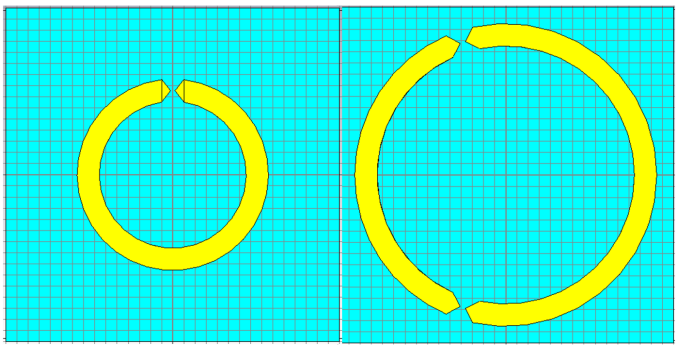

Figure 3.12. Tip shaped gaps applied to SSRR (left) and ASRR (right) geometries.

In simulations, flat and tip shaped gap versions of SSRR and ASRR structures excited by a pair of monopole antennas are compared for a more realistic representation of the measurement scheme. Monopole antenna pair was chose since it would be the excitation method of choice for initial tests as will be apparent in the subsequent sections. Simulation results are given in Figures 3.13 and 3.14. Obtained FOMs for i) SSRR and ii) ASRR geometries, having flat and tip shaped gaps are i) 0.42, 0.535, ii) 0.60, and 0.60, respectively. It is seen that tip shaping changed the sensitivity performance little for the ASRR case. For the SSRR, tip shaping increased sensitivity more than 25 %. Excitation with the monopole antenna seems to create a significant parallel resonance effect in simulation conditions.

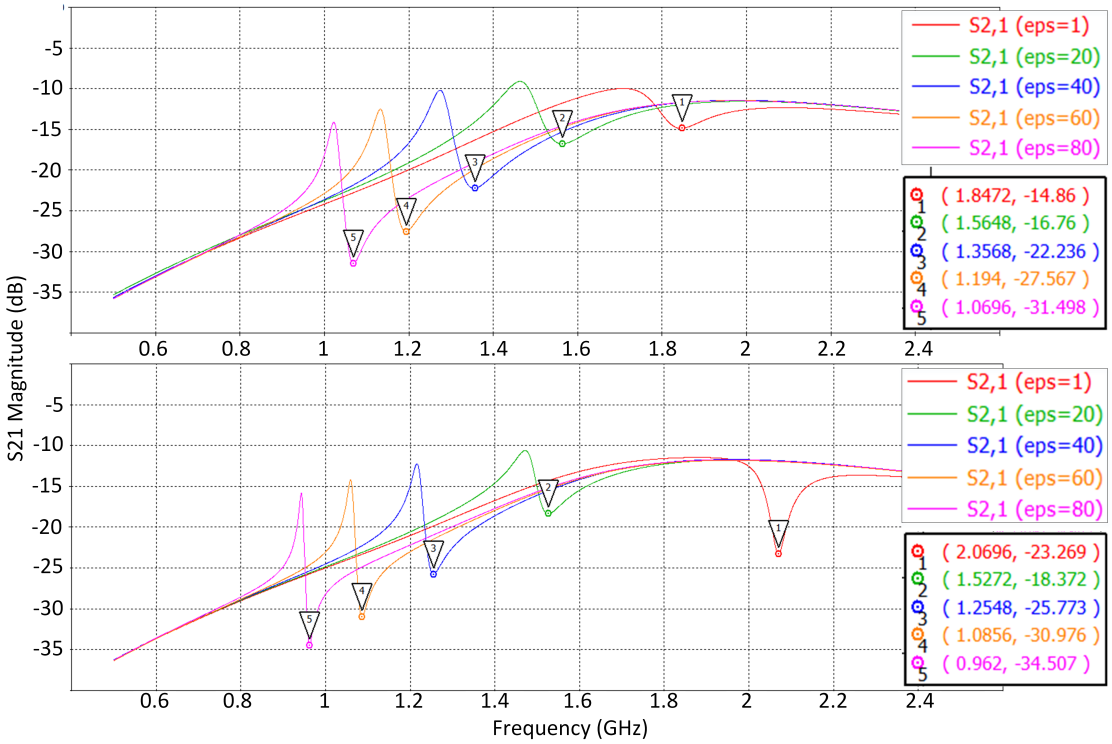

Figure 3.13. Dielectric sensitivity of SSRR structures with flat (top) and tip-shaped (bottom) gaps, under monopole antenna pair excitation.

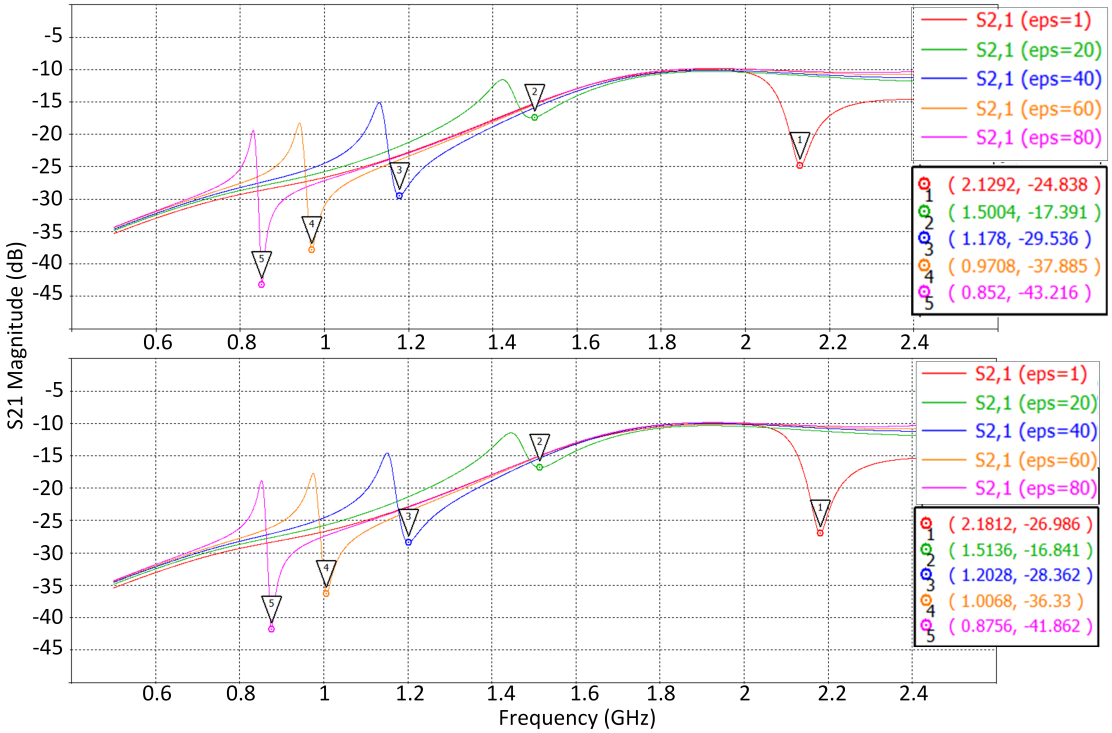

Figure 3.14. Dielectric sensitivity of ASRR structures with flat (top) and tip-shaped (bottom) gaps, under monopole antenna pair excitation.

3.2. Cost-Effective Fabrication

Finalized designs can easily be realized via PCB fabrication techniques in macro scale on commercially available FR4 substrates. This is often easier with simpler SRR geometries. More involved designs incorporating multiple gaps and smaller features may strain simpler fabrication applications in macro scale somewhat, since errors in features -especially the ones associated with the gaps- tend to cause deviations from the intended behavior. This was particularly the case for tip shaped gap applications, where small gap features were needed that could not be effectively patterned in a repeatable manner.

Masks for fabrication can be exported from the models prepared in CST or drawn in dedicated tools such as L-Edit. Two different processes for fabrication were applied for the realization of the resonators. In one technique, an adhesive material with polymer backing is fixed on the 35 μm Cu plated surface of an FR4 platform. The mask designs were then exported to a commercially available CO_2 laser cutting machine (Versa Laser VL-200). Laser engraving process burns away the polymer backing, leaving the adhesive as a residue, when applied at a sufficiently low power. Result of this operation performed on a sample mask can be seen in Figure 3.15. After the engraving, remaining adhesive with backing was peeled off from the FR4 board, which was then subjected to etching in acid bath composed of hydrochloric acid and hydrogen peroxide. Patterns protected by the molten adhesive remain on the surface, whereas the remaining Cu regions are etched away. Individual SRRs were then mechanically cut using guillotine-like tools. With this approach, it is possible to fabricate multiple devices on board with comparatively high resolution, while preserving good Cu and substrate thickness uniformity. On the other hand, more steps are required for the complete procedure, increasing the time required for the fabrication of SRRs. At times, it is also hard to control the parameters related to wet etching and engraving processes. Mechanical cutting of the samples as the last step can sometimes lead to cracks in the substrate, particularly when working with thicker substrates, reducing the repeatability of fabrication.

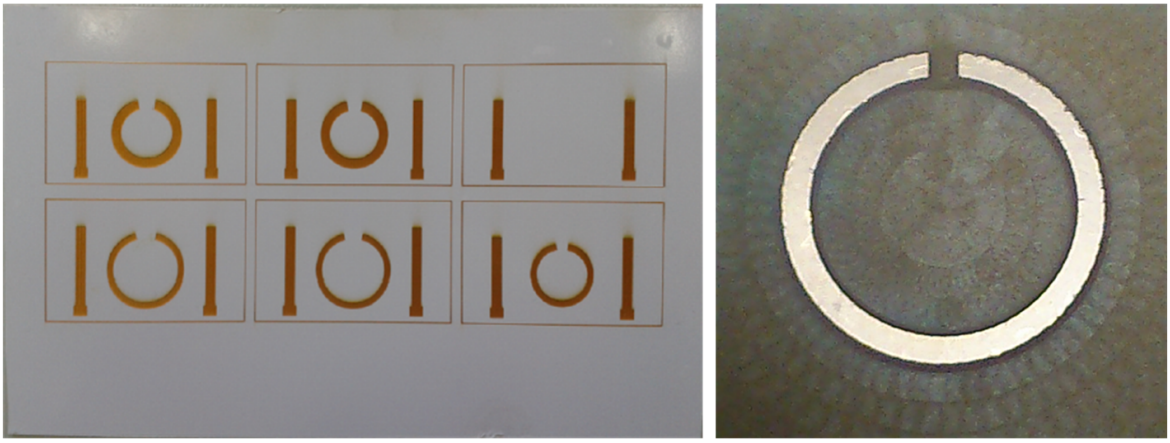

Figure 3.15. SRR samples fabricated with laser cutter before acid bath (left) and a SRR fabricated with PCB processing tool (right).

The second technique used for the fabrication of devices is the use of a PCB processing machine, which is LPKF S103 in this case. Such a tool shapes the PCB in mechanical ways via drilling, milling, and cutting. This is also a calibration-dependent process yielding acceptable resolutions in faster prototyping times. Potential distortions in surface uniformity of the conductive and substrate parts can occur. A sample SRR device fabricated with this technique is shown in Figure 3.15.

In later stages of the exploratory work it became apparent that it was important to place the liquid sample droplets at the same location of interest on the SRR surface. Similarly, measurement precision can be increased with droplets retaining their shapes for a longer period. Two additional steps were added to sensor fabrication to address these concerns. First one is to create an artificial reservoir-like feature on the sensor surface to hold the liquid together. A cost-effective way of doing this is to erode the FR4 substrate region in the SRR gap with additional engraving with the PCB prototyping machine, forming a depression on the surface where the droplet can be conveniently placed as shown in Figure 3.16.

Additionally, a hydrophobic coating of 7 μm parylene material, encouraging the droplet to retain its shape over a longer period of time on the surface of the sensor, was performed. This also has the advantage of isolating the liquid drop from the metallic regions, since potential increase in conductivity in the gap region or similarly potential

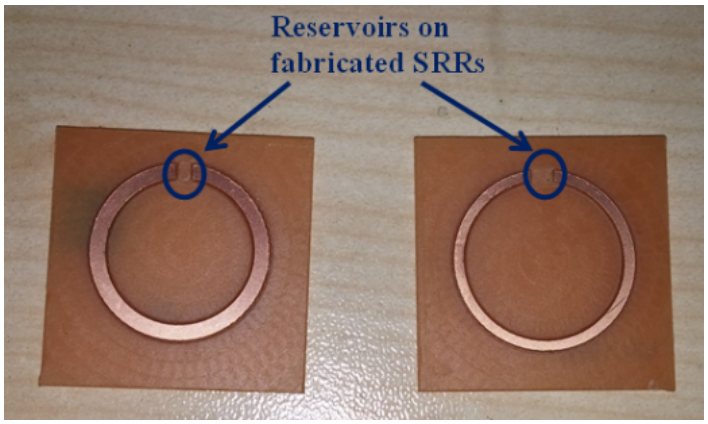

Figure 3.16. The fabricated SRRs with an eroded depression in the gap region acting as simple reservoirs.

risk of corrosion of the conductive material over time can affect sensor performance. Parylene is an ideal material of choice for this also because it is resistance to acid, heat, and oxidation.

3.3. Measurement Setup

Excitation of the SRR was done with a pair of planar monopole antennas with 30 mm × 3.5 mm × 35 μm dimensions fabricated on a 0.8 mm-thick FR4 substrate. Both monopole strips were perpendicularly mounted on an Al metal plate acting as a ground plane through a pair of holes, 5.4 cm apart from each other, drilled into it. The antennas show an optimized transmission performance at frequencies around 2 GHz, coinciding with f_0 of the fabricated resonators. In order to keep the sensor SRR along the shortest transmission path between the antennas and to perform measurement control at a higher precision, a 3D-printed custom-designed holder structure shown in Figure 3.17 was added to the setup. This holder essentially keeps the planar monopole strips and the SRR in plane and defines a more exact location to place the SRR to be worked with, provided that all SRR alternatives are fabricated on a substrate of a standardized size of 3 cm × 3 cm. The ground plane was mounted on an insulating table in a vertical position using two insulating bodies sandwiching the plate in between. Selected SRR geometries were fabricated on 35 μm-thick Cu coated FR4 substrate using PCB processing tool. A reservoir depression was added before it was

coated with 7 μm-thick parylene as described above. The monopole antenna pair was connected to a VNA (ZVB4, Rhode & Schwarz) for transmission measurements, with soldered SMA connectors. The VNA was calibrated before any set of measurements.

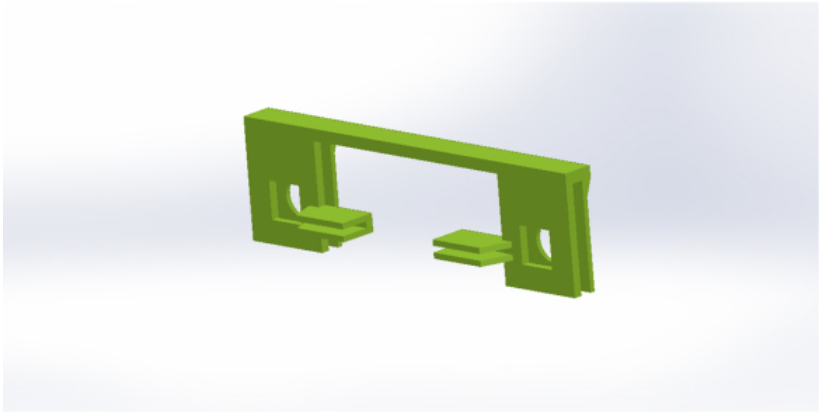

Figure 3.17. The resonator holder designed to fix the sensor substrates and monopole antennas in position, on the same plane.

Liquid samples, namely DI water and glucose solutions of different concentrations were applied as droplets using a micropipette with a precision of 2 %. Liquid volumes were chosen so that the droplet was large enough to fill the gap reservoir and lean against the resonator-gap interface but still small enough not to overflow from its confines.

For the measurements using GOx enzyme, it was extracted from commercially available fasTTest blood glucose test strips via physical methods. This includes the delamination of the test strip with a scalpel to expose the glucose sensitive part and at times cutting of the layer into a smaller size for more precise application. After this step, a small volume droplet was placed on the active part of the strip, dissolving the enzyme. This droplet was then collected once more with the micropipette to be applied to the glucose solution. Direct use of the microstrip on SRR surface cannot be done due to metallic electrode parts present in the microstrip. These would interfere with electromagnetic measurements. Pure glucose is obtained commercially. After every measurement that involves reagent solutions being applied to the sensor, surface was cleaned carefully with DI water so that no residues remain to interfere with subsequent measurement. Extra care was shown so that the parylene coating on sensor surface

was not eroded or peeled off. The aim is that the sensor f_0 return to its nominal value after the sample is removed from the sensor.

All measurements described in this chapter were done in laboratory environment at room temperature. Nominal S_{21} response of the monopole antenna pair was recorded separately to be used as a background reference. This allows easier determination of resonance characteristics of small amplitudes in cases where they may be otherwise overlooked. Figure 3.18 shows a photograph of the overall measurement setup. It was observed that the measurements should be performed at a mechanically stable environment and away from moving bodies, as much as possible. To address this, the VNA was controlled at a distance using a cable connected keyboard and mouse set.

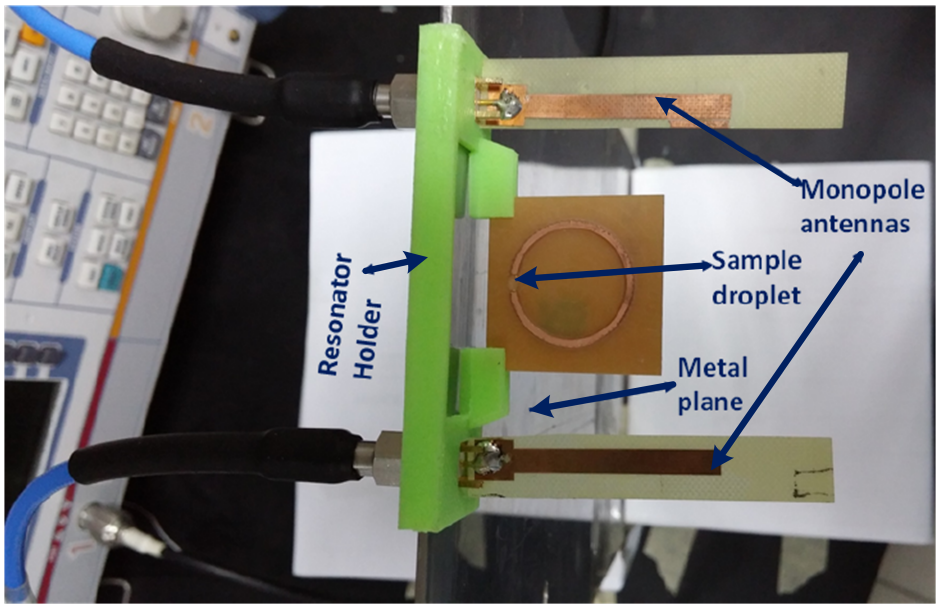

Figure 3.18. Initial measurement setup used for exploratory studies.

3.4. Exploratory Measurement Results

Several sets of experiments are conducted to observe basic sensor behavior as an initial step.

3.4.1. Effect of Volume and Position

The response of sensors under presence of liquid samples was observed. First DI water droplets of different volumes were applied at different positions of the SRRs. Expected outcome was to observe highest sensitivity to material presence closer to the gap of the structure, since this region is where the electrical field confinement is the highest as observed in the simulation environment. This was confirmed with the further discovery that the most sensitive region around and within the gap region is the interface between the conducting part and the dielectric, as shown in Figure 3.19.

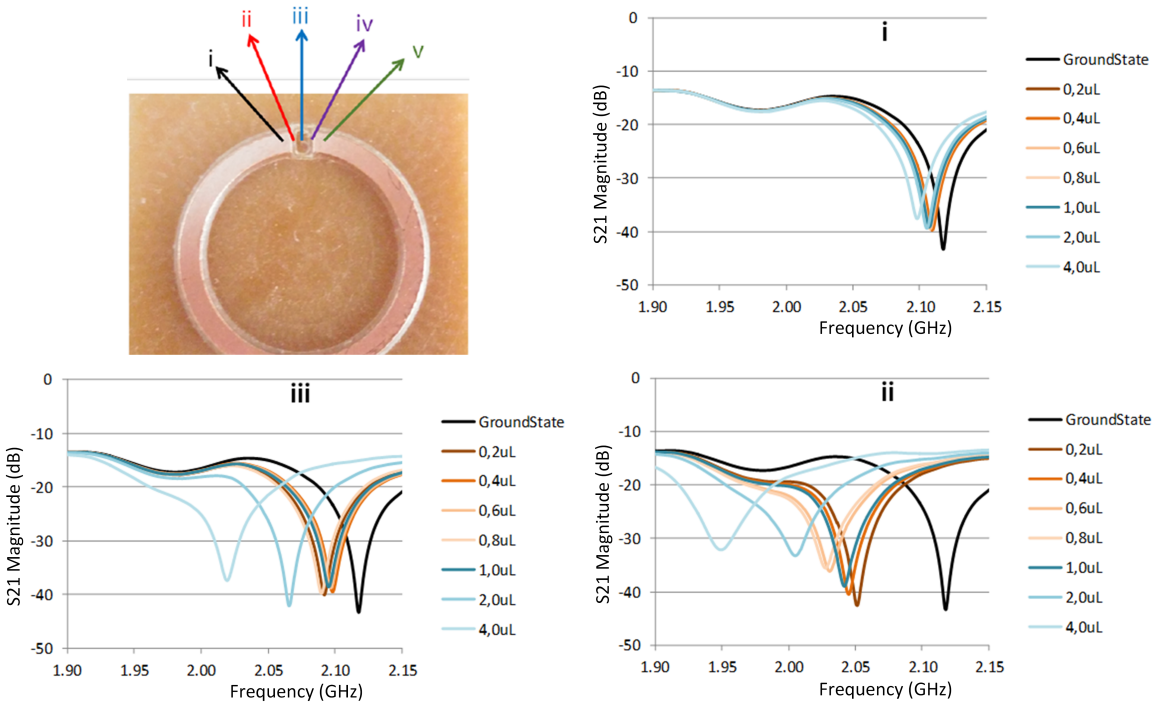

Figure 3.19. DI water samples of different volumes placed on the same SRR cause different amounts of shift when placed at different positions. The highest shift are observed around the gap region as expected, specifically at the conductor-substrate interface.

Application of DI water in different volumes showed a general trend to shift the resonance frequency to lower levels, although this behavior was not strictly consistent and not linear for the initial sets of measurements. The shift to lower frequencies was expected due to higher permittivity of water compared to that of the air, creating an increased capacitance, translating to a lower f_0. The inconsistencies and nonlinearities

were attested to the difficulty in precise positioning sample drops despite the presence of the reservoir structure.

In order to perform volume measurements at a higher range, a more pronounced reservoir made of rubber is placed around the gap region of the sensor, in which the liquid droplets were applied. This combined with taking the average of repeated experiments yielded a more consistent behavior of changing resonant frequencies. Results obtained with different volume DI water loads are given in Figure 3.20. Results demonstrate that the increased volume of liquid sample is inversely related to the f_0, which coincides with the dip of the transmission spectra. Amount of shift in consequent additions of liquid volume becomes less significant, i.e. there is a diminishing return effect.

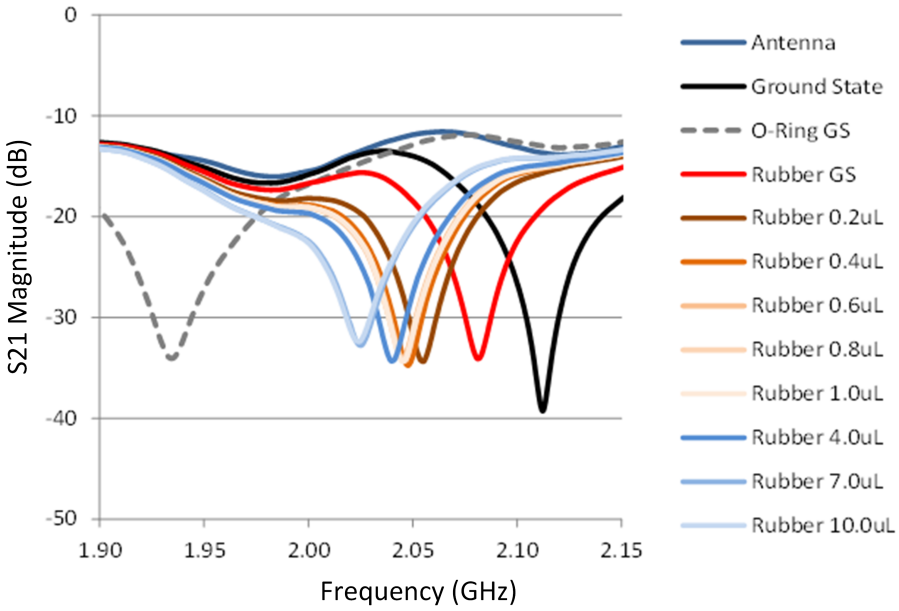

Figure 3.20. DI water samples of different volumes are applied to SRR with rubber reservoir.

3.4.2. Effect of Concentration

Next up, the response of the sensor to different levels of glucose concentration are studied. For this experiment, an SRR with g=2.1 mm, r=8 mm, w=1.5mm, t=0.035 mm dimensions are used. Corresponding nominal f_0 of the bare resonator is 2.12 GHz. Reservoir depression like the one added in the previous step was also incorporated.

Concentration sensitivity of the SRR device is investigated by applying 1.0 μL drops of varying glucose concentrations. Water droplet including the enzyme was added to the droplet containing the glucose concentration. The shifts in the dip frequency and magnitude 30 seconds after the introduction of the enzyme were recorded. The test was repeated five times for every concentration level. The gap reservoir was carefully cleaned with DI water after every measurement without removing the SRR structure from the holder. Obtained results are plotted in Figure 3.21. Plot shows the shifts from the ground state, which is a loading of DI water of the same volume. An increase in the shift amounts with an increase in concentration can be observed. Slopes of the trendlines fit to data are 65 MHz/g mL^{-1} and 11.55 dB/g mL^{-1}. Results show a clear relationship between the concentration and the sensor response. Minimum and maximum errors associated with the measurement are still relatively high, pointing to the fact that there is room for improvement in terms of precision. Reduction in Q can be explained in increased dielectric loss with increased glucose concentrations.

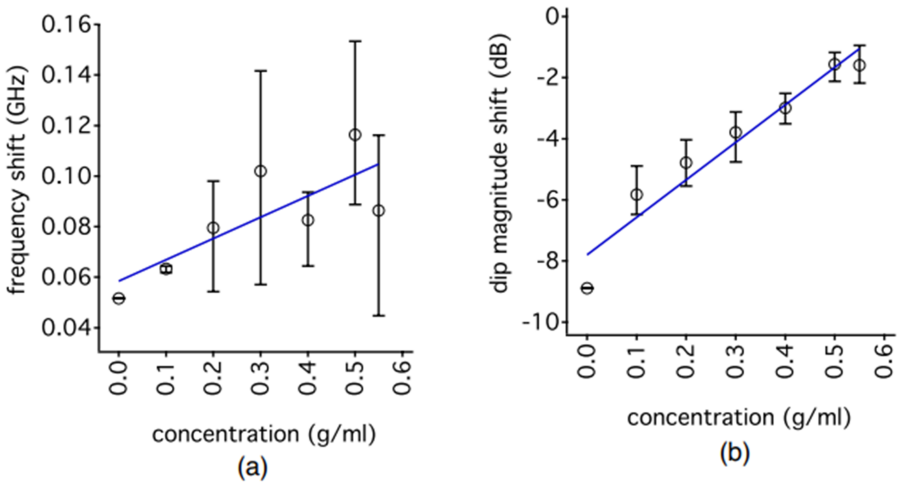

Figure 3.21. The amount of shift in (a) dip frequency and (b) dip magnitude 30 seconds after the enzyme introduction. Average of five measurements with minimum and maximum values marked with error bars are shown.

3.4.3. Effect of Reaction Time

In the last sets of exploratory measurements, response of SRR in time during the glucose solution-enzyme interaction for the duration of 10 minutes is observed for 30 second intervals. The change of the f_0 and magnitude due to enzyme introduction to

a 1.0 μL glucose solution of 0.55 g/mL concentration were recorded. The results are shown in Figure 3.22. An ongoing linear shift is observed throughout this time period, implying that the any interaction present was still continuing. According to this, shift rates of of 12.3 MHz/min and 0.37 dB/min are observed.

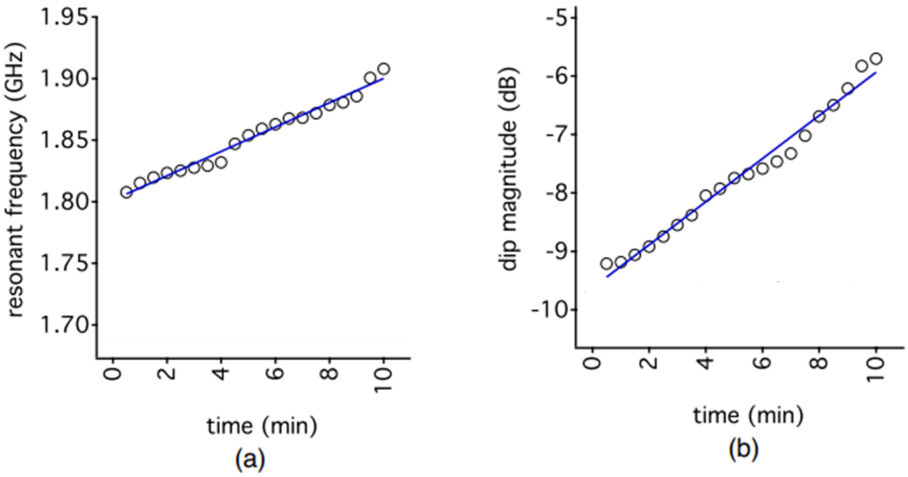

Figure 3.22. The recorded values of (a) resonance frequency and (b) transmission magnitude for a period of 10 minutes using a 1.0 μL solution of 0.55 g/mL glucose concentration.

3.5. Chapter Conclusion

Work done up to this point studies the application potential of an SRR based microwave glucose sensor. Different SRR architectures were tested in simulation environment and their sensitivities were investigated. Single loop SRR was chosen for its ability to effectively confine electrical fields at one focus and its simplicity. Selected SRR designs were designed and fabricated to operate at around 2 GHz. Fabrication process of the SRR structures and the experimental setup was designed and modified so that the a higher repeatability across the measurements could be achieved, which is necessary to see the effect of glucose concentration on the f_0 and resonance magnitude change.

It is seen that the incorporation of DI water and glucose solution causes a decrease in f_0 referenced to the nominal f_0 of the SRR. Increased glucose concentrations lead to higher f_0, since glucose solutions of higher concentrations demonstrate lower

permittivities. Dip frequency shifts as large as 41 MHz from the nominal state can be observed with the incorporation of liquid samples. A reduction in the quality factor is also observed, as the dip magnitude also increases. Both changes can be used to determine the glucose concentration of a liquid, as they are evidently correlated to the concentration.

4. PROPOSED GLUCOSE BIOSENSOR DESIGN

Biosensors are important devices used in a variety of applications ranging from medical diagnosis to environmental monitoring. Most prominent of these arguably is the management of diabetes, taking up to 85% of the market share [127]. Following the initial exploratory work, design of a glucose specific biosensor based on SRR sensing is demonstrated.

By definition, a biosensor incorporates a sensing element specific to the reagent or biomolecule being measured to ensure selectivity. As to how they transduce the sensed quantity into electrical signals, different approaches exist, namely electrochemical, optical, acoustic, thermometric, and magnetic [128, 129]. Large portion of the biosensors dedicated to management of blood glucose use electrochemical and optical transduction, as mentioned above. SRR variants have been used as alternatives to these.

This being said, measurand specific SRR based sensors were studied in the literature at a relatively limited scale [43, 121, 126, 133], where sensors committed to biosensing of glucose were even less visible. Biosensing schemes often require functionalization of the sensor surface, which significantly increases fabrication cost and adds further complexity to the system, hindering faster development of SRR based biosensing applications. To address this need, a SRR based biosensor incorporating glucose specific enzyme GOx for detection of glucose was developed.

4.1. SRR and Setup Design

Standard single loop SRR shape was continued to be used in this work. Design in this work was fabricated through a process similar to the one described in the previous chapter, with dimensions given in Section 3.4.2. A different approach was followed as part of the development of the reservoir. A masking layer made of polymer layers of 2.6 mm thickness was cut in the shape of the resonator with a CO_2 laser

cutter (Versa Laser VL-200). This mask layer was then fixed on the SRR substrate surface via an adhesive in a way that the cut out region exposes the conductor part of the SRR. Conductive polymer poly(3,4-ethylenedioxythiophene) polystyrene sulfonate (PEDOT:PSS) (Sigma-Aldrich 1.3 wt% in water) of 30 μL was applied in this reservoir after its activation. The decision that the liquid reservoir should utilize the conductor shape instead of the gap region is based on the fact that PEDOT:PSS is a conductive polymer and its presence in the gap region could destroy the resonance behavior at the designed frequency. This was a possibility since multiple application of liquids and cleaning could potentially destroy the parlyene coating on the surface.

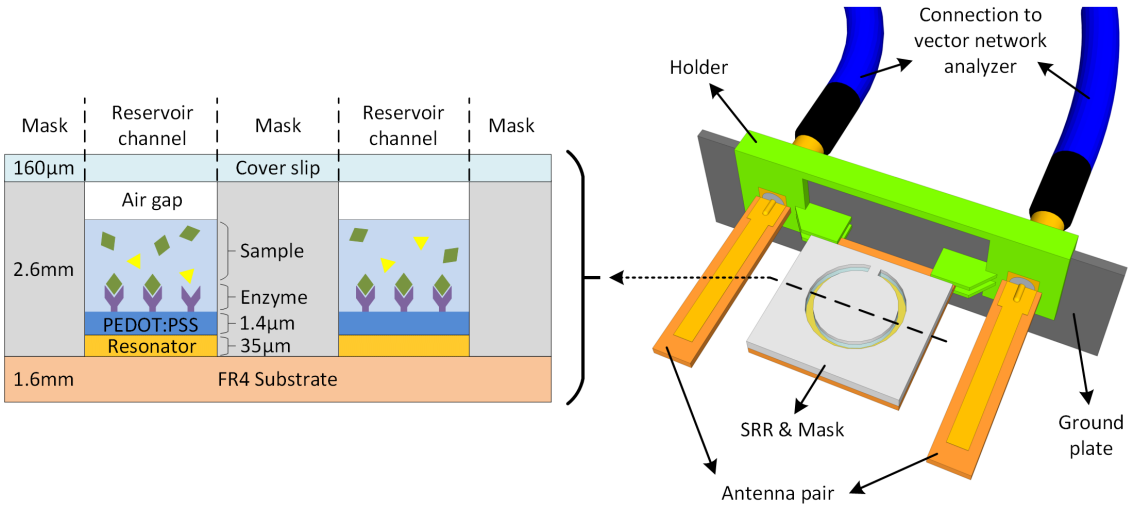

Figure 4.1. Cross-section of the SRR biosensor layers (left) and schematic representation the measurement system (right), from [203].

The enzyme GOx (Sigma-Aldrich, 50KU, type X-S from aspergillus niger) was to be immobilized within the matrix formed by the polymer placed in the reservoir. Prior to immobilization, the GOx was prepared in a buffer solution so that 15 mg of the enzyme product was dissolved in 25 ml of 0.1 M phosphate buffer of pH 6.5 containing 1.5 mM ethylenediaminetetraacetic acid as antimicrobial agent and 10 %w/v glycerol as stabilizer. 50 μL of this solution was then added to the PEDOT:PSS fixed reservoir. A cover slip was incorporated to seal the reservoir channel after addition of liquid samples to minimize reading interference that can occur due to liquid evaporation and contamination. Some air was left above the liquid sample to act as oxygen supplies.

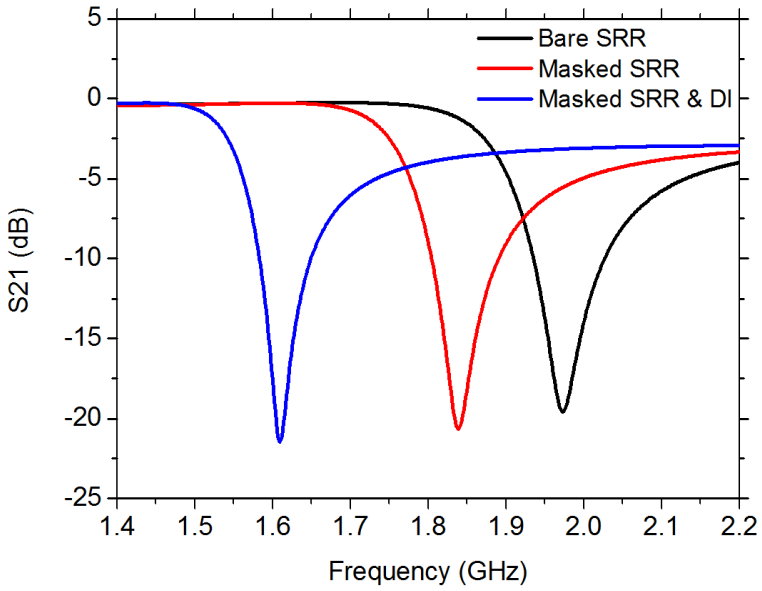

Figure 4.2. Transmission characteristics of the bare sensor, masked sensor, and the masked sensor with DI water loading as simulated, from [203].

Excitation of the the SRR and construction of the measurement setup was done in the same way explained in Section 3.3. Schematic representation of the setup and a cross-section showing the layers of the sensor structure are shown in Figure 4.1. Temperature changes were mollified with thermoelectric couplers (TEC1-12705) placed on the backside of the ground plane. These were controlled by a temperature controller device (Thor Labs TED 200C).

4.2. Experimental Results

4.2.1. Simulations

Resonance characteristics of bare sensor, masked sensor and masked sensor loaded with DI water in the reservoir was simulated in CST Microwave Studio. Figure 4.2 shows the results. Results suggest f_0 would appear at 1.97 GHz for the bare resonator. With the addition of the mask and application of DI water, the f_0 would shift to 1.84 GHz and to 1.61 GHz, respectively. This is something to be expected, since each addition is a further increase in dielectric permittivity.

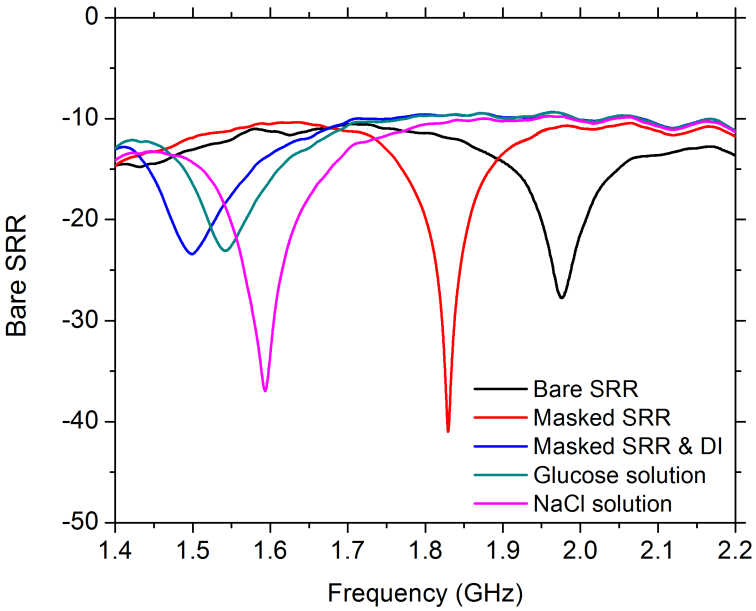

Figure 4.3. Measured transmission spectra for bare sensor, masked sensor, DI water loaded sensor, 0.33 M glucose solution loaded sensor, and 1 M NaCl solution loaded sensor, from [203].

4.2.2. Measurements

4.2.2.1. Basic Dielectric Loading. Experimental results obtained due to subsequent dielectric loading are presented at the first stage. Observed transmission parameters for the cases with bare sensor, masked sensor, DI water loaded sensor, glucose solution (0.33 M) loaded sensor, and NaCl solution loaded sensor (1 M) are presented in Figure 4.3. All liquid samples have a volume of 90 μL. Measured f_0 values are close to their simulated values. Obtained error rates for the bare sensor, masked sensor, and DI water loaded sensor are 0.1 %, 0.5 %, and 7.3 %, respectively. Experimentally obtained f_0 positions of DI water loaded sensor, glucose loaded sensor, and NaCl loaded sensor seem to agree with the literature. This is based on the ε_r values for the solutions at these concentration levels, which are 77.9, 75, and 68, respectively [204–206].

4.2.2.2. Sensor Response to Glucose Solutions - Without Enzyme. As the next step glucose solutions at different concentration levels were applied to the sensor prior to enzyme incorporation to the sensor. Following each measurement, sensor surface was carefully cleaned with DI water and dried afterwards. Sensor response in terms of

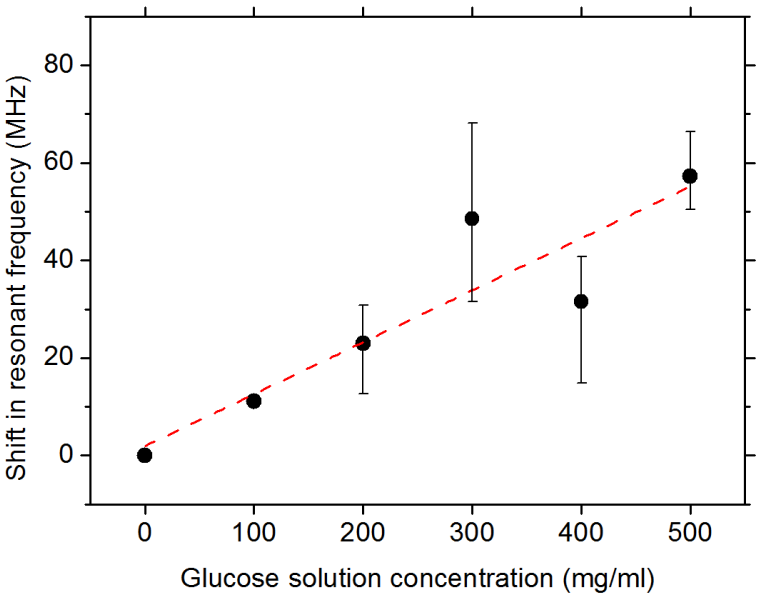

Figure 4.4. Relative shift observed in f_0 1.5 minutes following the introduction of glucose solution in the sensor reservoir. Three measurements per concentration level were made and averages are plotted, along with the minimum-maximum error bars, from [203].

shifts in f_0 with respect to concentration levels were plotted in Figure 4.4. Averages of three measurements per concentration level are reported. Tendency is a shift to higher frequency levels with increased concentrations of glucose in solution. Trendline fit to data is shown as a dashed line ($R^2 = 0.79$) forming basis for sensor sensitivity. Equation describing this line is given as:

$$y = 0.107\,x + 1.927 \tag{4.1}$$

which implies that the sensitivity for this experiment was 0.107 MHz/mg mL^{-1}.

4.2.2.3. Sensor Response to Glucose, and Control - With Enzyme. Aqueous solutions of different reagents, namely glucose (25 mg mL^{-1}), fructose (40 mg mL^{-1}), sucrose (80 mg mL^{-1}) and NaCl (25 mg mL^{-1}) solutions were applied to the sensor incorporating enzyme to demonstrate sensor specificity. Change in f_0 was observed in continuous time for a time interval of 25 minutes. The results are shown in Figure 4.5. In order to compare responses better, relative shifts with respect to initial value were presented

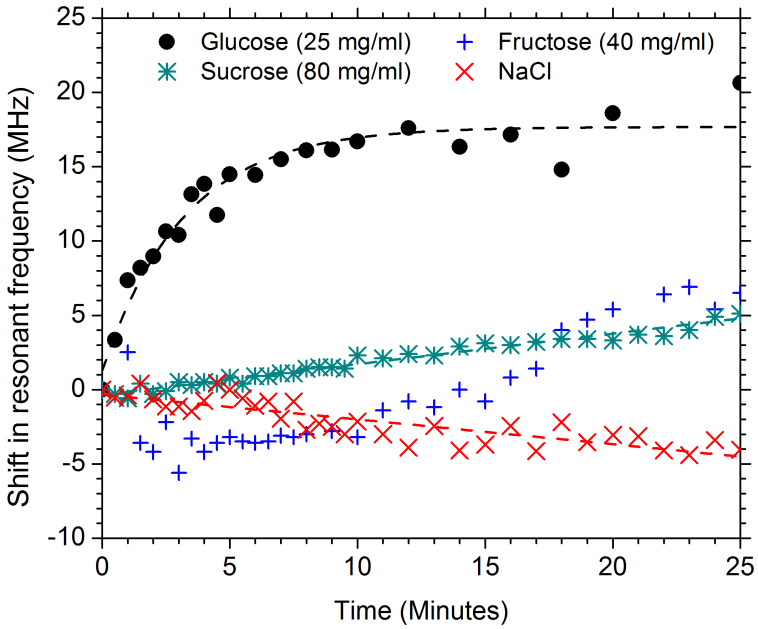

Figure 4.5. Change of f_0 values relative to their initial values for aqueous solutions of glucose, fructose, sucrose, and NaCl solutions as measured by the sensor incorporating GOx within 25 minutes, from [203].

for better comparison.

Dashed lines show exponential or linear fits to f_0 change behavior in time and have $R^2 = 0.93$, $R^2 = 0.71$, and $R^2 = 0.98$ for glucose, NaCl, and sucrose solution cases, respectively. Behavior associated with the glucose solution fits to an exponential, whereas the other two are linear fits. Saturating behavior of the exponential is expected from an enzymatic reaction coming into a balance, since the enzyme activity decreases with a decrease in concentration of the target analyte. This exponential fit to glucose is in agreement with the relationship modeling the concentration change of a substance in a first order chemical reaction over time as shown as follows [207]:

$$\Delta f_0(t) = f_0(0)\left(1 - e^{-kt}\right) = S\,[G](0)\left(1 - e^{-kt}\right) \tag{4.2}$$

where $f_0(\tau)$ is the time dependent function of f_0, S is the sensitivity constant relating the glucose concentration to f_0 (being equal to 0.107 MHz/mg mL^{-1} for this sensor as calculated above), $[G](\tau)$ is the time dependent function of glucose concentration, and

k denotes the reaction constant. It is important to note that fructose, sucrose, and NaCl solutions do not follow a similar response, demonstrating changes that are rather small, compared to the glucose solution. Looking at the graph, 15 minutes after the sample application, absolute f_0 shift responses of the sensor to glucose, sucrose, NaCl, and fructose solutions are 17.5 MHz, 3.1 MHz, 2.5 MHz, and 0.8 MHz, respectively. In other words, the response to glucose solution is more than 5 times that of the closest control reagent. This implies a high selectivity in favor of the target substance that is glucose, owing to the incorporation of the biospecific element.

4.3. Chapter Conclusion

A biosensor system specific to glucose using SRR based transducing was demonstrated. SRR used in the sensing system is the basic single loop SRR. Resonator was initially designed using the analytical model presented in Section 2.2. Methods demonstrated in Chapter 3 were applied in the whole process. Design improvement and and modeling of certain measurement conditions were performed with different SRR variant geometries were performed via FEA. Cost-effective fabrication methods were employed and measurements were performed with a setup of low complexity. Operation of the fabricated sensor was in good agreement with the simulation results, with the highest error rate being 7.3 %, and theoretical expectations.

Sensing capability of the sensor system was demonstrated with liquid samples of different electrical characteristics. Following incorporation of the GOx enzyme, measurements done with glucose solutions of different concentrations yielded a glucose sensitivity level at 0.107 MHz/mg mL^{-1}. Specificity of the sensor was demonstrated via its interaction with other analytes. Results of this work, which were published in [203, 208], demonstrate the potential of SRR structures in target-specific sensing of glucose, even when it is part of a rather simple system. However, there was room for improvement on certain aspects of the system.

Measurement with SRRs are prone to fluctuations in the change of physical characteristics of the medium. This can be alleviated by adoption of a double measurement

scheme. Using an additional resonator as a reference, it will be possible to track the signal component caused by background variations, which can then be subtracted from the total signal. Additionally, presence of a ground plane perpendicular to the orientation of the sensor and antennas makes the system bulkier. A planar arrangement would increase the applicability of the sensor system. It is also desired to use a scheme that employs the SRR gap region for increased sensitivity and a more sophisticated way of containing liquid samples for increased precision and repeatability.

5. FURTHER IMPROVEMENTS TO ORIGINAL DESIGN

Motivated by the conclusions drawn from the exploratory work and the initial biosensor design, ways to improve and modify the system were studied subsequently.

5.1. Differential Measurement

One of the most prominent challenges faced by SRR senors is their susceptibility to interference caused by external changes, such as temperature and humidity fluctuations, and changing proximity to objects and persons. To suppress the effects of external interference such as these, it is possible to model the SRR output changes related to physical effects. As an example, to address the effect of temperature on SRR readings, a temperature correction function was derived and applied in the analysis of results from constant temperature and time varying temperature cases in [209]. Following this approach of course means an additional calibration step is needed after every new sensor and system design. Moreover, such a calibration study should be performed for every physical quantity interfering with sensor operation.

Another idea as an alternative to suppress signals related to external interference is to use not one, but two sensors. This pair would be following a differential measurement approach, inspired by the differential amplifier used in electronic systems [210]. In a possible application of this approach, two sensors exist where one of the would be loaded with the sample under test, whereas the other would not, acting as a reference sensing the signals arising from background changes. The sensed quantity would be the difference between the shifts of resonance frequencies from both sensor. Even though this approach increases the sensor complexity, the advantages it provides can outweigh its cost. At the time of the publication of the glucose biosensor presented in Chapter 4 [203], examples dedicated to differential measurement with SRRs were present in a limited corpus. In [211], a skin contact based glucose sensor is built comprising of two SRRs designed at slightly different frequencies of 1.74 GHz vs. 1.50 GHz. The sensors are stacked on top of each other and read by the same two ports

with slightly different frequencies measured via multiplexing. The lower SRR, being close to skin performs the measurement of glucose levels, while the upper one, being desensitized to the measurand due to its location, responds to changes in temperature only. Approach presented here proved to be highly effective in realization of a skin-contact based glucose sensor system.

In this section, it is aimed to propose an improvement to measurement precision using two SRRs in a differential measurement scheme. Effectively, this becomes a problem of arranging different sensors effectively and efficiently within the same space, belonging to the same measurement system.

5.1.1. Simulations of Differential Measurement Alternatives

For the simulations, it was decided to use resonators that have slightly different resonance frequencies, as was the case for [211]. SSRR type sensors were used in simulations, where their gap regions were loaded with semi-spherical dielectric loads, as done in Section 3.1.1. Once again, different electric permittivities were assigned to these dielectric loads. Specifically, one of the resonators was loaded with a dielectric of ε_r of 80, whereas the other resonator was loaded with only a slightly higher ε_r, the maximum being 90. This is done as such since the electric permittivity of liquid solutions tend not to be very different than that of the pure water. Excitation was done with monopoole or dipole antenna pairs for different cases. Directions mentioned in the following Subsections are based on the following definitions:

(i) x axis is the direction in which electromagnetic transmission between two antennas occurs.
(ii) y axis is in plane with the antennas, but is perpendicular to x axis.
(iii) z axis is perpendicular to the antenna and resonator planes.

5.1.1.1. Stacking Resonators in x Axis. In this approach, two resonators are placed one after the other in x direction, in simulation environment. In other words, both

resonators are between an antenna pair coupled to each other. This scheme causes an increase in antenna separation. Monopole antennas are used in signal excitation since they tolerate antenna separation better based on previous simulations. Simulated model and the results are shown in Figure 5.1. The response to the said resonator types to differential dielectric loads are shown in Figures 5.1. S_{21} magnitude plot shows two resonance dips associated with two resonators of different f_0 values. Changing dielectric load of only one resonator does not affect the resonance characteristics of the other. Their f_0 difference has a sensitivity to dielectric changes of 5.1 MHz.

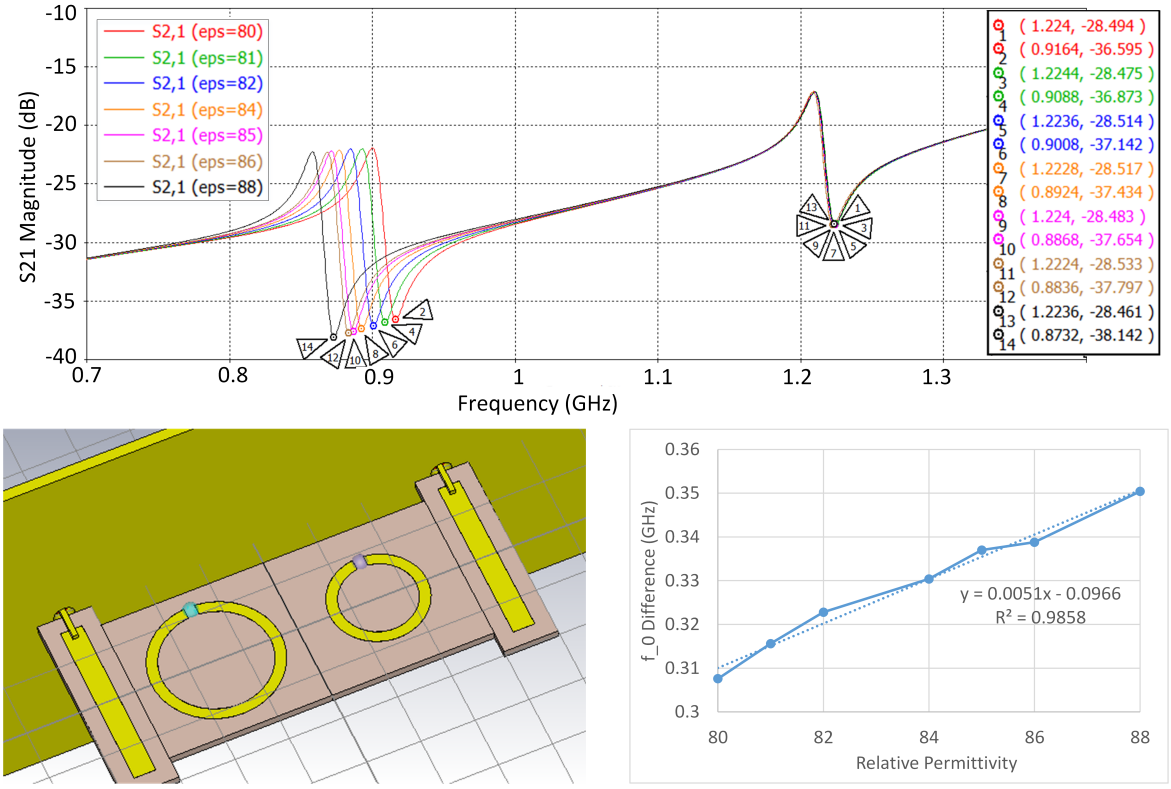

Figure 5.1. S_{21} magnitude vs. frequency of double SSRRs stacked in x direction (top), its simulation model (bottom let), and difference of f_0 of both SSRRs at different load permittivites (bottom right).

5.1.1.2. Stacking Resonators in y Axis. Here, two resonators are be placed so that their substrates make contact in the y direction. Different from the previous case, this does not affect the antenna separation. Dipole and monopole antennas may both be utilized for such a configuration, However, the former would be more advantageous, since it would be possible to drive the resonators in a truly symmetrical fashion.

Stacking two SSRRs in y direction in a monopole antenna excitation scenario will cause one of them to be placed further away from the ground plane, disrupting symmetry. Dipole antenna excitation of a SSRR pair and results of this arrangement are presented in Figure 5.2. In this arrangement, we see that f_0 of the reference resonator (the one with static dielectric loading) is affected by the change in the the electric permittivity of the other dielectric loading. This shows that the resonators are coupled too closely to each other to interfere with each other's readings. Even though this is an undesirable outcome, it is still possible to perform a differential measurement based on the outputs of both resonator pairs.

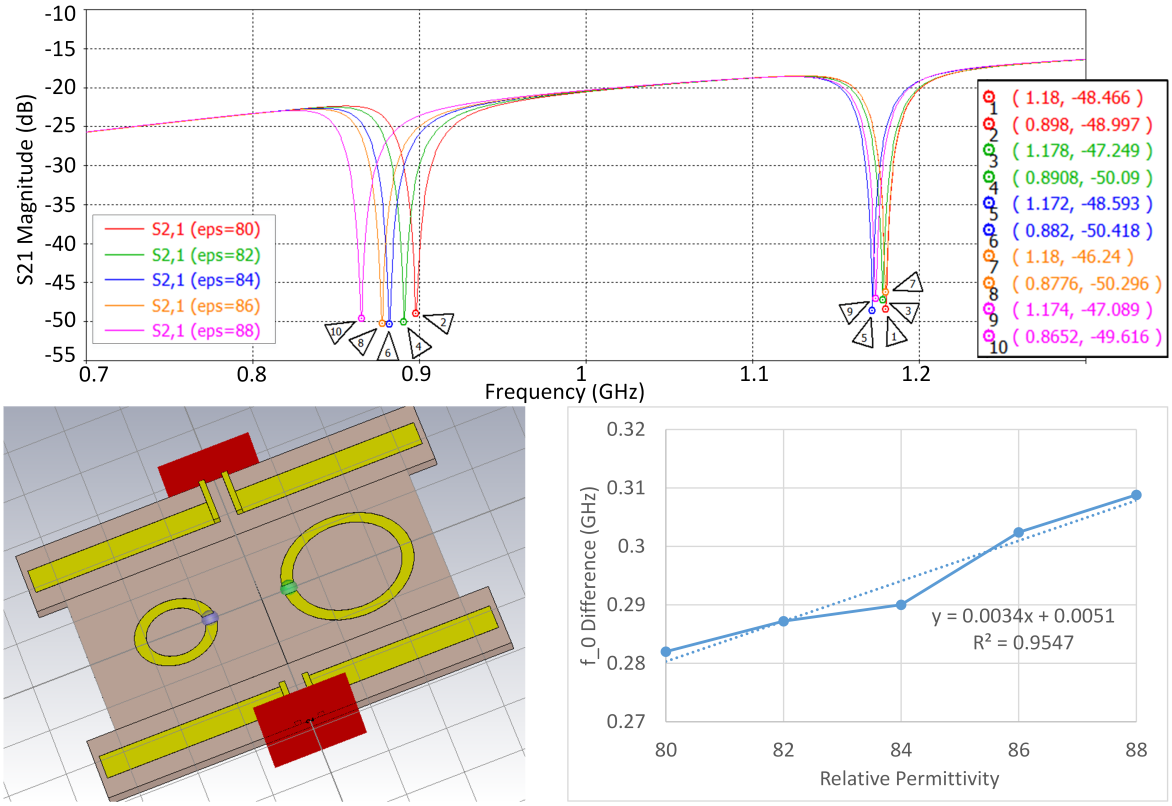

Figure 5.2. S_{21} magnitude vs. frequency of double SSRRs stacked in y direction (top), its simulation model (bottom let), and difference of f_0 of both SSRRs at different load permittivites (bottom right).

5.1.1.3. Stacking Resonators in z Axis. The third possible way to arrange two resonators in a measurement scheme is when they are placed on top of each other, separated by a substrate. This scheme can again be excited efficiently with monopole antennas. This provides the most compact differential measurement setup. Simula-

tion results and the relevant model are shown in 5.3 where the substrate separating both resonators were hidden from the view for clarity. Differential measurement performance is not satisfactory, since the difference of resonator outputs remained stationary for small changes in ε_r. This indicates that there is even higher coupling present between dielectric loads of opposite resonators, rendering the scheme useless.

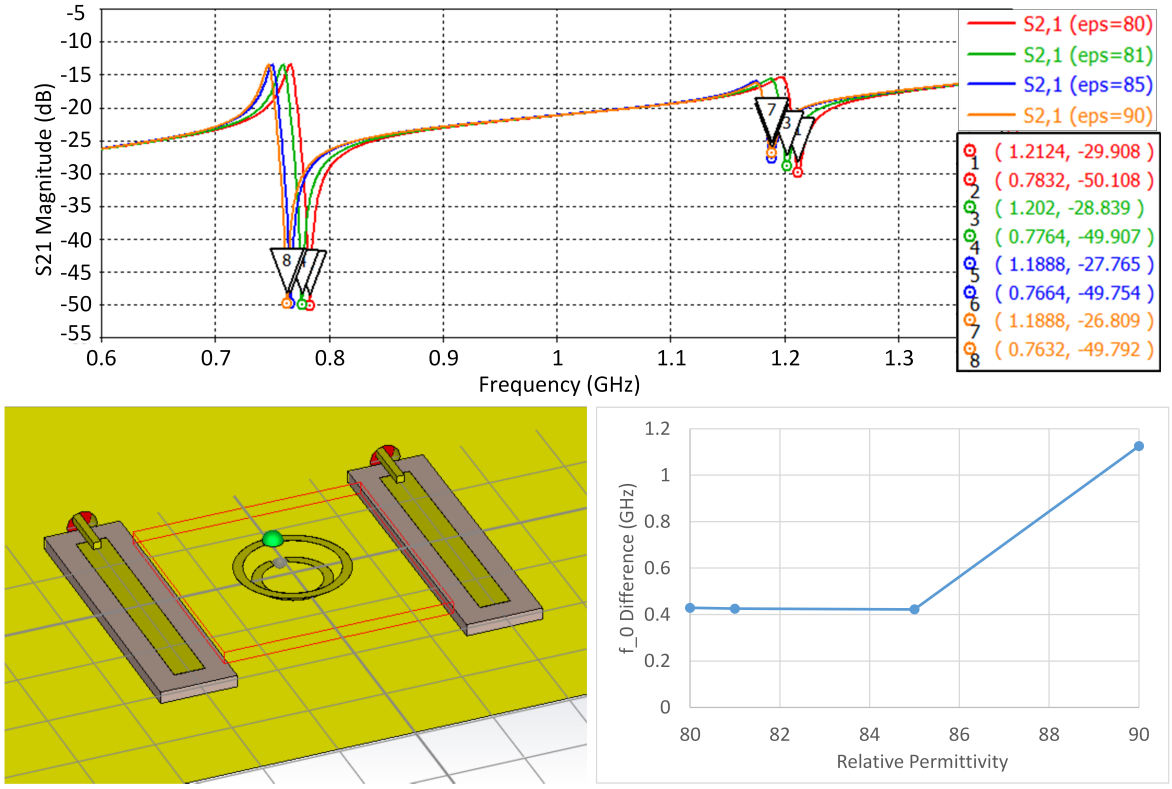

Figure 5.3. S_{21} magnitude vs. frequency of double SSRRs stacked in Z direction (top), its simulation model (bottom let), and difference of f_0 of both SSRRs at different load permittivites (bottom right).

5.1.2. Implementation, Measurement, and Results

Simulation results obtained in the previous section suggests that transmission measurement based differential measurement approaches are better suited to stacking resonators in x direction. This can be done via excitation the resonators with a pair of monopole antennas, as mentioned above. It should be noted that this requires an increase in separation between the antennas, requiring an alteration in the current measurement setup.

Standardizing maximum sizes associated with substrates on which antenna strips and resonators are patterned, which are 30 mm × 30 mm and 40 mm × 4 mm, respectively, it is possible to design a versatile setup platform. Incorporation of a holder is desirable, since SRR based sensing is often affected by displacements. That is why a planar structure allowing application of various differential measurement approaches and steady placement of resonator and antenna structures were designed. Drawn pieces of the holder and an example of use with a monopole antenna pair is shown in Figure 5.4.

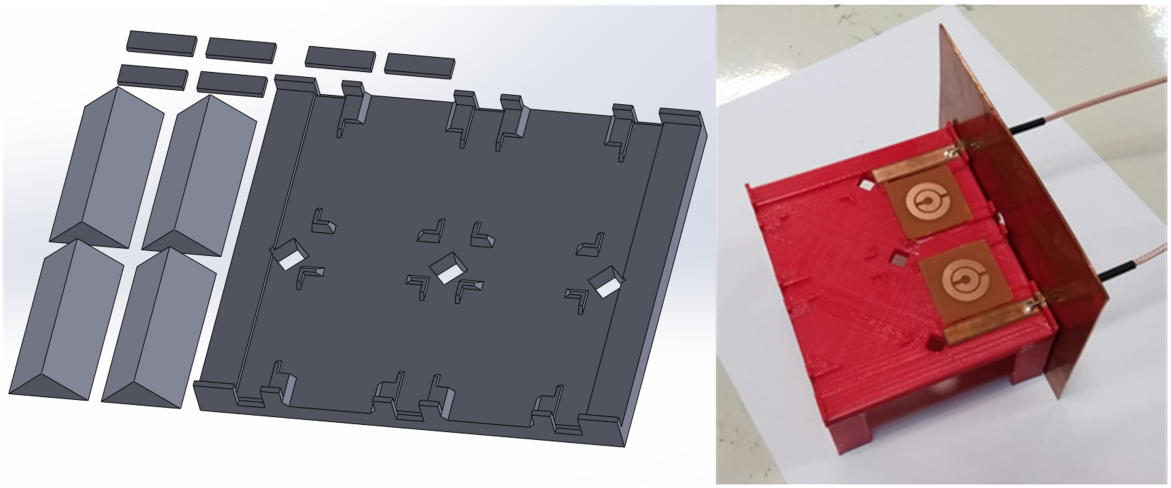

Figure 5.4. Computer aided design of the holder structure (left) and its use after fabrication with a pair of monopole antennas (right).

A new set of resonators in accordance with the dimensional limits were designed to be used in the measurements with simulated resonant frequencies at 2 GHz. The designs were fabricated on 0.035 mm copper coated FR4 structures of 1.6 mm thickness with acid etching PCB fabrication procedure. The resonators were fabricated mostly in identical pairs, even though the simulations were done with resonators with slight f_0 discrepancies. This decision was made based on the fact that even if the differences between two resonators would be minor, their responses to changes in physical quantities would be different. This in turn would decrease the effectiveness of the differential measurement. Following the fabrication of the resonators, reservoirs cut from acrylate blocks with laser cutters were placed in their gap regions and were fixed with commercial adhesives. Care was taken to ensure that identical resonator pairs were loaded with the reservoir in an identical manner.

Glucose solutions of different concentrations were added to the reservoir via a micropipette, without using enzymes. Using identical resonators in these schemes have the disadvantage that when the resonance dips on the S_{21} are too close to each other, they collapse into one resonance dip that is not easily resolvable into two different signals. To be able to track signals separately, the measurement was done so that the measuring resonator was loaded with the solution, while the reference resonator was kept unloaded. Different ways of implementing differential measurement approaches were experimentally tried. These are presented in below:

5.1.2.1. Stacking in x Direction. This approach is one of the ones tried in simulation environment. Two identical resonators were placed side by side between two monopole antennas. This configuration has reduced complexity, but may sacrifice slightly from symmetry since transmission occurs from one antenna to the other, and the resonator distances from transmitting and receiving antennas are different. Tracking is done via measurement of S_{21} parameters, which are loaded by two different resonators. The measurement setup is shown in Figure 5.5 along with the measurement results. The linear fit to absolute differences between the f_0s of both resonators had $R^2 = 0.86$. Increased distance of antennas themselves and the distance between antennas and resonators may potentially reduce sensor performance in such a scheme.

5.1.2.2. Stacking in y Direction. This is the second approach that was tested in the simulation environment. Here, the resonators are placed back to back and are excited by a pair of dipole antennas. It was desired to keep resonators slightly apart to reduce the effect of cross-coupling. Therefore, a different holder structure was used for this part. Measurement setup and results are shown in Figure 5.6. Results indicate that cross-coupling is still an issue, as the resonance frequency of the reference resonator seemed to have shifted by a significant factor during the measurement. It should be noted that the actual sensitivity is even lower for data points related to non-zero concentration values. Moreover, the difference data had very low linearity with the trendline fit resulting in $R^2 = 0.67$.

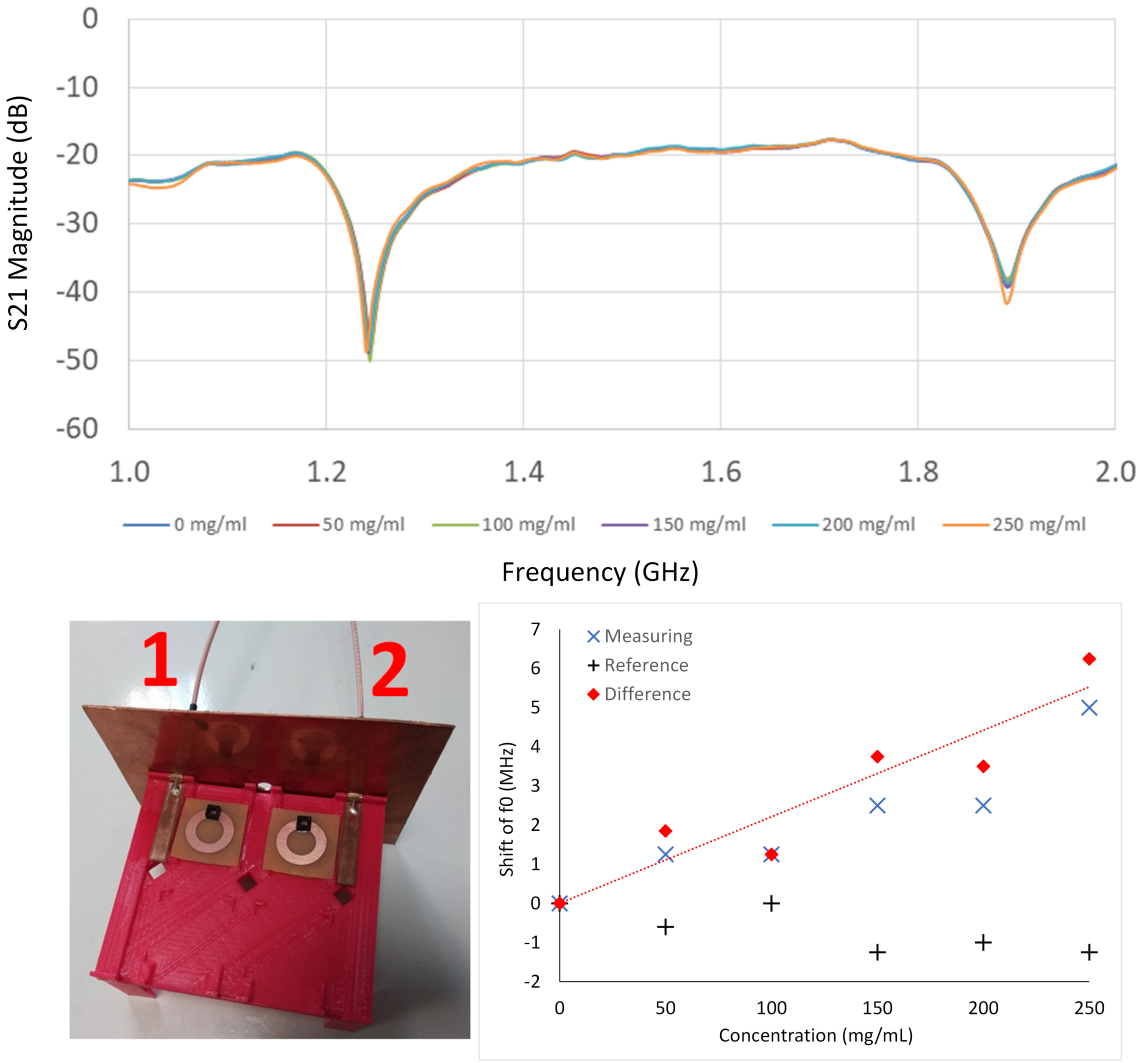

Figure 5.5. S_{21} magnitude for differential measurement via stacking resonators in x direction (top), its measurement setup (bottom left), and sensitivity of the system to glucose solution changes (bottom right).

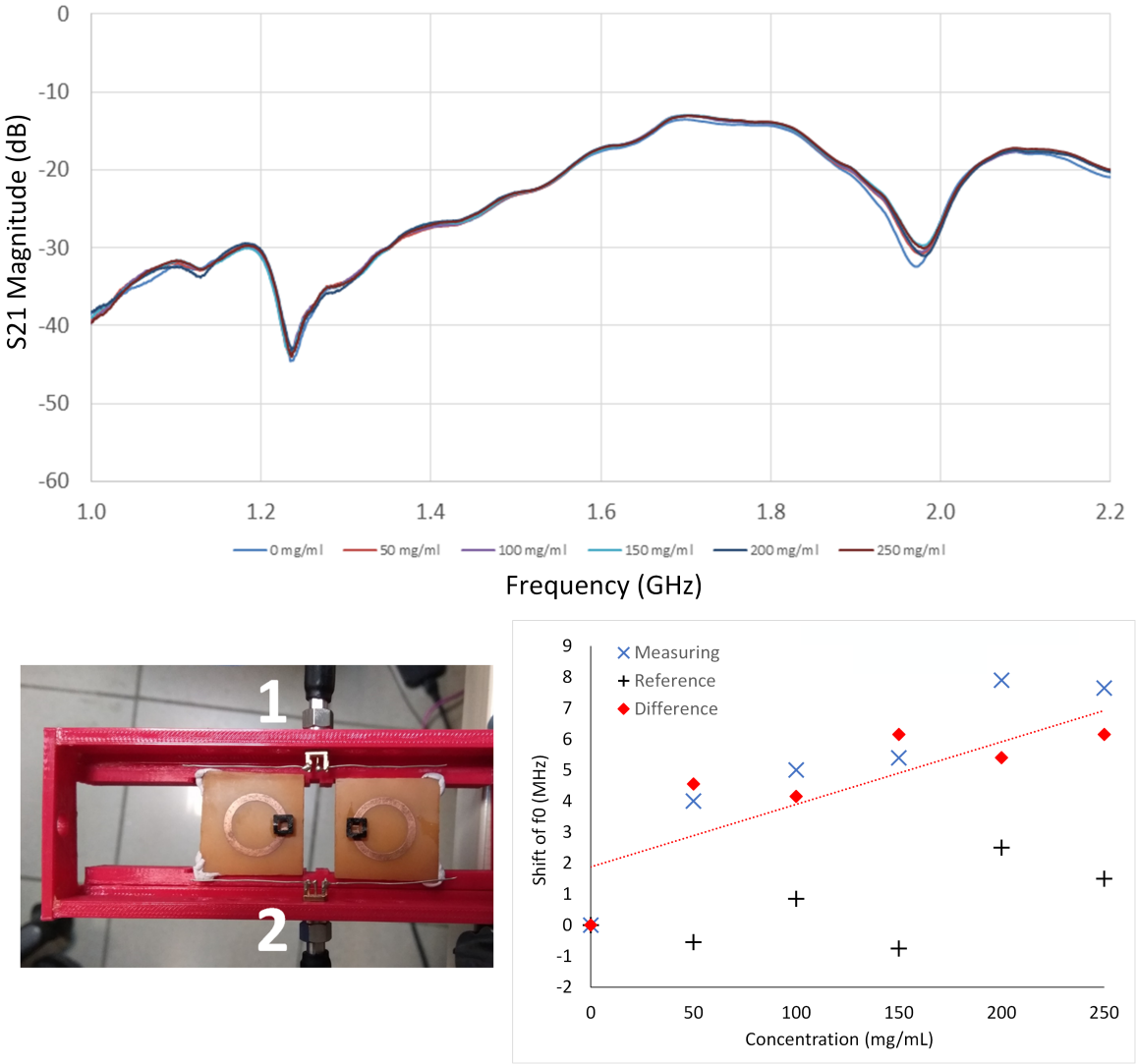

Figure 5.6. S_{21} magnitude for differential measurement via stacking resonators in y direction (top), its measurement setup (bottom left), and sensitivity of the system to glucose solution changes (bottom right).

5.1.2.3. Splitting Both Ports. This is a step away from the simulated cases in an attempt to try a new approach. Seeing that cross-coupling and increasing antenna distances have affects on differential measurement, it is aimed to isolate the resonators and measurements from each other. Two identical setups implemented on two identical holders were used for this configuration. Setups were placed in significant distance from each other. To maintain the ability to measure signals from both resonators simultaneously with a single VNA having two ports, signals had to be split and combined, since we need four ports to measure two S_{21} from two resonators.

In order to do this, radio frequency splitter/combiner tools were used. The transmitting port of the network analyzer was split into two paths with an RF splitter/combiner (Mini Circuits ZFSC-2-372-S+, rated bandwidth at 3.7 GHz) and the receiving ports are combined with a rat race coupler rated at 11 GHz. Measurement results are presented in Figure 5.7. Resonators being off-frequency from the rated values and also imperfect efficiency of the introduced RF elements caused losses, resulting in low Qs associated with the measuring resonator. Despite this, it is seen that reading linearity is still low, with trendline fit having $R^2 = 0.77$. Use of couplers specifically designed for this setup may increase this performance further.

5.1.2.4. Splitting the Transmission Port. This is a hybrid approach, where only one port of the VNA is split into two paths with the RF splitter/combiner used above. There is only one receiver port, common to both sensors. While there is still Q loss due to splitting of transmission path, this approach can reduce the complexity and setup size of the full split approach. Moreover it is possible to maintain simultaneous measurement capability and keep cross-coupling low. The measurement setup is presented in Figure 5.8.

Cross-coupling immunity and symmetry of operation can be tested with placing only one resonator at a time, and comparing the resonance characteristics with the case where both resonators are present. As shown in Figure 5.9, having only one resonator (denoted as resonator A and B) in place and having both resonators present

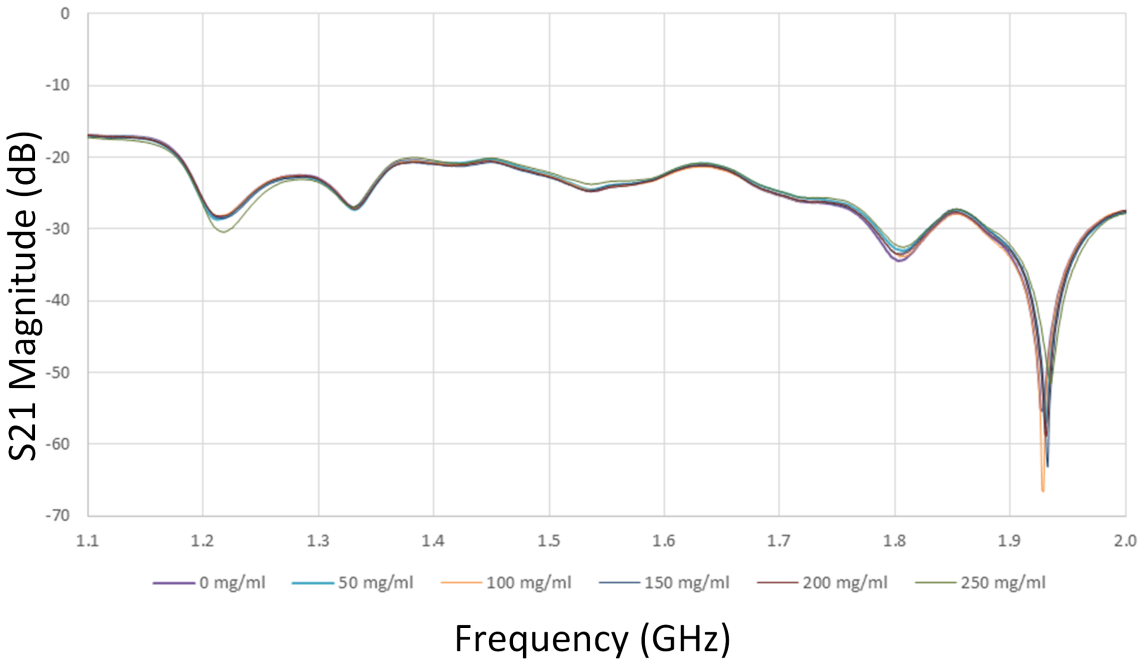

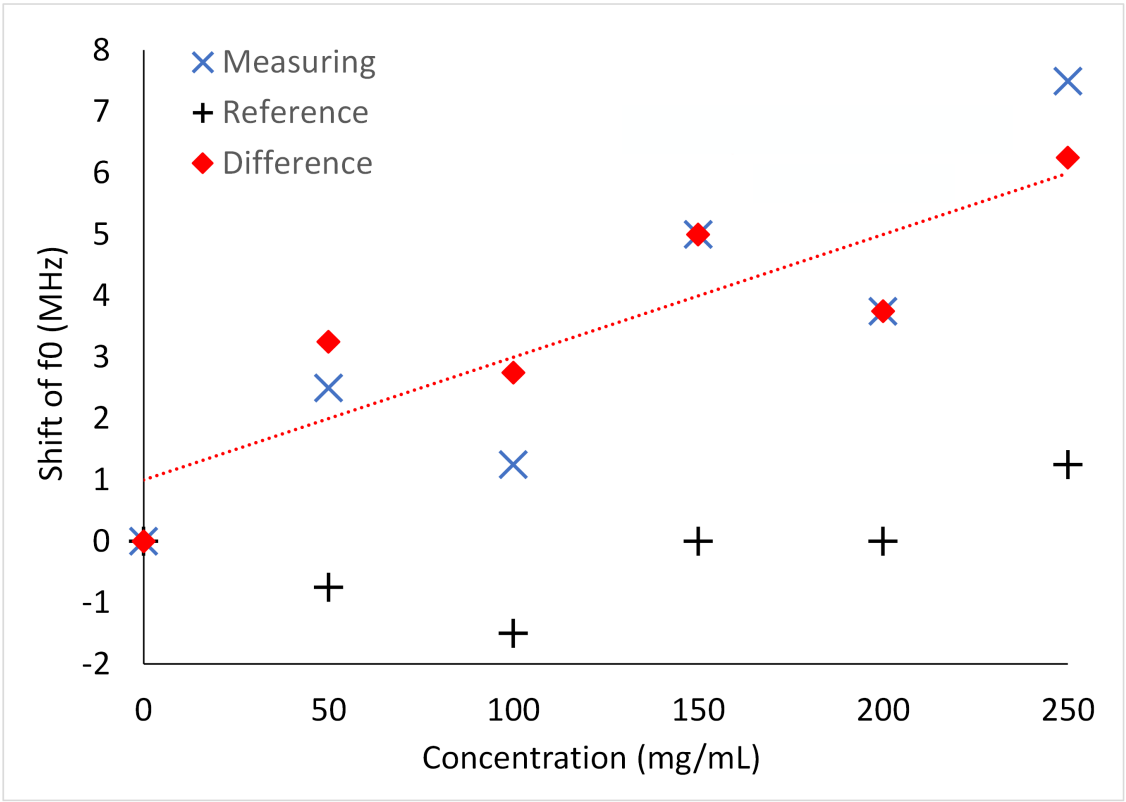

Figure 5.7. S_{21} magnitude for differential measurement via full isolation (top) and sensitivity of the system to glucose solution changes (bottom).

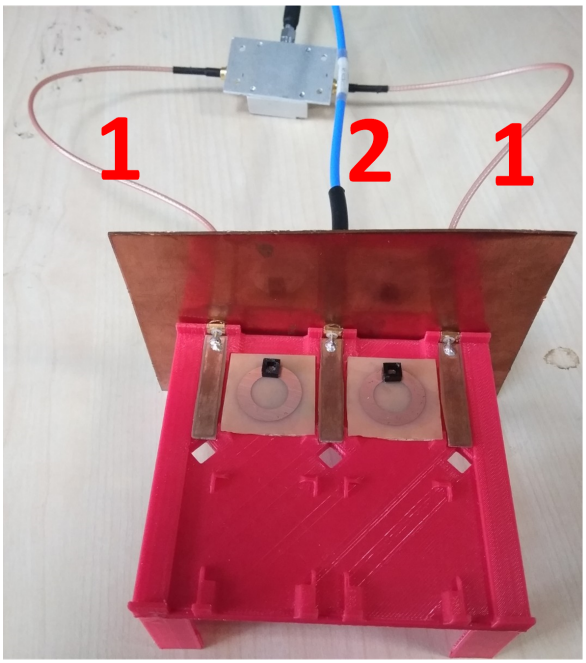

Figure 5.8. Setup for split transmission port differential measurement.

in setup creates a small difference of f_0. This can be in part related to measurement errors caused by reduced Q of the system. Swapping the places of the resonators do not cause a change in f_0, confirming system symmetry.

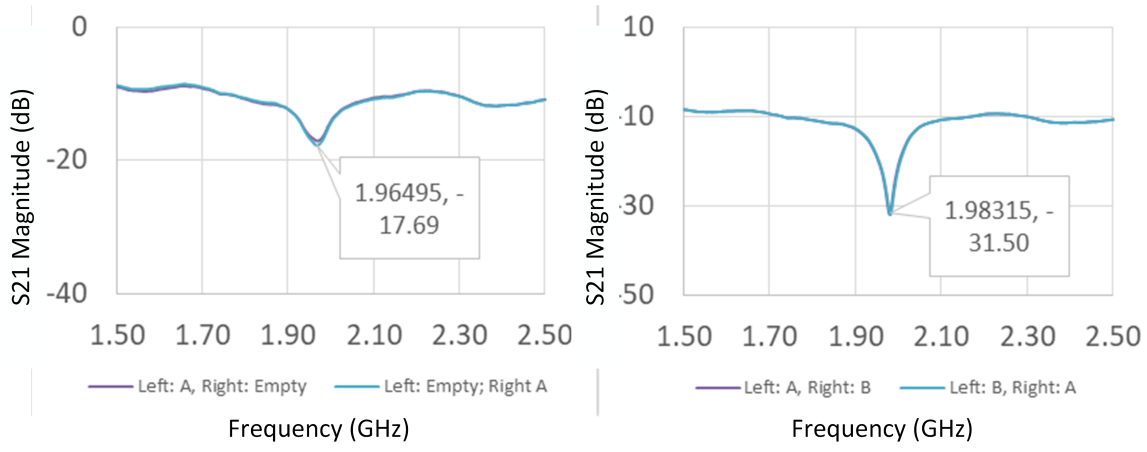

Figure 5.9. S_{21} spectra measured with split port differential measurement setup for a pair of identical resonators (denoted A and B) when only one resonator is present (left) and when both of them are present in both possible arrangements (right).

Following this step, instead of concentrated reservoirs placed on the gap, long, channel shaped reservoirs were cut from acrylate using the laser cutter. These were then fixed on the surface of a newly designed pair of resonators manually using com-

mercial adhesives. Resonant frequencies of structure pairs before and after the channel incorporation is given in Figure 5.10 [212]. It was seen that the channel addition lowers the f_0 by around 60 Mhz for each case while reducing the quality factor as well. Otherwise, resonance characteristics of individual resonators of the same pair are in good agreement with the highest error rate being 1.0 %.

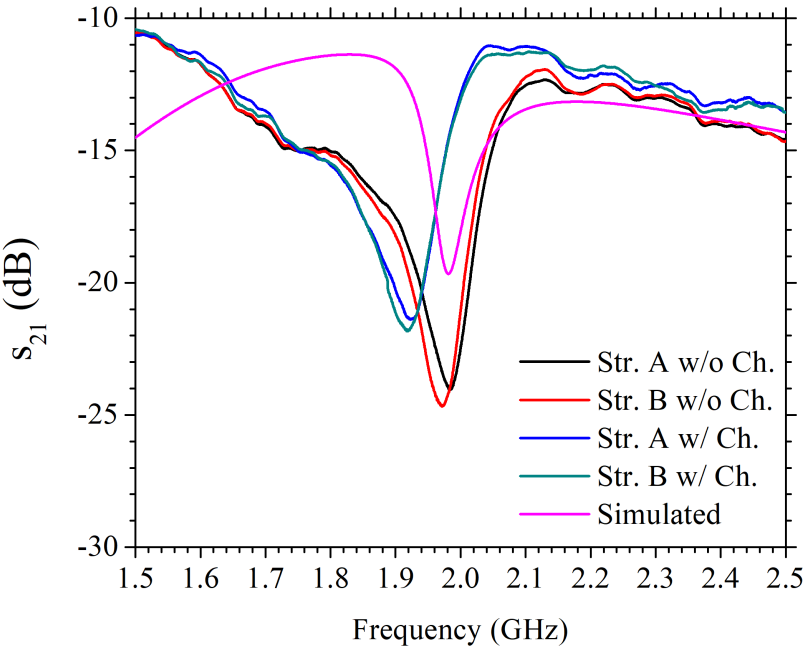

Figure 5.10. Resonant frequencies of bare resonators and resonators with long reservoirs used in the tests, from [212].

Basic sensitivity to dielectric loading is observed by applying DI water of different volumes to the channel of the measuring resonator. Similar to the examples above, the reference resonator was kept empty. The results are presented in Figure 5.11 [212]. It is interesting to note that when there is no loading, both resonators contribute to a higher Q factor, which is lowered by about 16 dB when both resonances are split. There is also a small difference between the f_0 values before and after splitting. Nevertheless, the characteristics of the reference resonator is not responding to the volumetric load change in the measuring resonator. Increased volume of dielectric loading is shifting the f_0 of the measuring resonator to lower frequencies, as expected.

Differential measurement of glucose concentration was performed with transmission splitting approach as well. The concentration range of the applied glucose was

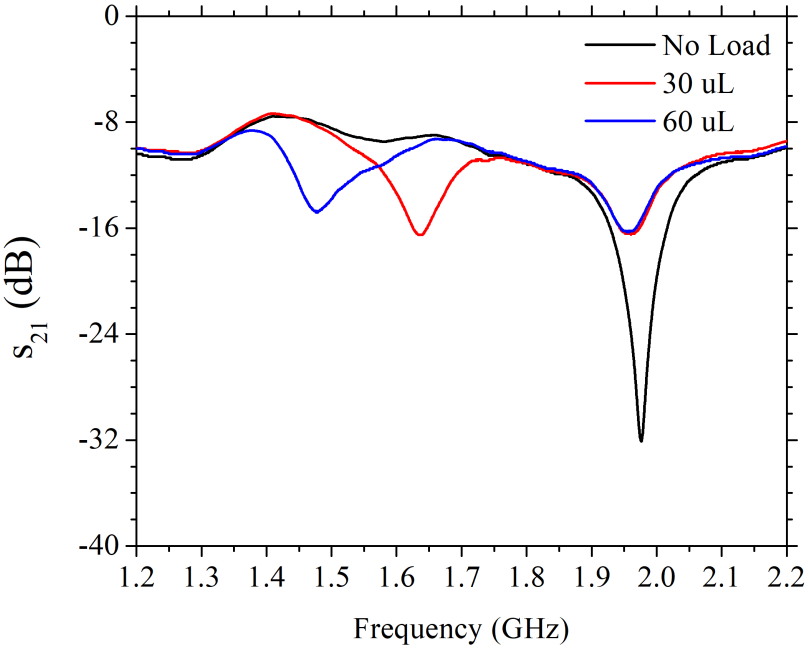

Figure 5.11. Shift of f_0 with DI water loading of different volumes, as presented in [212].

reduced to be limited by the pataphysiological levels. Solution was applied to measuring reservoir with a micropipette, while reference sensor was kept unloaded again. f_0 changes of both sensors and their absolute difference are presented in Figure 5.12 [212]. A correlation to shift in f_0 of the measuring sensor is visible. On the other hand, shift of f_0 of the reference resonator is more random and seemingly unaffected by changes in glucose concentration. A line fit to difference data, which is the actual sensor output, shows an increased linearity ($R^2 = 0.905$). Sensitivity derived from this system was 34.72 MHz/mg mL^{-1}.

5.1.3. Discussion on Differential Measurement Applications

It is seen that different approaches to differential measurement can be adopted with certain benefits. Transmission port splitting offers a compromise that addresses the aims of this measurement scheme well. The approach provides symmetry, simultaneous measurement and allows antenna transmission with reduced losses. The approach made it possible for the measurement of smaller changes in glucose concentrations in aqueous solutions with high sensitivity. This being said, the noisy nature of

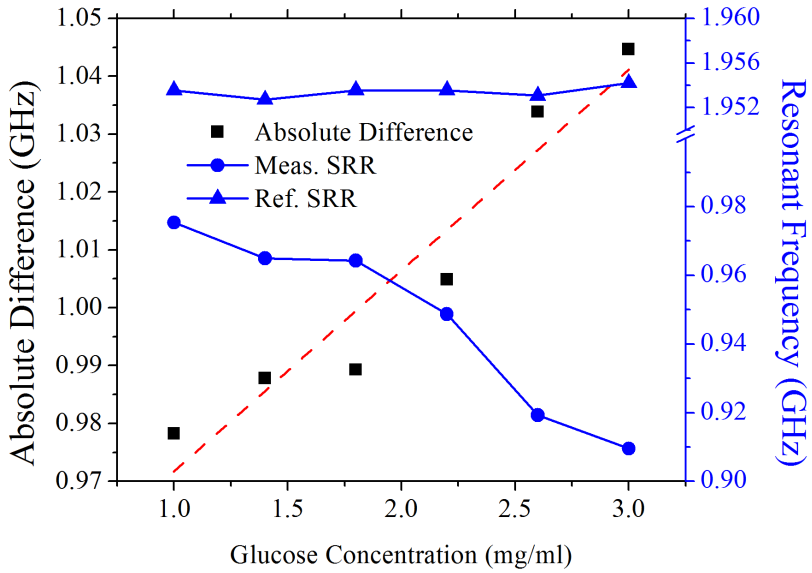

Figure 5.12. Split transmission port f_0 shifts for the reference and measuring resonators and their absolute differences as the sensor output, from [212].

transmission measurement can still sometimes pose problems. Moreover, necessity to include a ground plane while working with monopole antennas still causes an increase in system size. It is desirable to have a planar system at hand to fully exploit the compactness potential of the SRR structures.

Nevertheless, transmission port splitting approach demonstrated in this section was one of earlier cases of the use of differential measurement with SRRs to increase measurement repeatability and was published in [212]. Differential measurement propositions for planar and fully symmetric sensor systems were proposed at similar times and after. Rectangular SRRs coupled to a microstrip splitter/combiner configuration demonstrated in [213] for differential liquid characterization can be used for this purpose. It should be noted that the use of splitters can cause loss in coupling efficiency and reduced quality factors in responses of individual sensors. One way to address this issue is to use multiple identical SRR structures loading a single transmission line in a symmetrical manner as exemplified in [214]. Here, a pair of identical rectangular double SRR structures are loading a transmission line on its either sides, where one is acting as a reference and the other is performing the measurement. Even though the SRRs are more closely placed they still can perform in an uncoupled

manner. A way to increase measurement efficiency in an envisioned versatile sensor platform can be the incorporation of a multitude of resonators to a single measurement system to achieve multi-band measurement or to cover a wider range of the frequency spectrum, such as the ones described in [215, 216].

5.2. Loop Antennas and Reflection Measurement

Excitation of the resonators so far was done by the use of monopole antennas. As discussed above, these have the disadvantage of including a ground plane perpendicular to the resonator plane. For a truly planar measurement scheme, other excitation alternatives can be considered. Arguably the most promising one is the loop antenna. It has the advantages of being fully planar and size-effective. They dont require any ground planes or additional metallization and can be easily coupled to SRR structures, which are in essence loop structures themselves.

Using a loop antenna per resonator, it is possible to perform reflection measurements. In this scheme the SRR, absorbing the electromagnetic energy at its specific resonance frequency, will create a dip in the reflection (S_{11}) spectra of the antenna. Reflection measurements requiring a single port contributes to reduced size and cost-effectiveness. Moreover, reflection spectrum of an antenna tends to be significantly freer of noise. One potential interference could be the one occurring with the antenna's own resonance. However, designing an SRR at an f_0 remaining below the resonance of a loop antenna is trivial. A sample simulation case is presented in Figure 5.13, where dielectric load induced changes in resonance characteristics of an SRR placed at the center of a loop antenna is shown. According to the simulations, highest sensitivity to dielectric changes are obtained when the SSRR is located at the center and oriented so that its gap is turned away from the port of the loop antenna.

It is also quite convenient to perform differential measurements using a VNA with loop antennas since two ports of the VNA can simply be tracking two reflection spectra, namely S_{11} and S_{22}, from two separate antennas coupled to two separate resonators. A simple version of this is demonstrated in Figure 5.14. In this scheme, the antennas and

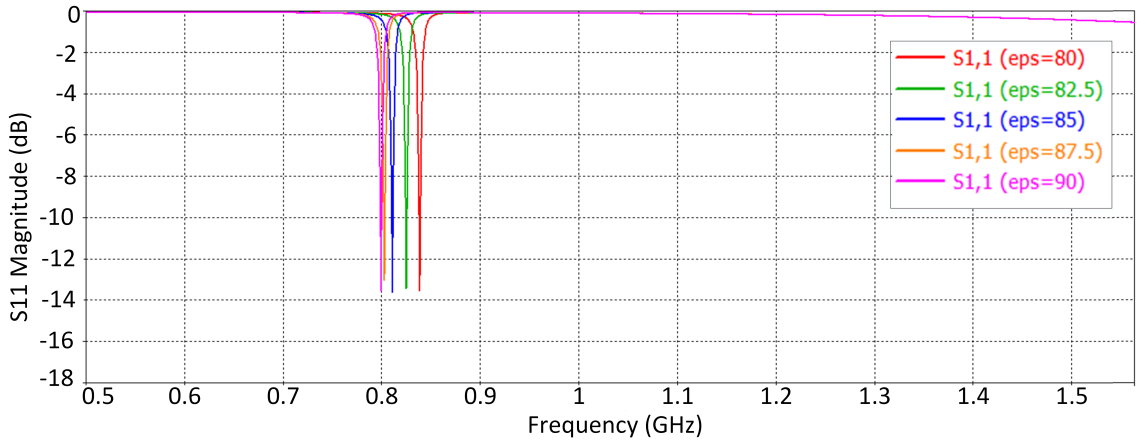

Figure 5.13. Simulated S_{11} spectra of an SRR with 2 GHz nominal f_0, loaded with different dielectric media, coupled to a 2.5 GHz loop antenna.

resonators can be placed at any distance without the concern of transmission power loss. With the advantages they present they are promising candidates to be applied in SRR based sensing platforms.

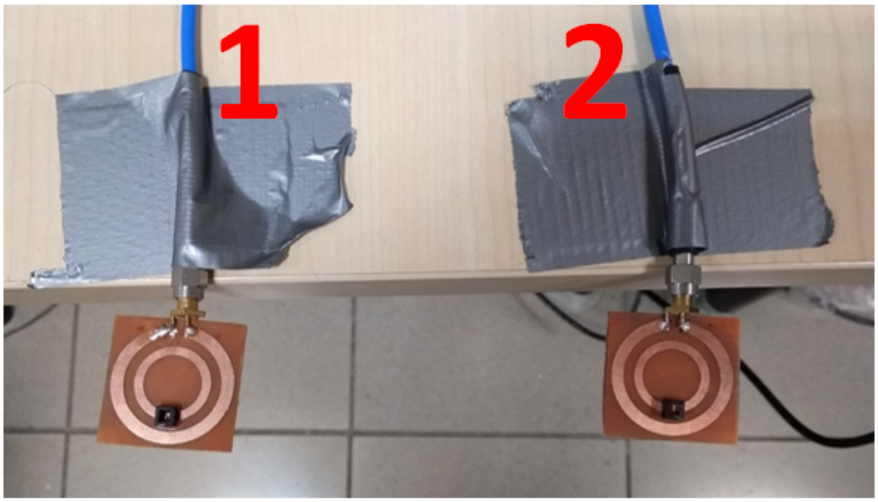

Figure 5.14. Measurement setup for the differential reflection measurement with loop antennas.

5.3. Incorporation of Microfluidics

Recently, considerable effort was devoted to the development of sensor systems incorporating microfluidic elements for a wide range of fields, including environmental analysis, food monitoring, security, forensics, and healthcare [217–223]. Healthcare

applications are particularly interesting since microfluidic lab-on-chip (LOC) platforms that can undertake basic diagnosis and detection of biomolecules have the potential to replace conventional laboratory-based systems. Such systems can be operated by the non-expert and can be easily distributed [224, 225]. Multiplexed microfluidic designs can handle sensing of various samples or analytes in short time [226]. They have the advantage of working with low amounts of sample volumes, while consuming low power [227]. All these make them promising for development of cost-effective and portable sensors, addressing to cases where access to conventional and costly sensing methods are rather limited.

Many of the microfluidic LOC sensors demonstrated in the literature have transducers relying on electrochemical, optical, or mechanical interactions [223, 225, 228–236]. Despite their effectiveness, these approaches can introduce certain restrictions to the system [237]. Conventional electrochemical and mechanical methods require contact with the sensors and thus are invasive [115,238]. In contrast, optical transduction is often costly and may require additional steps such as labeling, increasing complexity [106]. In this sense, systems using SRR sensors and microfluidic elements together are being studied in order to bring the best of both worlds together [1, 104, 105, 107]: SRRs can provide portable, noninvasive, and cost-effective transducer alternatives to microfluidics, whereas microfluidics can help solve the sample confinement issue to increase measurement linearity and repeatability. Even though bare SRR sensor designs may be sufficient for development of some skin contact based systems, SRR sensor systems relying on characterization of liquid samples are likely to integrate microfluidic elements on them because of this.

Motivated by this, studies where microchannels are integrated to SRR and microwave glucose sensors have been demonstrated in literature with microfluidic elements formed of polymethyl methacrylate or [239] polytetrafluoroethylene [178] tubes, and microfabricated PDMS microchannels [114, 200, 240, 241]. In terms of distribution of sample over the capacitive regions of the resonator, use of microfabricated channels provide an opportunity with CSRR sensors, since their shape can be manipulated to follow the slit in conductor comprising the complementary resonator as

applied in [240, 241]. SRR based glucose sensor systems developed for differential or multi-band measurement methods have also been incorporating microfluidic elements lately [209, 215, 242, 243].

This section describes the addition of microfluidic elements to the SRR sensor structure for the benefit of increased sensor performance.

5.3.1. Initial Fabrication and Measurements

As part of the initial experiments, some ready-made microchannel structures fabricated in the Department of Nanoscience and Nanoengineering of Istanbul Technical University were used. Microchannels were made of PDMS material and were bonded on 1.1 mm thick soda lime glass substrates. For the fabrication of the microchannels, conventional optical lithography processes were used to create a master mold for casting of PDMS. Two layers of SU-8 3050 negative photoresist were spin-coated with an equal thickness of 100 μm to achieve a total thickness of 200 μm. PDMS was then cast on this mold and then cured and sliced. Substrates were placed in a vacuum oven at 50 °C for 15 minutes to achieve a stable plasma activated bonding. Fabricated sample microchannels that were used in the work described in this part are shown in Figure 5.15.

The resonators were designed as SSRR structures, with f_0 at 2 GHz, coupled to loop antennas fabricated on the same FR4 substrate via acid etching method. Dimensions of a single SSRR and loop antenna pair and their simulated resonance characteristics are shown in Figure 5.16 [57]. Fixing of microchannels was done with simple methods. The differential measurement scheme based on reflection tracking with loop antennas that is used in the experiments is schematized in Figure 5.17 [57]. For measurements using glucose solutions, a concentration range of 1.4 $\mathrm{mg\,mL^{-1}}$ - 3.0 $\mathrm{mg\,mL^{-1}}$ was used. Liquid samples were applied with a syringe connected to a Teflon tube to measuring the channels. Glucose measurements were performed four times at each concentration level.

Figure 5.15. Four pairs of microchannels obtained for experiments. Top left right pair was to used in the subsequently presented results since it lets through a higher sample volume.

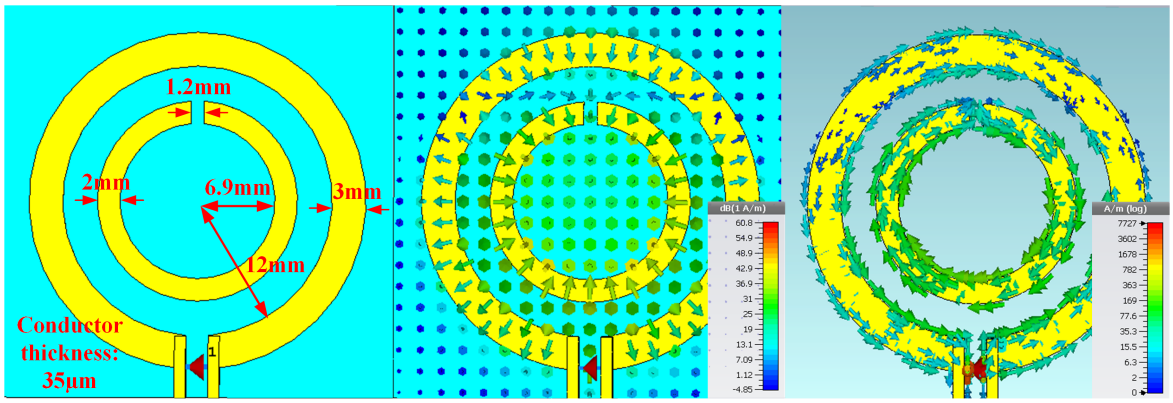

Figure 5.16. Geometric dimensions of a single SSRR loop antenna pair (left), their simulated h fields (middle), and surface currents (right) at resonance, as presented in [57].

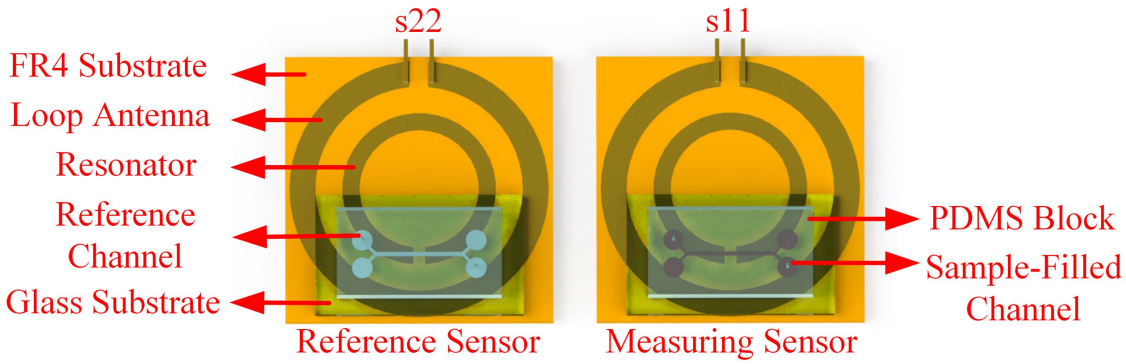

Figure 5.17. Elements of microfluidic differential measurement structure, as presented in [57].

As first part of the measurements, dielectric loading of different types were performed to either resonator. Reflection measurements obtained with bare resonators, resonators with PDMS microchannels placed on them, and when these channels are filled with DI water are presented in Figure 5.18 [57]. Following the fabrication, resonators had an f_0 that is in line with the analytical model and close to each other. As the electric permittivity increases due to dielectric loading, f_0 shifts to lower frequencies, as expected. Due to imperfections related to channel placement, amount of f_0 shift related to the placement of the channel showed some discrepancy.

Following the first step, response to glucose solutions of various concentrations were observed. Averages of the observed shifts from the f_0 measured before loading at each glucose concentration level are shown in Figure 5.19 [57]. Error bars show the minimum and maximum error ranges. It can be seen that the reference sensor also has a random shift response, despite being unloaded. This shift pattern seems to be repeated in the measurement sensor output as well, pointing to a background signal coupling to measurements. The sensor output, which is the difference between these two signals, is suppressing this background signal and attains a signal of high linearity, with the trendline fit having $R^2 = 0.9$. Based on the slope of the trendline, obtained sensitivity is 0.92 MHz/mg mL^{-1}.

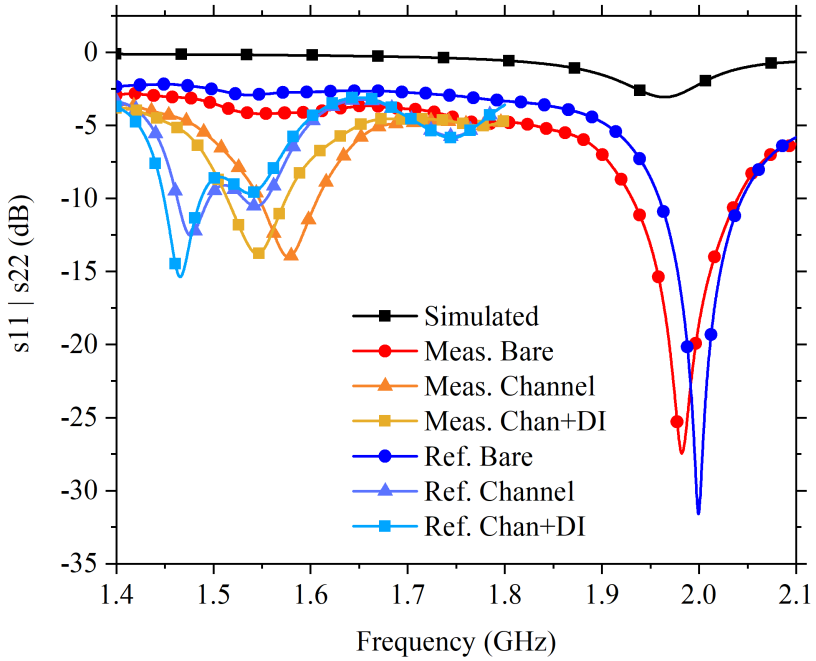

Figure 5.18. S_{11} and S_{22} responses of measuring and reference sensors for bare resonators, resonators with added microchannels, and with microchannels loaded with DI water, as presented in [57].

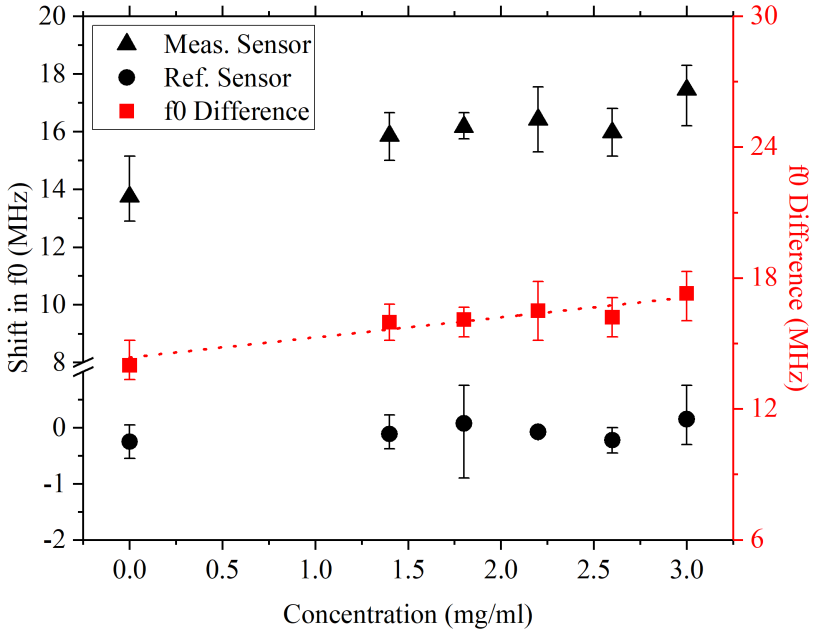

Figure 5.19. f_0 shifts related to loading of glucose in different concentrations, while the microchannel of the reference resonator was kept empty, as presented in [57].

5.3.2. Discussion on Microfluidic Integrated SRR Sensor

In the work described above, resonators coupled to loop antennas were tested for sensing of glucose in aqueous solutions. Reflection measurements provided VNA readings with clearer spectra, making sensitivity measurements more precise. A differential measurement scheme is applied. Results of this study, which were published in [57], indicate a good performance of the differential measurement approach, providing high linearity of the output.

This device can be improved further by direct incorporation of microchannels to the resonator substrates. In the present case, the PDMS microchannels were bonded on glass substrates, which in turn then placed on FR4 resonator substrates. This introduces an additional dielectric between the sensor and the analyte, which can potentially reduce sensitivity. Potential incorporation of the biosensitive elements in the future can be done with more ease with the use of other materials. That is why, an improved iteration of this design will be presented in the following, fabricated using materials highly compatible with conventional biosensor designs.

5.4. Gold SRRs on Glass Substrates with PDMS Microchannels

Bonding of PDMS type microchannels can be performed on glass substrates as shown in the previous section. In order to achieve a direct integration of PDMS microchannels with resonators can thus be performed via fabrication of SRR resonators on glass substrates directly. As the conductive part to form the resonator and antenna elements, it was decided to use gold. Gold and glass are both agreeable materials of choice in fabrication of biosensor systems due to their functionalizability. Additionally, gold is quite inert in macroscales, remaining unaffected from chemical reactions. Moreover they are compatible with conventional clean room fabrication techniques. Dimensions of the designed system and the cross-section showing its layers are drawn in Figure 5.20 [244].

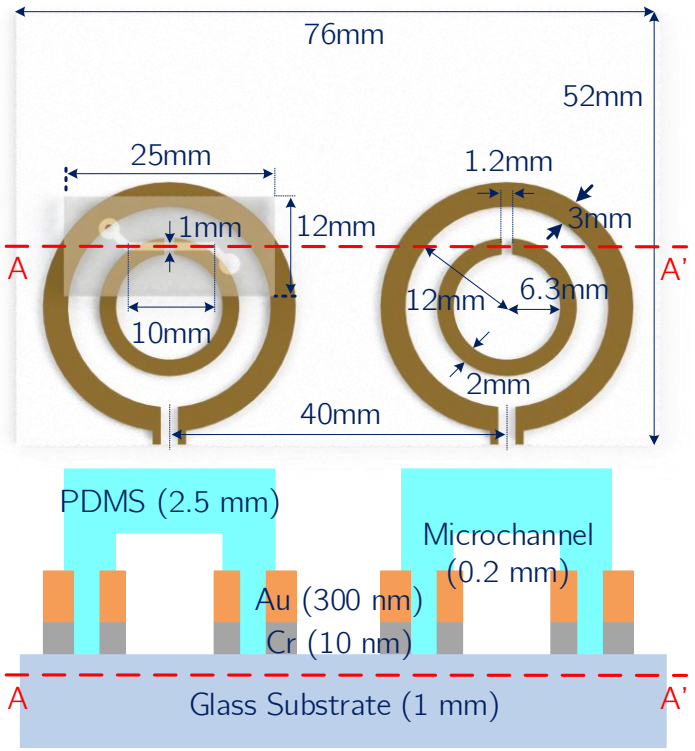

Figure 5.20. Geometric dimensions of the designed gold SRR on glass substrate sensor system, from [244].

5.4.1. Fabrication of Resonators and Microchannels

Fabrication steps of the sensor components are summarized in Figure 5.21. After cleaning of the glass substrates with isopropyl alcohol, acetone, and DI water, they were treated with TI PRIME to promote photoresist adhesion. TI PRIME was spin coated on the substrate at 4000 rpm for 45 seconds and then was baked at 110 °C for two minutes. After this step, AZ5214 photoresist was also spun at 4000 rpm for 50 seconds and was baked at 120 °C for five minutes. Ultraviolet (UV) light was applied (dose = 40, separation = 60, exposure = 1100) through an ink pattern printed on acetate paper, acting as a photolithography mask. A second UV exposure was applied followed by a reverse bake of 120 °C for another two minutes. The sample was then developed for 90 seconds. Following these steps, the substrate was placed in chamber for sputtering of 10 nm Cr, acting as an adhesion promoter, and 300 nm of Au. This was followed by a conventional lift off process, where the photoresist parts were etched and the desired conductive patterns, which include the pair of resonators and loop antennas, were formed on the glass.

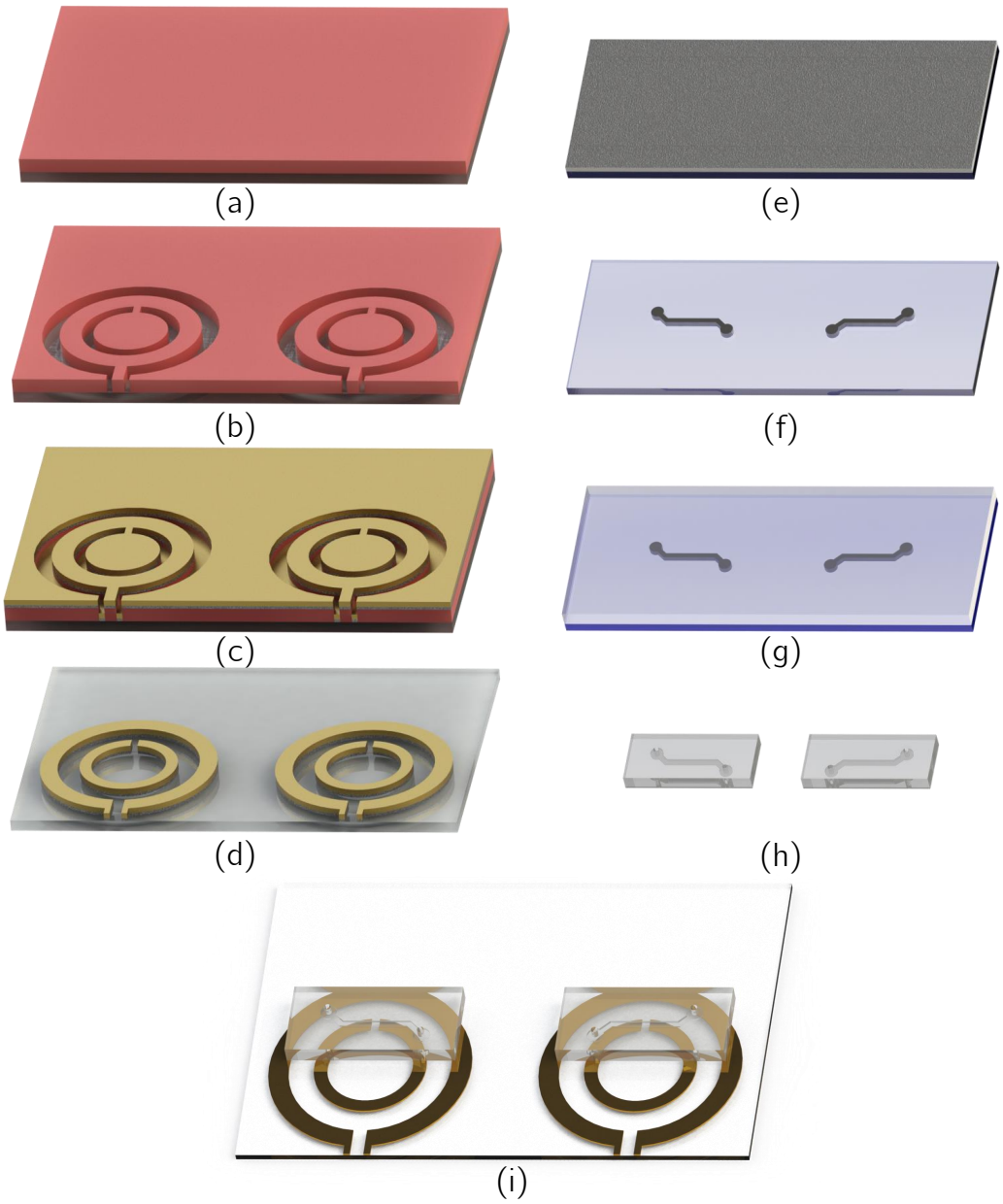

Figure 5.21. Fabrication of the gold SRR on glass substrate sensor system. Spin coating of photoresist on surface treated substrate (a). UV exposure and etching of the photoresist (b). Cr (10 nm) and Au (300 nm) deposition (c). Photoresist removal (d). Spin coating of SU-8 on substrate (e). Formation of mold via photolitography patterning (f). Pouring, degassing, and curing of PDMS and curing agent mixture on mold (g). Slicing and puncturing (h). Alignment and bonding of microchannels (i). Redrawn from [244].

PDMS microchannels were fabricated via mold casting of PDMS in liquid form. The mold itself was made via photolithography patterning of 200 μm thick SU-8 3050 negative photoresist. Microchannels themselves have 1 mm width and 10 mm length. This thickness was achieved by two consecutive spin coating of the material, as explained in the previous Section. PDMS material and the glass substrate were bonded together with a plasma activation process. It is possible to couple the microchannels to the resonators in a variety of ways. In order to obtain the highest sensitivity to dielectric changes, simulated responses to dielectric loads, having the electrical characteristics of DI water and the shape of the microchannel, placed on different locations on sensor surface in different orientations were compared. The results shown in Figure 5.22 indicate that for highest sensitivity, the microchannel should be placed in a transverse orientation to SRR gap so that it passes through midway of the gap/conductor interface. This is in agreement with the theory as described in Section 2.3. Bonding of the microchannels to the substrate was done in accordance to this. Before the bonding of plasma activated PDMS and glass substrates, a droplet of methanol was added in between to create a sliding layer for alignment of the microchannels to the sensors. Identical alignment of microchannels on individual resonators were aimed for better differential measurement performance. The microchannels were positioned so that they cross the gap of the resonator in a transverse manner.

One SMA connector was bonded to each of the loop antenna ports to provide the conductive connection to the VNA (Rohde & Schwarz - ZVB4). In order to prevent the solder contact from mechanical loading that may occur, solder contacts were sealed in epoxy. To provide further mechanical stability to the sensor system and the cables, 3D printed holder structures were used in measurements as well. Two additional holders were also added to support the connection cables in an attempt to reduce mechanical stress due to the cable weights as well. Sensor system and related holder elements are shown in Figure 5.23.

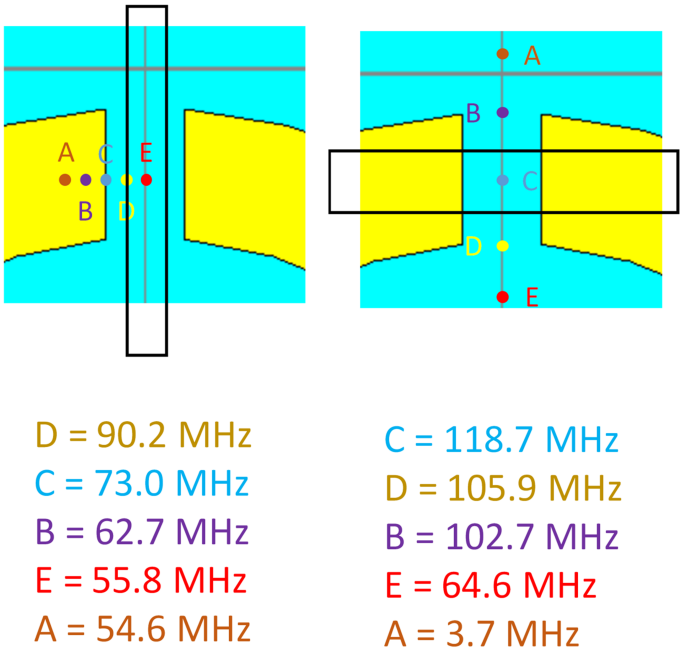

Figure 5.22. Simulated f_0 shift due to a dielectric load in the shape of the microchannel in different orientations and positions, demonstrating the dielectric sensitivity of the sensor in different cases. Black rectangle frame showing orientation of the microchannel is not to scale.

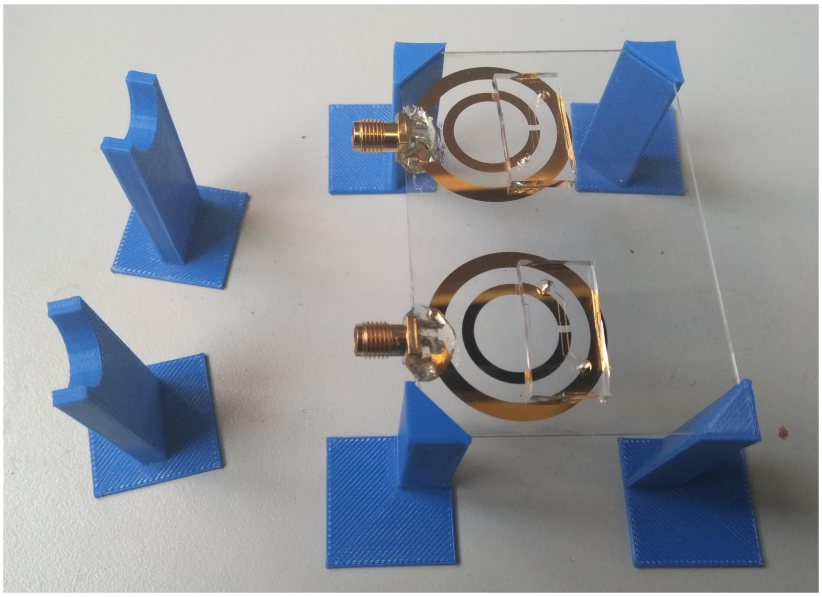

Figure 5.23. Microchannel integrated resonators with soldered SMA connectors and their holder structures.

5.4.2. Experimental Setup and Results

Via the SMA connectors, the resonators were connected to the VNA. Using two ports of the VNA, simultaneous tracking of the reflection spectra were measured for both sensors. Even though it is possible to achieve stable bonding with plasma activation, PDMS microchannels are prone to separation from glass surface if too much pressure is applied on them. That is why the samples needed be applied to microchannels in a slow and controlled manner. As a solution, syringes used for sample injection were used with 3D stage based structures. These stages allow for millimetric adjustment of position and thus using them makes it possible to control the syringes with higher precision. Syringes were connected to the microchannels via Teflon tubes with 0.5 mm diameter. Liquid sample injection was carried on until the microchannel was fully loaded with the material. After this point, the injection was stopped until the recordings were carried out, which were made 10 seconds following the full loading of the microchannel. The overall setup is shown in Figure 5.24 [244].

Reflection measurements were carried out first with the dielectric loading conditions, results of which are demonstrated in Figure 5.25. Both unloaded sensors have f_0 of 1.74 GHz, shifting to 1.45 GHz after microchannels were loaded with DI water. While both sensors achieve a good f_0 parity, their Q is different, which may be related to the sputterer being off-calibration, yielding varying metal thicknesses across the substrate. Q for the measuring sensor is as high as 124, even with the PDMS microchannel integrated on it. It should be noted that 300 nm thickness of Au is lower than the skin depth relevant to the operation frequencies, which varies between 1.68 μm and 1.95 μm. This actually increases resistive losses and potentially reduces the quality factor.

Following this, aqueous solutions of glucose in concentration range of 3.2 mM - 16.1 mM were applied to the measuring sensor microchannel. Three measurements at each concentration values were recorded. Figure 5.26 shows the averages of measurements for both the measuring and reference sensor. Data marked with red color indicates the difference between two readings, instead of the difference of shifts as

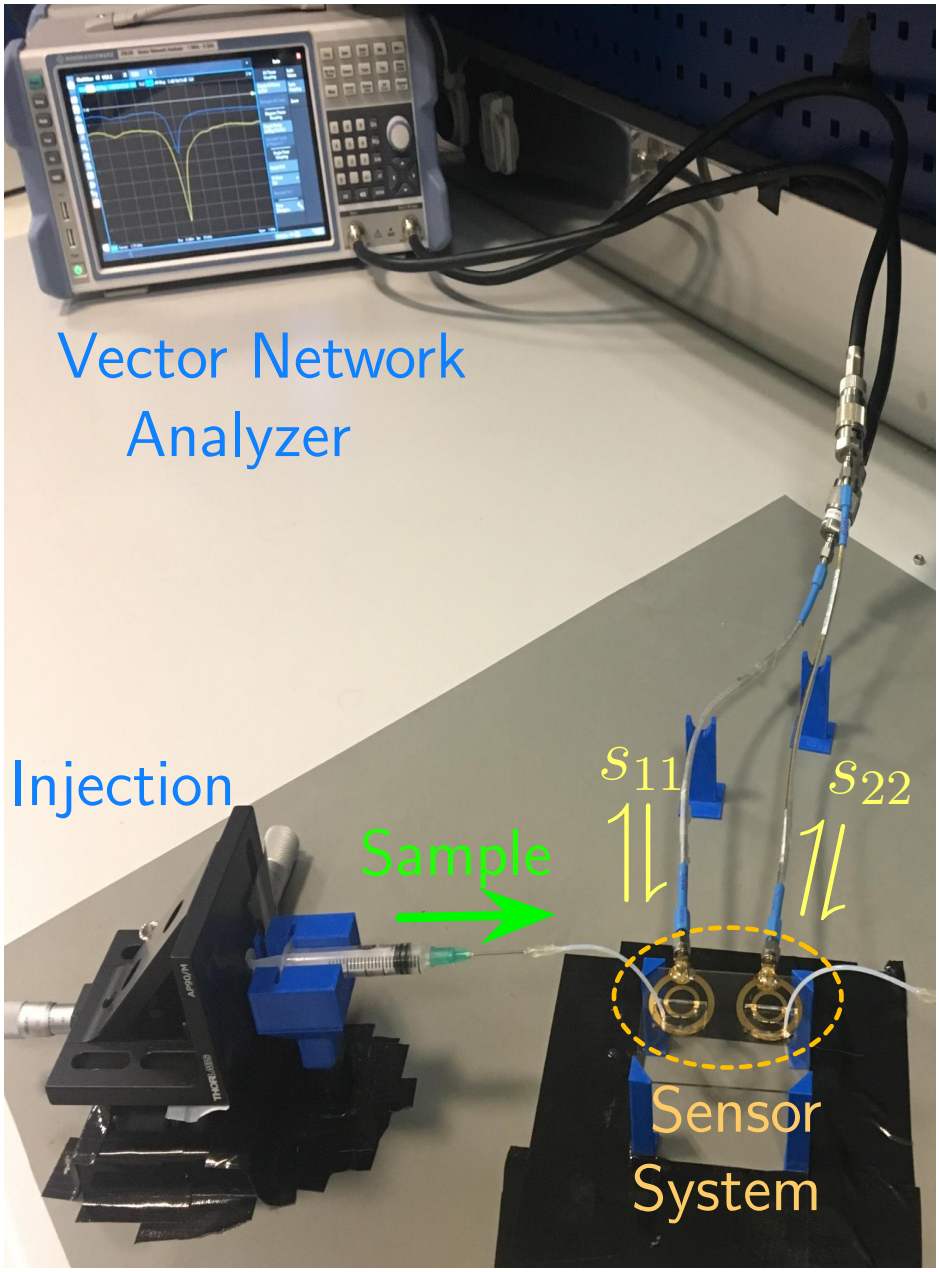

Figure 5.24. Entire measurement setup of gold SRR on glass substrates sensor system, as shown in [244].

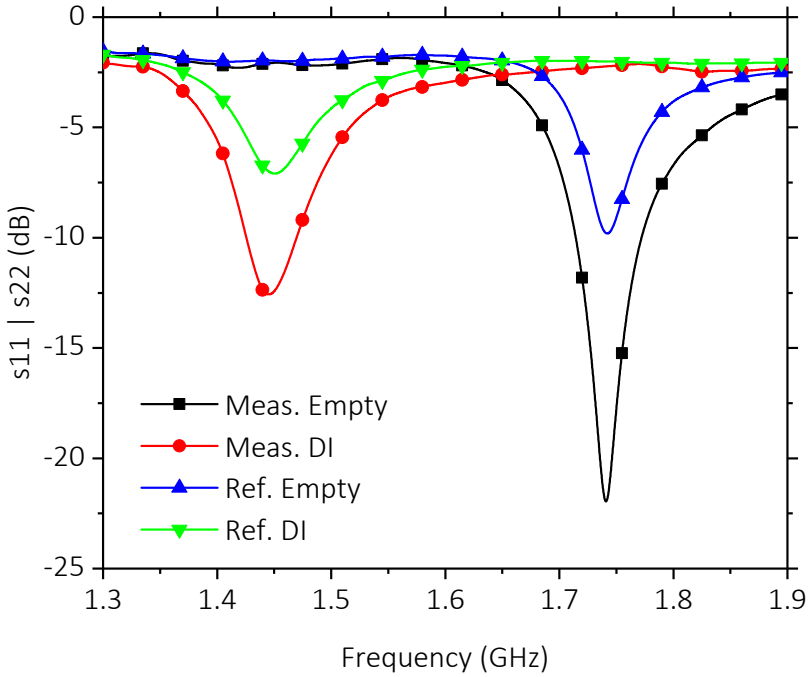

Figure 5.25. S_{11} and S_{22} as measured belonging to sensors integrated with microchannels when they are empty and when they are loaded with DI water. Measuring sensor attains a $Q = 124$ while unloaded. Redrawn from [244].

was presented in previous sensing tests. Error bars indicate the standard deviation of measurements, with worst case measurement error falling from 3 MHz of the previous microchannel integrated sensor design to 1.2 MHz in this one. Added trendlines show a significant improvement in measurement linearity when differential measurement approach is used since measurement sensor trendline fit has $R^2 = 0.48$ whereas the difference trendline fit has $R^2 = 0.96$. Based on the fit to difference data, sensitivity to glucose concentration of the design is 0.16 MHz/mM.

5.5. Discussion on Gold SRR on Glass Substrate Sensors

In this part, a loop antenna excited SRR based sensing system incorporating microfluidic channels and employing a differential measurement approach, fabricated with materials compatible with biosensing applications was presented. Simulation and fabrication steps can be performed with conventional methods. In its improved form, the sensor system is able to reject background noises and improve measurement lin-

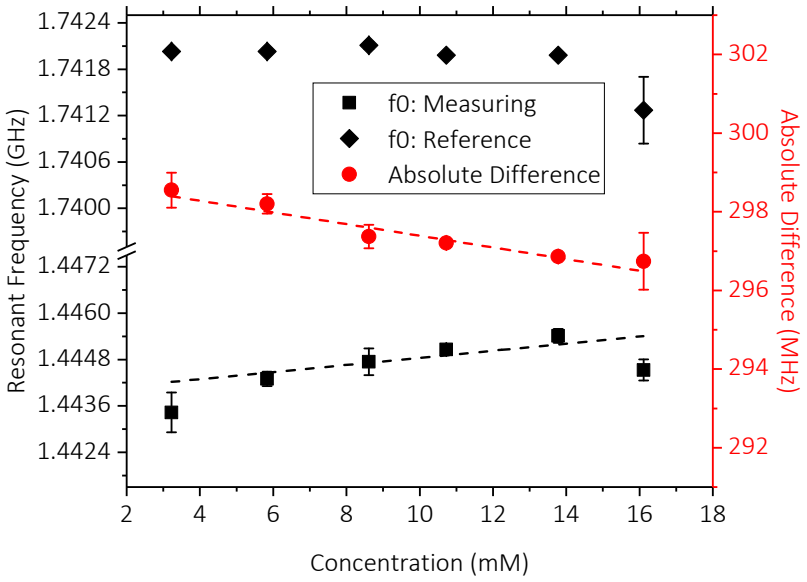

Figure 5.26. Measured f_0 of the measuring and reference sensors of the improved design, and their differences at different glucose concentrations, as presented in [244].

earity and repeatability. High Q obtained has also a significant contribution to this and the detection limit, since a sharper resonance characteristic is good for better resolution of smaller f_0 changes. Obtained sensitivity is in the order of similar sensor approaches investigated in the literature [200]. Use of loop antennas for reading makes it possible to design a fully planar system with a contactless reading potential. Microfluidic channels can be now in direct contact with the sample. This is important for future applications, where biospeceific elements can be immobilized on the sensor surface to allow fully selective sensing of glucose. Material choice of gold and glass are also in alignment with this vision, since there are examples of immobilization of GOx, an enzyme specific to glucose, on glass or gold substrates [245–248].

6. CONCLUSION AND FUTURE WORK

In this thesis, development of an SRR based sensor aiming to detect glucose concentrations in aqueous solutions was presented. After a relevant literature review and theoretical study, exploratory work was performed to demonstrate sensing potential with SRR structures. This was carried out to the point where one of the earliest glucose specific SRR based sensor in the literature was demonstrated. For specificity, GOx enzyme was used. The enzyme was immobilized on the sensor surface with a PEDOT:PSS polymer matrix. Due to conductive nature of the polymer, the sensitive gap region of the resonator could not be utilized. To hold the liquid samples, a cost-effective laser-cut polymer reservoir in the shape of the resonator was used. Specificity was demonstrated via a comparison of the sensor response to other reagents as well, namely fructose, sucrose, and NaCl.

This design was later improved in steps. A second resonator was added to the system so that differential measurements can be carried out. In such a scheme, one of the resonators act as a reference and measure the background signal, whereas the measuring resonator perform the whole measurement. Difference of their outputs is the actual sensor output and to a large degree can suppress the background signal. Monopole antenna excitation was then abandoned in favor of loop antennas, since they allow fully planar designs while not incorporating any ground planes, allowing for more effective contactless measurement schemes.

To contain liquid samples more effectively and to demonstrate the potential of SRR based sensors in the growing field of microfluidics and LOC applications, microfluidic channels were then incorporated to the system in development. The initial example used microchannels fabricated separately and then manually added to the system. This was further developed by fabrication of microchannels along with the sensors and direct bonding of them to sensor surfaces, owing to the fact that new sensor materials allowing it. Improved sensor was demonstrated to be competent in sensing of glucose in aqueous solutions, achieving improved linearity and sensitivity.

Work done until this point demonstrated the feasibility of sensing of reagents in aqueous solutions with SRR based sensors, which are cost-effective, portable, and easy to use. The basic biosensor design and conceptual improvements were published [57, 203, 208, 212, 244]. Still there is room for improvement still in sensor sensitivity, precision, specificity, and particularly interfacing.

6.1. Current State and Future Work

Recent developments in research of SRR based sensing of glucose looks particularly promising for the contact-based detection of glucose levels with SRRs. In a remarkable study, a portable device, complete with readout electronics and interface [249], for noninvasive monitoring of blood glucose detected through a contact with the tongue of the patient was demonstrated and tested on 352 individuals [250]. The sensor is the basic rectangular SRR structure coupled to readout ports. This being said, even though the relationship between the sensor output and blood glucose level obtained from reference readings are coherent, the effect of other biological components may have interfered with the reading. Final sensor design presented in this work can also be improved with added specificity, since it does not incorporate any specific elements targeting glucose. In fact, there still is a limited corpus of SRR based glucose sensors in the literature that claim reagent specificity.

In a recent example, an enzyme-free glucose-specific SRR based sensor using on phenylboronic acid (PBA) hydrogel is presented [251]. Sensor system is formed of a pair of rectangular SRRs, sandwiching the PBA layer, which swells or deswells based on its reversible binding to sugar molecules. Both binding activity changing the dielectric and the change in physical distance between SRRs due to swelling could contribute to the shift in resonance frequency. Due to the sensor being responsive to reagents such as galactose and fructose as well, the selectivity problem is addressed only partially. Nevertheless, this approach can pose an interesting alternative to enzymatic solutions, since it does not suffer from shorter lifetimes associated with enzyme degradation. Materials chosen for the finalized design are compatible with functionalization processes used for immobilization of biospecific elements [252].

Currently, SRR based sensor readings are often being done with VNA equipment, which inherently defines the bandwidth and limit of detection. These devices are also often costly and bulky. A truly portable SRR based sensor will require interfacing with electronic microsystem, of which few examples exist [250]. An approach to address the need for an electronic readout system was presented in [192]. Here, it is suggested that by making the frequency selective elements that are SRRs part of a positive feedback loop, it was possible to devise oscillators providing signals of the selected frequency. In these forms, processing of resonator outputs can be done in less complex electronic environments, helping SRR based sensors to achieve their true potential.

REFERENCES

1. Chen, T., S. Li and H. Sun, "Metamaterials Application in Sensing", *Sensors*, Vol. 12, No. 3, pp. 2742–2765, 2012.

2. Eleftheriades, G. V. and N. Engheta, "Metamaterials: Fundamentals and Applications in the Microwave and Optical Regimes [Scanning the Issue]", *Proceedings of the IEEE*, Vol. 99, No. 10, pp. 1618–1621, 2011.

3. Gokhale, V. J., O. A. Shenderova, G. E. McGuire and M. Rais-Zadeh, "Infrared Absorption Properties of Carbon Nanotube/Nanodiamond Based Thin Film Coatings", *Journal of Microelectromechanical Systems*, Vol. 23, No. 1, pp. 191–197, 2014.

4. Schurig, D., J. J. Mock, B. J. Justice, S. A. Cummer, J. B. Pendry, A. F. Starr and D. R. Smith, "Metamaterial Electromagnetic Cloak at Microwave Frequencies", *Science*, Vol. 314, No. 5801, pp. 977–980, 2006.

5. Smolyaninov, I. I., Y.-J. Hung and C. C. Davis, "Magnifying Superlens in the Visible Frequency Range", *Science*, Vol. 315, No. 5819, pp. 1699–1701, 2007.

6. Liu, Z., H. Lee, Y. Xiong, C. Sun and X. Zhang, "Far-Field Optical Hyperlens Magnifying Sub-Diffraction-Limited Objects", *Science*, Vol. 315, No. 5819, pp. 1686–1686, 2007.

7. Gangwar, K., Paras and R. P. S. Gangwar, "Metamaterials: Characteristics, Process and Applications", *Advance in Electronic and Electric Engineering*, Vol. 4, No. 1, pp. 97–106, 2014.

8. Veselago, V. G., "The electrodynamics of substances with simultaneously negative values of ϵ and μ", *Soviet Physics Uspekhi*, Vol. 10, No. 4, pp. 509–514, 1968.

9. Pendry, J. B., A. J. Holden, D. J. Robbins and W. J. Stewart, "Magnetism from conductors and enhanced nonlinear phenomena", *IEEE Transactions on Microwave Theory Techniques*, Vol. 47, No. 11, pp. 2075–2084, 1999.

10. Smith, D. R., W. J. Padilla, D. C. Vier, S. C. Nemat-Nasser and S. Schultz, "Composite Medium with Simultaneously Negative Permeability and Permittivity", *Physical Review Letters*, Vol. 84, No. 18, pp. 4184–4187, 2000.

11. Shelby, R. A., D. R. Smith and S. Schultz, "Experimental Verification of a Negative Index of Refraction", *Science*, Vol. 292, No. 5514, pp. 77–79, 2001.

12. Grbic, A. and G. V. Eleftheriades, "Experimental verification of backward-wave radiation from a negative refractive index metamaterial", *Journal of Applied Physics*, Vol. 92, No. 10, pp. 5930–5935, 2002.

13. Brito, D. B., *Metamaterial Inspired Improved Antennas and Circuits*, Ph.D. Thesis, Electromagnetism, Telecom ParisTech, 2010.

14. Yeh, L. K., C. Y. Chen and H. R. Chuang, "A Millimeter-Wave CPW CMOS On-Chip Bandpass Filter Using Conductor-Backed Resonators", *IEEE Electron Device Letters*, Vol. 31, No. 5, pp. 399–401, 2010.

15. Linden, S., C. Enkrich, M. Wegener, J. Zhou, T. Koschny and C. M. Soukoulis, "Magnetic Response of Metamaterials at 100 Terahertz", *Science*, Vol. 306, No. 5700, pp. 1351–1353, 2004.

16. Ishikawa, A., T. Tanaka and S. Kawata, "Negative Magnetic Permeability in the Visible Light Region", *Physical Review Letters*, Vol. 95, No. 23, pp. 237401–1–237401–4, 2005.

17. Wan Nordin, M. A., M. T. Islam and N. Misran, "A compact wideband coplanar waveguide fed metamaterial-inspired patch antenna for wireless application", *Applied Physics A*, Vol. 109, No. 4, pp. 961–965, 2012.

18. Gil, M., J. Bonache and F. Martín, "Metamaterial filters: A review", *Metamaterials*, Vol. 2, No. 4, pp. 186 – 197, 2008.

19. Torun, H., S. Sadeghzadeh, H. Bilgin and A. D. Yalcinkaya, "A micromachined freestanding terahertz absorber with an array of metallic patches", *AIP Advances*, Vol. 6, No. 3, pp. 035323–1–035323–13, 2016.

20. Zhang, X. and Z. Liu, "Superlenses to overcome the diffraction limit", *Nature Materials*, Vol. 7, No. 6, pp. 435–441, 2008.

21. Alu, A. and N. Engheta, "Plasmonic and metamaterial cloaking: physical mechanisms and potentials", *Journal of Optics A: Pure and Applied Optics*, Vol. 10, No. 9, pp. 093002–1–093002–18, 2008.

22. Ashworth, P. C., E. Pickwell-MacPherson, E. Provenzano, S. E. Pinder, A. D. Purushotham, M. Pepper and V. P. Wallace, "Terahertz pulsed spectroscopy of freshly excised human breast cancer", *Optics Express*, Vol. 17, No. 15, pp. 12444–12454, 2009.

23. Baena, J., R. Marques, F. Medina and J. Martel, "Artificial magnetic metamaterial design by using spiral resonators", *Physical Review B*, Vol. 69, No. 014402, pp. 1–5, 2004.

24. Ozbay, E., I. Bulu and H. Caglayan, "Transmission, refraction, and focusing properties of labyrinth based left-handed metamaterials", *Physica Status Solidi (b)*, Vol. 244, No. 4, pp. 1202 – 1210, 2007.

25. Chen, H., L. Ran, J. Huangfu, X. Zhang, K. Chen, T. Grzegorczyk and J. Kong, "Magnetic properties of S-shaped split ring resonators", *Progress in Electromagnetics Research*, Vol. 51, No. 1, pp. 231–247, 2005.

26. Wu, B.-I., W. Wang, J. Pacheco, X. Chen, T. Grzegorczyk and J. Kong, "A study of using metamaterials as antenna substrate to enhance gain", *Progress in*

Electromagnetics Research, Vol. 51, No. 1, pp. 295–328, 2005.

27. Marques, R., F. Mesa, J. Martel and F. Medina, "Comparative Analysis of Edge- and Broadside-Coupled Split Ring Resonators for Metamaterial Design - Theory and Experiments", *IEEE Transactions on Antennas and Propagation*, Vol. 51, No. 10, pp. 2572 – 2581, 2003.

28. Burokur, S. N., M. Latrach and S. Toutain, "Study of the effect of Dielectric Split Ring Resonators on microstrip line transmission", *Microwave and Optical Technology Letters*, Vol. 44, No. 5, pp. 445 – 448, 2005.

29. Marques, R. and F. Medina, "Role of bianisotropy in negative permeability and left-handed metamaterials", *Physical Review B*, Vol. 65, No. 14, pp. 144440–1–144440–6, 2002.

30. Melik, R., E. Unal, N. K. Perkgoz, B. Santoni, D. Kamstock, C. Puttlitz and H. V. Demir, "Nested Metamaterials for Wireless Strain Sensing", *IEEE Journal of Selected Topics in Quantum Electronics*, Vol. 16, No. 2, pp. 450–458, 2010.

31. Ozbey, B., E. Unal, H. Ertugrul, O. Kurc, C. M. Puttlitz, V. B. Erturk, A. Altintas and H. V. Demir, "Wireless Displacement Sensing Enabled by Metamaterial Probes for Remote Structural Health Monitoring", *Sensors*, Vol. 14, No. 1, pp. 1691–1704, 2014.

32. Zhou, J., *Study of Left-Handed Materials*, Ph.D. Thesis, Electrical and Computer Engineering, Iowa State University, 2008.

33. Sydoruk, O., E. Tatartschuk, E. Shamonina and L. Solymar, "Analytical formulation for the resonant frequency of split rings", *Journal of Applied Physics*, Vol. 105, No. 1, pp. 014903–1–014903–5, 2009.

34. Baena, J. D., J. Bonache, F. Martin, R. M. Sillero, F. Falcone, T. Lopetegi, M. A. G. Laso, J. Garcia-Garcia, I. Gil, M. F. Portillo and M. Sorolla,

"Equivalent-circuit models for split-ring resonators and complementary split-ring resonators coupled to planar transmission lines", *IEEE Transactions on Microwave Theory and Techniques*, Vol. 53, No. 4, pp. 1451–1461, 2005.

35. Alici, K. B., F. Bilotti and E. Ozbay, "Miniaturized negative permeability materials", *Applied Physics Letters*, Vol. 91, No. 7, pp. 071121–1–071121–4, 2007.

36. Ekmekci, E. and G. Turhan-Sayan, "Reducing the electrical size of magnetic metamaterial resonators by geometrical modifications: a comparative study for single-sided and double-sided multiple SRR, spiral and U-spiral resonators", *IEEE Antennas and Propagation Society International Symposium*, pp. 1–4, 2008.

37. Bilotti, F., A. Toscano and L. Vegni, "Design of Spiral and Multiple Split-Ring Resonators for the Realization of Miniaturized Metamaterial Samples", *IEEE Transactions on Antennas and Propagation*, Vol. 55, No. 8, pp. 2258–2267, 2007.

38. Capolino, F., *Theory and Phenomena of Metamaterials*, Metamaterials Handbook, CRC Press, 2009.

39. Yasar-Orten, P., E. Ekmekci and G. Turhan-Sayan, "Equivalent Circuit Models for Split-ring Resonator Arrays", *PIERS Proceedings*, 2010.

40. Zheludev, N. I., "The Road Ahead for Metamaterials", *Science*, Vol. 328, No. 5978, pp. 582–583, 2010.

41. Su, L., J. Mata-Contreras, P. Vélez and F. Martín, "A Review of Sensing Strategies for Microwave Sensors Based on Metamaterial-Inspired Resonators: Dielectric Characterization, Displacement, and Angular Velocity Measurements for Health Diagnosis, Telecommunication, and Space Applications", *International Journal of Antennas and Propagation*, Vol. 2017, No. 5619728, pp. 1–14, 2017.

42. Jaksic, Z., S. Vukovic, J. Matovic and D. Tanaskovic, "Negative Refractive Index

Metasurfaces for Enhanced Biosensing", *Materials*, Vol. 4, No. 1, pp. 1–36, 2011.

43. Lee, H.-J. and J.-G. Yook, "Biosensing using split-ring resonators at microwave regime", *Applied Physics Letters*, Vol. 92, No. 25, pp. 254103–1–254103–4, 2008.

44. Ishimairu, A., S. Jaruwatanadilok and Y. Kuga, "Generalized surface plasmon resonance sensors using metamaterials and negative index materials", *Progress in Eletromagnetics Research*, Vol. 51, No. 1, pp. 139–152, 2005.

45. Huang, M. and J. J. Yang, *Microwave Sensor Using Metamaterials*, Intech Press: Vienna, Austria, 2011.

46. Vaddiraju, S., I. Tomazos, D. J. Burgess, F. C. Jain and F. Papadimitrakopoulos, "Emerging synergy between nanotechnology and implantable biosensors: A review", *Biosensors and Bioelectronics*, Vol. 25, No. 7, pp. 1553 – 1565, 2010.

47. Tao, H., S. Hwang, M. Liu, B. Panilaitis, M. A. Brenckle, D. L. Kaplan, R. D. Averitt, J. A. Rogers and F. G. Omenetto, "Fully Implantable and Resorbable Metamaterials", *Conference on Lasers and Electro-Optics*, pp. 1–2, Optical Society of America, 2012.

48. Tao, H., W. J. Padilla, X. Zhang and R. D. Averitt, "Recent Progress in Electromagnetic Metamaterial Devices for Terahertz Applications", *IEEE Journal of Selected Topics in Quantum Electronics*, Vol. 17, No. 1, pp. 92–101, 2011.

49. Park, S., S. Yoon and Y. Ahn, "Dielectric constant measurements of thin films and liquids using terahertz metamaterials", *RSC Advances*, Vol. 6, No. 73, pp. 69381–69386, 2016.

50. Tao, H., C. M. Bingham, A. C. Strikwerda, D. Pilon, D. Shrekenhamer, N. I. Landy, K. Fan, X. Zhang, W. J. Padilla and R. D. Averitt, "Highly flexible wide angle of incidence terahertz metamaterial absorber: Design, fabrication, and characterization", *Physical Review B*, Vol. 78, No. 24, pp. 2411031–1–2411031–4,

2008.

51. Landy, N. I., C. M. Bingham, T. Tyler, N. Jokerst, D. R. Smith and W. J. Padilla, "Design, theory, and measurement of a polarization-insensitive absorber for terahertz imaging", *Physical Review B*, Vol. 79, No. 12, pp. 125104–1–125104–6, 2009.

52. Memon, M. U. and S. Lim, "Review of Electromagnetic-Based Crack Sensors for Metallic Materials (Recent Research and Future Perspectives)", *Metals - Open Access Metallurgy Journal*, Vol. 6, No. 8, pp. 172–1–172–22, 2016.

53. Schueler, M., C. Mandel, M. Puentes and R. Jakoby, "Metamaterial Inspired Microwave Sensors", *IEEE Microwave Magazine*, Vol. 13, No. 2, pp. 57–68, 2012.

54. Lee, H.-J., H.-S. Lee, K.-H. Yoo and J.-G. Yook, "DNA sensing using split-ring resonator alone at microwave regime", *Journal of Applied Physics*, Vol. 108, No. 1, pp. 014908–1–014908–7, 2010.

55. Kim, N., R. Dhakal, K. Adhikari, E. Kim and C. Wang, "A reusable robust radio frequency biosensor using microwave resonator by integrated passive device technology for quantitative detection of glucose level", *Biosensors and Bioelectronics*, Vol. 67, No. 15, pp. 687 – 693, 2015.

56. Gao, L., L. Lin, J. Hao, W. Wang, R. Ma, H. Xu, J. Yu, N. Lu, W. Wang and L. Chi, "Fabrication of split-ring resonators by tilted nanoimprint lithography", *Journal of Colloid and Interface Science*, Vol. 360, No. 1, pp. 320 – 323, 2011.

57. Camli, B., E. Altinagac, H. Kizil, H. Torun, G. Dundar and A. D. Yalcinkaya, "Loop Antenna Driven Double Microwave Resonator-Based Sensors Incorporating PDMS Microchannels on Glass Substrates", *Proceedings*, Vol. 2, No. 13, pp. 1064–1–1064–4, 2018.

58. Muller, A. A., R. Abdul Khadar, E. A. Casu, A. Krammer, M. Cavalieri,

A. Schuler, J. Zhang and A. M. Ionescu, "A Novel Reconfigurable CMOS Compatible Ka Band Bandstop Structure Using Split-Ring Resonators and Vanadium Dioxide (VO2) Phase Change Switches", *IEEE MTT-S International Microwave Symposium (IMS)*, pp. 865–868, 2019.

59. Jiang, Y., X. Liu, X. Huang, Y. Shang, M. Yan and H. Yu, "Lab-on-CMOS: A multi-modal CMOS sensor platform towards personalized DNA sequencing", *IEEE International Symposium on Circuits and Systems (ISCAS)*, pp. 2266–2269, 2016.

60. Liang, Y., H. Yu, C. Yang, N. Li, X. Li, X. Liu, J. Zhao, W. Yang and Y. Wang, "CMOS sub-THz on-chip communication with SRR modulator and SPP interconnect", *IEEE MTT-S International Microwave Workshop Series on Advanced Materials and Processes for RF and THz Applications (IMWS-AMP)*, pp. 1–3, 2015.

61. Kim, N.-Y., K. K. Adhikari, R. Dhakal, Z. Chuluunbaatar, C. Wang and E.-S. Kim, "Rapid, Sensitive, and Reusable Detection of Glucose by a Robust Radiofrequency Integrated Passive Device Biosensor Chip", *Scientific Reports*, Vol. 5, No. 7807, pp. 1–9, 2015.

62. Gundogdu, T., M. Gökkavas, K. Güven, M. Kafesaki, C. Soukoulis and E. Ozbay, "Simulation and micro-fabrication of optically switchable split ring resonators", *Photonics and Nanostructures - Fundamentals and Applications*, Vol. 5, No. 2–3, pp. 106 – 112, 2007.

63. Im, D.-K., D. Im and K. Lee, "SOI CMOS Miniaturized Tunable Bandpass Filter with Two Transmission Zeros for High Power Applications", *Progress in Eletromagnetics Research Symposium Proceedings*, 2012.

64. Melik, R., E. Unal, N. Perkgoz, C. Puttlitz and H. Demir, "Flexible metamaterials for wireless strain sensing", *Applied Physics Letters*, Vol. 95, No. 18, pp. 181105–1–181105–4, 2009.

65. Sadeqi, A., H. R. Nejad and S. Sonkusale, "Low-cost metamaterial-on-paper chemical sensor", *Optics Express*, Vol. 25, No. 14, pp. 16092–16100, 2017.

66. Tao, H., L. R. Chieffo, M. A. Brenckle, S. M. Siebert, M. Liu, A. C. Strikwerda, K. Fan, D. L. Kaplan, X. Zhang, R. D. Averitt and F. G. Omenetto, "Metamaterials on Paper as a Sensing Platform", *Advanced Materials*, Vol. 23, No. 28, pp. 3197–3201, 2011.

67. Zahertar, S., E. Laurin, L. E. Dodd and H. Torun, "Embroidered Rectangular Split-Ring Resonators for the Characterization of Dielectric Materials", *IEEE Sensors Journal*, Vol. 20, No. 5, pp. 2434–2439, 2020.

68. Mata-Contreras, J., C. Herrojo and F. Martín, "Application of Split Ring Resonator (SRR) Loaded Transmission Lines to the Design of Angular Displacement and Velocity Sensors for Space Applications", *IEEE Transactions on Microwave Theory and Techniques*, Vol. 65, No. 11, pp. 4450–4460, 2017.

69. Naqui, J. and F. Martín, "Angular Displacement and Velocity Sensors Based on Electric-LC (ELC) Loaded Microstrip Lines", *IEEE Sensors Journal*, Vol. 14, No. 4, pp. 939–940, 2014.

70. Ebrahimi, A., W. Withayachumnankul, S. Al-Sarawi and D. Abbott, "Metamaterial-Inspired Rotation Sensor With Wide Dynamic Range", *IEEE Sensors Journal*, Vol. 14, No. 8, pp. 2609–2614, 2014.

71. Naqui, J., M. Durán-Sindreu and F. Martín, "Novel Sensors Based on the Symmetry Properties of Split Ring Resonators (SRRs)", *Sensors (Basel, Switzerland)*, Vol. 11, No. 8, pp. 7545–53, 2011.

72. Horestani, A. K., Z. Shaterian, D. Abbott and C. Fumeaux, "Application of metamaterial-inspired resonators in compact microwave displacement sensors", *1st Australian Microwave Symposium (AMS)*, pp. 19–20, 2014.

73. Lee, C., B. Bai, Q. Song, Z. Wang and G. Li, "Microwave Resonator for Eye Tracking", *IEEE Transactions on Microwave Theory and Techniques*, Vol. 67, No. 12, pp. 5417–5428, 2019.

74. Li, J., W. Withayachumnankul, S. Chang and D. Abbott, "Metamaterial-based strain sensors", *Seventh International Conference on Intelligent Sensors, Sensor Networks and Information Processing*, pp. 30–32, 2011.

75. Dijvejin, Z. A., K. K. Kazemi, K. Alasvand Zarasvand, M. H. Zarifi and K. Golovin, "Kirigami-Enabled Microwave Resonator Arrays for Wireless, Flexible, Passive Strain Sensing", *ACS Applied Materials & Interfaces*, Vol. 12, No. 39, pp. 44256–44264, 2020.

76. Salim, A., A. H. Naqvi, E. Park, A. D. Pham and S. Lim, "Inkjet printed kirigami inspired split ring resonator for disposable, low cost strain sensor applications", *Smart Materials and Structures*, Vol. 29, No. 1, pp. 015016–1–015016–19, 2019.

77. Kou, H., Q. Tan, Y. Wang, G. Zhang, S. Shujing and J. Xiong, "A microwave SIW sensor loaded with CSRR for wireless pressure detection in high-temperature environments", *Journal of Physics D: Applied Physics*, Vol. 53, No. 8, pp. 085101–1–085101–11, 2019.

78. Ekinci, G., A. Calikoglu, S. N. Solak, A. D. Yalcinkaya, G. Dundar and H. Torun, "Split-ring resonator-based sensors on flexible substrates for glaucoma monitoring", *Sensors and Actuators A: Physical*, Vol. 268, No. 1, pp. 32 – 37, 2017.

79. Calikoglu, A., G. Dundar, A. D. Yalcinkaya and H. Torun, "Laser-Machined Split-Ring Resonators Embedded in a Polymer Matrix for Glaucoma Monitoring", *Proceedings*, Vol. 1, No. 4, pp. 531–1–531–4, 2017.

80. Eom, S. and S. Lim, "Stretchable Complementary Split Ring Resonator (CSRR)-Based Radio Frequency (RF) Sensor for Strain Direction and Level Detection", *Sensors*, Vol. 16, No. 10, pp. 1667–1–1667–12, 2016.

81. Kairm, H., D. Delfin, M. A. I. Shuvo, L. A. Chavez, C. R. Garcia, J. H. Barton, S. M. Gaytan, M. A. Cadena, R. C. Rumpf, R. B. Wicker, Y. Lin and A. Choudhuri, "Concept and Model of a Metamaterial-Based Passive Wireless Temperature Sensor for Harsh Environment Applications", *IEEE Sensors Journal*, Vol. 15, No. 3, pp. 1445–1452, 2015.

82. Ekmekci, E. and G. Turhan-Sayan, "Multi-functional metamaterial sensor based on a broad-side coupled SRR topology with a multi-layer substrate", *Applied Physics A*, Vol. 110, No. 1, pp. 189–197, 2013.

83. Xia, Y. and L. Wang, "A Wireless Sensor Using Left-Handed Metamaterials", *4th International Conference on Wireless Communications, Networking and Mobile Computing*, pp. 1–3, 2008.

84. Tao, H., M. A. Brenckle, M. Yang, J. Zhang, M. Liu, S. M. Siebert, R. D. Averitt, M. S. Mannoor, M. C. McAlpine, J. A. Rogers, D. L. Kaplan and F. G. Omenetto, "Silk-Based Conformal, Adhesive, Edible Food Sensors", *Advanced Materials*, Vol. 24, No. 8, pp. 1067–1072, 2012.

85. Compaleo, J. D., *Split Ring Resonator Design for Agricultural Based Applications*, Ph.D. Thesis, Wright State University, 2015.

86. Jilani, M. T., W. P. Wen, M. A. Zakariya and L. Y. Cheong, "Microstrip ring resonator based sensing technique for meat quality", *IEEE Symposium on Wireless Technology Applications (ISWTA)*, pp. 220–224, 2013.

87. Chakyar, S. P., S. S. K., A. Murali, S. T. A., J. Andrews and J. V. P., "Determination of permittivity of pulses and cereals using metamaterial split ring resonator", *AIP Conference Proceedings*, Vol. 1849, No. 1, pp. 020024–1–020024–6, 2017.

88. Zhang, Y., J. Zhao, J. Cao and B. Mao, "Microwave Metamaterial Absorber for Non-Destructive Sensing Applications of Grain", *Sensors*, Vol. 18, No. 6, pp. 1912–1–1912–10, 2018.

89. Redzwan, S., M. D. Perez, J. Velander and R. Augustine, "Study of Maturity Fruit Assessment using Permittivity and Microwave Reflectivity Measurements for Quality Classification", *IEEE Conference on Antenna Measurements & Applications (CAMA)*, pp. 1–3, 2018.

90. Amin, E. M., N. C. Karmakar and B. Winther-Jensen, "Polyvinyl-Alcohol (PVA)-Based Humidity Sensor in Microwave Frequency", *Progress In Electromagnetics Research B*, Vol. 54, No. 1, pp. 149–166, 2013.

91. Kim, H. S., S. H. Cha, B. Roy, S. Kim and Y. H. Ahn, "Humidity sensing using THz metamaterial with silk protein fibroin", *Optics Express*, Vol. 26, No. 26, pp. 33575–33581, 2018.

92. Abbasi, Z., P. Shariaty, Z. Hashisho and M. Daneshmand, "SilicaGel-Integrated Chipless RF Tag for Humidity Sensing", *18th International Symposium on Antenna Technology and Applied Electromagnetics (ANTEM)*, pp. 1–2, 2018.

93. Park, J.-K., T.-G. Kang, B.-H. Kim, H.-J. Lee, H. H. Choi and J.-G. Yook, "Real-time Humidity Sensor Based on Microwave Resonator Coupled with PEDOT:PSS Conducting Polymer Film", *Scientific Reports*, Vol. 8, No. 439, pp. 1–8, 2018.

94. Abbasi, Z. and M. Daneshmand, "Contactless pH Measurement Based on High Resolution Enhanced Q Microwave Resonator", *IEEE/MTT-S International Microwave Symposium - IMS*, pp. 1156–1159, 2018.

95. Vivek, A., K. Shambavi and Z. C. Alex, "A review: metamaterial sensors for material characterization", *Sensor Review*, Vol. 39, No. 3, pp. 417–432, 2019.

96. Savin, A., R. Steigmann and G.-S. Dobrescu, "Metamaterial Sensors for Structural Health Monitoring", *ASME 12th Biennial Conference on Engineering Systems Design and Analysis, ESDA*, 2014.

97. Albishi, A. M. and O. M. Ramahi, "Microwaves-Based High Sensitivity Sensors

for Crack Detection in Metallic Materials", *IEEE Transactions on Microwave Theory and Techniques*, Vol. 65, No. 5, pp. 1864–1872, 2017.

98. Yun, T. and S. Lim, "High-Q and miniaturized complementary split ring resonator-loaded substrate integrated waveguide microwave sensor for crack detection in metallic materials", *Sensors and Actuators A: Physical*, Vol. 214, No. 1, pp. 25 – 30, 2014.

99. Alahnomi, R. A., Z. Zakaria, Z. M. Yussof, T. Sutikno, A. Alhegazi and A. I. Abu-Khadrah, "Enhanced symmetrical split ring resonator for metallic surface crack detection", *Telkomnika (Telecommunication Computing Electronics and Control)*, Vol. 17, No. 4, pp. 2107–2115, 2019.

100. Xie, Y., X. Yang, H. Xiao and Y. Wang, "A split-ring resonator probe for assessing subsurface wood defects", *Review of Scientific Instruments*, Vol. 90, No. 12, pp. 125004–1–125004–7, 2019.

101. Lee, C. and C. Yang, "Thickness and Permittivity Measurement in Multi-Layered Dielectric Structures Using Complementary Split-Ring Resonators", *IEEE Sensors Journal*, Vol. 14, No. 3, pp. 695–700, 2014.

102. Gkantou, M., M. Muradov, G. S. Kamaris, K. Hashim, W. Atherton and P. Kot, "Novel Electromagnetic Sensors Embedded in Reinforced Concrete Beams for Crack Detection", *Sensors*, Vol. 19, No. 23, pp. 5175–1–5175–14, 2019.

103. Kim, B., Y. Lee, H. Lee, Y. Hong, J. Yook, M. H. Chung, W. Cho and H. H. Choi, "A gas sensor using double split-ring resonator coated with conducting polymer at microwave frequncies", *IEEE Sensors*, pp. 1815–1818, 2014.

104. Wiltshire, B., K. Mirshahidi, K. Golovin and M. H. Zarifi, "Robust and sensitive frost and ice detection via planar microwave resonator sensor", *Sensors and Actuators B: Chemical*, Vol. 301, No. 126881, pp. 1–5, 2019.

105. Moghadas, H. and V. K. Mushahwar, "Passive microwave resonant sensor for detection of deep tissue injuries", *Sensors and Actuators B: Chemical*, Vol. 277, No. 1, pp. 69 – 77, 2018.

106. Salim, A. and S. Lim, "Review of Recent Metamaterial Microfluidic Sensors", *Sensors*, Vol. 18, No. 1, pp. 232–1–232–25, 2018.

107. Rydosz, A., E. Maciak, K. Wincza and S. Gruszczynski, "Microwave-based sensors with phthalocyanine films for acetone, ethanol and methanol detection", *Sensors and Actuators B: Chemical*, Vol. 237, No. 1, pp. 876 – 886, 2016.

108. Withayachumnankul, W., K. Jaruwongrungsee, A. Tuantranont, C. Fumeaux and D. Abbott, "Metamaterial-based microfluidic sensor for dielectric characterization", *Sensors and Actuators A: Physical*, Vol. 189, No. 1, pp. 233 – 237, 2013.

109. Ebrahimi, A., J. Scott and K. Ghorbani, "Ultrahigh-Sensitivity Microwave Sensor for Microfluidic Complex Permittivity Measurement", *IEEE Transactions on Microwave Theory and Techniques*, Vol. 67, No. 10, pp. 4269–4277, 2019.

110. Cai, J., Y. J. Zhou and X. M. Yang, "A metamaterials-loaded quarter mode SIW microfluidic sensor for microliter liquid characterization", *Journal of Electromagnetic Waves and Applications*, Vol. 33, No. 3, pp. 261–271, 2019.

111. Seo, Y., M. U. Memon and S. Lim, "Microfluidic Eighth-Mode Substrate-Integrated-Waveguide Antenna for Compact Ethanol Chemical Sensor Application", *IEEE Transactions on Antennas and Propagation*, Vol. 64, No. 7, pp. 3218–3222, 2016.

112. Salim, A. and S. Lim, "Complementary Split-Ring Resonator-Loaded Microfluidic Ethanol Chemical Sensor", *Sensors*, Vol. 16, No. 11, pp. 1802–1–1802–13, 2016.

113. Chuma, E. L., Y. Iano, G. Fontgalland and L. L. Bravo Roger, "Microwave Sensor for Liquid Dielectric Characterization Based on Metamaterial Complementary Split Ring Resonator", *IEEE Sensors Journal*, Vol. 18, No. 24, pp. 9978–9983, 2018.

114. Govind, G. and M. J. Akhtar, "Metamaterial-Inspired Microwave Microfluidic Sensor for Glucose Monitoring in Aqueous Solutions", *IEEE Sensors Journal*, Vol. 19, No. 24, pp. 11900–11907, 2019.

115. Zarifi, M. H., H. Sadabadi, S. H. Hejazi, M. Daneshmand and A. Sanati-Nezhad, "Noncontact and Nonintrusive Microwave-Microfluidic Flow Sensor for Energy and Biomedical Engineering", *Scientific Reports*, Vol. 8, No. 139, pp. 1–10, 2018.

116. Mohammadi, S., R. Narang, M. Mohammadi Ashani, H. Sadabadi, A. Sanati-Nezhad and M. H. Zarifi, "Real-time monitoring of Escherichia coli concentration with planar microwave resonator sensor", *Microwave and Optical Technology Letters*, Vol. 61, No. 11, pp. 2534–2539, 2019.

117. Awang, R. A., F. J. Tovar-Lopez, T. Baum, S. Sriram and W. S. T. Rowe, "Meta-atom microfluidic sensor for measurement of dielectric properties of liquids", *Journal of Applied Physics*, Vol. 121, No. 9, pp. 094506–1–094506–8, 2017.

118. Shih, K., P. Pitchappa, M. Manjappa, C. P. Ho, R. Singh and C. Lee, "Microfluidic metamaterial sensor: Selective trapping and remote sensing of microparticles", *Journal of Applied Physics*, Vol. 121, No. 2, pp. 023102–1–023102–7, 2017.

119. Puentes, M., M. Maasch, M. Schubler and R. Jakoby, "Frequency Multiplexed 2-Dimensional Sensor Array Based on Split-Ring Resonators for Organic Tissue Analysis", *IEEE Transactions on Microwave Theory and Techniques*, Vol. 60, No. 6, pp. 1720–1727, 2012.

120. Lee, H.-J., J.-H. Lee, S. Choi, I.-S. Jang, J.-S. Choi and H.-I. Jung, "Asymmetric split-ring resonator-based biosensor for detection of label-free stress biomarkers",

Applied Physics Letters, Vol. 103, No. 5, pp. 053702–1–053702–5, 2013.

121. Torun, H., F. Cagri Top, G. Dundar and A. D. Yalcinkaya, "An antenna-coupled split-ring resonator for biosensing", *Journal of Applied Physics*, Vol. 116, No. 12, 2014.

122. Liu, C.-F., M.-H. Wang and L.-S. Jang, "Microfluidics-based hairpin resonator biosensor for biological cell detection", *Sensors and Actuators B: Chemical*, Vol. 263, No. 1, pp. 129 – 136, 2018.

123. Park, S. J., S. H. Cha, G. A. Shin and Y. H. Ahn, "Sensing viruses using terahertz nano-gap metamaterials", *Biomedical Optics Express*, Vol. 8, No. 8, pp. 3551–3558, 2017.

124. La Spada, L., F. Bilotti and L. Vegni, "Metamaterial biosensor for cancer detection", *IEEE Sensors*, pp. 627–630, 2011.

125. Emami Nejad, H., A. Mir and A. Farmani, "Supersensitive and Tunable Nano-Biosensor for Cancer Detection", *IEEE Sensors Journal*, Vol. 19, No. 13, pp. 4874–4881, 2019.

126. Reinecke, T., J.-G. Walter, T. Kobelt, A. Ahrens, T. Scheper and S. Zimmermann, "Design and evaluation of split-ring resonators for aptamer-based biosensors", *Journal of Sensors and Sensor Systems*, Vol. 7, No. 1, pp. 101–111, 2018.

127. Turner, A. P. F., "Biosensors: sense and sensibility", *Chemical Society Reviews*, Vol. 42, No. 8, pp. 3184–3196, 2013.

128. Chen, C., Q. Xie, D. Yang, H. Xiao, Y. Fu, Y. Tan and S. Yao, "Recent advances in electrochemical glucose biosensors: a review", *RSC Advances*, Vol. 3, No. 14, pp. 4473–4491, 2013.

129. Guo, X., "Surface plasmon resonance based biosensor technique: A review",

Journal of Biophotonics, Vol. 5, No. 7, pp. 483–501, 2012.

130. Katardjiev, I. and V. Yantchev, "Recent developments in thin film electro-acoustic technology for biosensor applications", *Vacuum*, Vol. 86, No. 5, pp. 520 – 531, 2012.

131. Yakovleva, M., S. Bhand and B. Danielsson, "The enzyme thermistor—A realistic biosensor concept. A critical review", *Analytica Chimica Acta*, Vol. 766, No. 1, pp. 1 – 12, 2013.

132. Llandro, J., J. J. Palfreyman, A. Ionescu and C. H. W. Barnes, "Magnetic biosensor technologies for medical applications: a review", *Medical & Biological Engineering & Computing*, Vol. 48, No. 10, pp. 977–998, 2010.

133. Jaruwongrungsee, K., U. Waiwijit, W. Withayachumnankul, T. Maturos, D. Phokaratkul, A. Tuantranont and A. Wisitsoraat, "Real-time and label-free biosensing with microfluidic-based split-ring-resonator sensor", *IEEE 15th International Conference on Nanotechnology (IEEE-NANO)*, pp. 1091–1094, 2015.

134. Geng, Z., X. Zhang, Z. Fan, X. Lv and H. Chen, "A Route to Terahertz Metamaterial Biosensor Integrated with Microfluidics for Liver Cancer Biomarker Testing in Early Stage", *Scientific Reports*, Vol. 7, No. 16378, pp. 1–11, 2017.

135. Jaksic, Z., O. Jaksic and J. Matovic, "Performance limits to the operation of nanoplasmonic chemical sensors: noise-equivalent refractive index and detectivity", *Journal of Nanophotonics*, Vol. 3, No. 1, pp. 031770–1–031770–13, 2009.

136. Jaksic, Z. and Z. Djuric, "Cavity enhancement of Auger-suppressed detectors: a way to background-limited room-temperature operation in 3-14- μm range", *IEEE Journal of Selected Topics in Quantum Electronics*, Vol. 10, No. 4, pp. 771–776, 2004.

137. Djuric, Z., "Mechanisms of noise sources in microelectromechanical systems",

Microelectronics Reliability, Vol. 40, No. 6, pp. 919 – 932, 2000.

138. Bolla, A. S. and R. Priefer, "Blood glucose monitoring- an overview of current and future non-invasive devices", *Diabetes & Metabolic Syndrome: Clinical Research & Reviews*, Vol. 14, No. 5, pp. 739 – 751, 2020.

139. Korostynska, O., A. Mason and A. Al-Shamma'a, "Microwave sensors for the non-invasive monitoring of industrial and medical applications", *Sensor Review*, Vol. 34, No. 2, pp. 182–191, 2014.

140. Siddiqui, S. A., Y. Zhang, J. Lloret, H. Song and Z. Obradovic, "Pain-Free Blood Glucose Monitoring Using Wearable Sensors: Recent Advancements and Future Prospects", *IEEE Reviews in Biomedical Engineering*, Vol. 11, No. 1, pp. 21–35, 2018.

141. Vashist, S. K., D. Zheng, K. Al-Rubeaan, J. H. Luong and F.-S. Sheu, "Technology behind commercial devices for blood glucose monitoring in diabetes management: A review", *Analytica Chimica Acta*, Vol. 703, No. 2, pp. 124 – 136, 2011.

142. Oliver, N. S., C. Toumazou, A. E. G. Cass and D. G. Johnston, "Glucose sensors: a review of current and emerging technology", *Diabetic Medicine*, Vol. 26, No. 3, pp. 197–210, 2009.

143. Hwang, D.-W., S. Lee, M. Seo and T. D. Chung, "Recent advances in electrochemical non-enzymatic glucose sensors – A review", *Analytica Chimica Acta*, Vol. 1033, No. 1, pp. 1 – 34, 2018.

144. Zhang, Z., Z. Chen, F. Cheng, Y. Zhang and L. Chen, "Highly sensitive on-site detection of glucose in human urine with naked eye based on enzymatic-like reaction mediated etching of gold nanorods", *Biosensors and Bioelectronics*, Vol. 89, No. 2, pp. 932 – 936, 2017.

145. Ito, N., M. Miyashita and S. Ikeda, "1 - Portable urine glucose sensor", K. Mitsubayashi, O. Niwa and Y. Ueno (Editors), *Chemical, Gas, and Biosensors for Internet of Things and Related Applications*, pp. 3 – 12, Elsevier, 2019.

146. Arakawa, T., Y. Kuroki, H. Nitta, P. Chouhan, K. Toma, S. ichi Sawada, S. Takeuchi, T. Sekita, K. Akiyoshi, S. Minakuchi and K. Mitsubayashi, "Mouthguard biosensor with telemetry system for monitoring of saliva glucose: A novel cavitas sensor", *Biosensors and Bioelectronics*, Vol. 84, No. 1, pp. 106 – 111, 2016.

147. Diouf, A., B. Bouchikhi and N. El Bari, "A nonenzymatic electrochemical glucose sensor based on molecularly imprinted polymer and its application in measuring saliva glucose", *Materials Science and Engineering: C*, Vol. 98, No. 1, pp. 1196 – 1209, 2019.

148. Chen, J., X. Zhu, Y. Ju, B. Ma, C. Zhao and H. Liu, "Electrocatalytic oxidation of glucose on bronze for monitoring of saliva glucose using a smart toothbrush", *Sensors and Actuators B: Chemical*, Vol. 285, No. 1, pp. 56 – 61, 2019.

149. Xuan, X., H. S. Yoon and J. Y. Park, "A wearable electrochemical glucose sensor based on simple and low-cost fabrication supported micro-patterned reduced graphene oxide nanocomposite electrode on flexible substrate", *Biosensors and Bioelectronics*, Vol. 109, No. 1, pp. 75 – 82, 2018.

150. Yoon, H., J. Nah, H. Kim, S. Ko, M. Sharifuzzaman, S. C. Barman, X. Xuan, J. Kim and J. Y. Park, "A chemically modified laser-induced porous graphene based flexible and ultrasensitive electrochemical biosensor for sweat glucose detection", *Sensors and Actuators B: Chemical*, Vol. 311, No. 127866, pp. 1–10, 2020.

151. Liao, Y., H. Yao, A. Lingley, B. Parviz and B. P. Otis, "A 3-μW CMOS Glucose Sensor for Wireless Contact-Lens Tear Glucose Monitoring", *IEEE Journal of Solid-State Circuits*, Vol. 47, No. 1, pp. 335–344, 2012.

152. Romeo, A., A. Moya, T. S. Leung, G. Gabriel, R. Villa and S. Sánchez, "Inkjet printed flexible non-enzymatic glucose sensor for tear fluid analysis", *Applied Materials Today*, Vol. 10, No. 1, pp. 133 – 141, 2018.

153. Jiang, C., M. Sun, Z. Wang, Z. Chen, X. Zhao, Y. Yuan, Y. Li and C. Wang, "A Portable Real-Time Ringdown Breath Acetone Analyzer: Toward Potential Diabetic Screening and Management", *Sensors (Basel, Switzerland)*, Vol. 16, No. 8, pp. 1199–1–1199–15, 2016.

154. Srivastava, A., M. K. Chowdhury, S. Sharma and N. Sharma, "Measurement of glucose by using modulating ultrasound with optical technique in normal and diabetic human blood serum", *International Conference on Advances in Engineering Technology Research (ICAETR)*, pp. 1–5, 2014.

155. Yilmaz, T., R. Foster and Y. Hao, "Radio-Frequency and Microwave Techniques for Non-Invasive Measurement of Blood Glucose Levels", *Diagnostics*, Vol. 9, No. 1, pp. 6–1–6–34, 2019.

156. Turgul, V. and I. Kale, "Permittivity extraction of glucose solutions through artificial neural networks and non-invasive microwave glucose sensing", *Sensors and Actuators A: Physical*, Vol. 277, No. 1, pp. 65 – 72, 2018.

157. Villena Gonzales, W., A. T. Mobashsher and A. Abbosh, "The Progress of Glucose Monitoring—A Review of Invasive to Minimally and Non-Invasive Techniques, Devices and Sensors", *Sensors*, Vol. 19, No. 4, pp. 800–1–800–45, 2019.

158. Omer, A. E., S. Safavi-Naeini, R. Hughson and G. Shaker, "Blood Glucose Level Monitoring Using an FMCW Millimeter-Wave Radar Sensor", *Remote Sensing*, Vol. 12, No. 3, pp. 385–1–385–25, 2020.

159. Shaker, G., K. Smith, A. E. Omer, S. Liu, C. Csech, U. Wadhwa, S. Safavi-Naeini and R. Hughson, "Non-Invasive Monitoring of Glucose Level Changes Utilizing a mm-Wave Radar System", *International Journal of Mobile Human Computer*

Interaction, Vol. 10, No. 3, pp. 10–29, 2018.

160. Bahar, A. A. M., Z. Zakaria, A. A. M. Isa, R. A. Alahnomi and N. A. Rahman, "Complex Permittivity Measurement Based on Planar Microfluidic Resonator Sensor", *18th International Symposium on Antenna Technology and Applied Electromagnetics (ANTEM)*, pp. 1–5, 2018.

161. Abedeen, Z. and P. Agarwal, "Microwave sensing technique based label-free and real-time planar glucose analyzer fabricated on FR4", *Sensors and Actuators A: Physical*, Vol. 279, No. 1, pp. 132 – 139, 2018.

162. Melikyan, H., E. Danielyan, S. Kim, J. Kim, A. Babajanyan, L. Jungha, B. Friedman and K. Lee, "Non-invasive in vitro sensing of D-glucose in pig blood", *Medical Engineering & Physics*, Vol. 34, No. 3, pp. 299–304, 2011.

163. Saha, S., H. Cano-Garcia, I. Sotiriou, O. Lipscombe, I. Gouzouasis, M. Koutsoupidou, G. Palikaras, R. Mackenzie, T. Reeve, P. Kosmas and E. Kallos, "A Glucose Sensing System Based on Transmission Measurements at Millimetre Waves using Micro strip Patch Antennas", *Scientific Reports*, Vol. 7, No. 6855, pp. 1–11, 2017.

164. Juan, C. G., E. Bronchalo, G. Torregrosa, E. Ávila, N. García and J. M. Sabater-Navarro, "Dielectric characterization of water glucose solutions using a transmission/reflection line method", *Biomedical Signal Processing and Control*, Vol. 31, No. 1, pp. 139 – 147, 2017.

165. Hofmann, M., G. Fischer, R. Weigel and D. Kissinger, "Microwave-Based Noninvasive Concentration Measurements for Biomedical Applications", *IEEE Transactions on Microwave Theory and Techniques*, Vol. 61, No. 5, pp. 2195–2204, 2013.

166. Salim, A., S.-H. Kim, J. Y. Park and S. Lim, "Microfluidic Biosensor Based on Microwave Substrate-Integrated Waveguide Cavity Resonator", *Journal of*

Sensors, Vol. 2018, No. 1324145, pp. 1–14, 2018.

167. Kim, S., H. Melikyan, J. Kim, A. Babajanyan, J.-H. Lee, L. Enkhtur, B. Friedman and K. Lee, "Noninvasive in vitro measurement of pig-blood d-glucose by using a microwave cavity sensor", *Diabetes Research and Clinical Practice*, Vol. 96, No. 3, pp. 379 – 384, 2012.

168. Kim, J., A. Babajanyan, A. Hovsepyan, K. Lee and B. Friedman, "Microwave dielectric resonator biosensor for aqueous glucose solution", *Review of Scientific Instruments*, Vol. 79, No. 8, pp. 086107–1–086107–3, 2008.

169. Zeising, S., J. Kirchner, H. F. Khalili, D. Ahmed, M. Lübke, A. Thalmayer and G. Fischer, "Towards Realisation of a Non-Invasive Blood Glucose Sensor Using Microstripline", *IEEE International Instrumentation and Measurement Technology Conference (I2MTC)*, pp. 1–6, 2020.

170. Cebedio, M. C., L. A. Rabioglio, I. E. Gelosi, R. A. Ribas, A. J. Uriz and J. C. Moreira, "Analysis and Design of a Microwave Coplanar Sensor for Non-Invasive Blood Glucose Measurements", *IEEE Sensors Journal*, Vol. 20, No. 18, pp. 10572–10581, 2020.

171. Byford, J. A., K. Y. Park and P. Chahal, "Metamaterial inspired periodic structure used for microfluidic sensing", *IEEE 65th Electronic Components and Technology Conference (ECTC)*, pp. 1997–2002, 2015.

172. Chretiennot, T., D. Dubuc and K. Grenier, "Microwave-Based Microfluidic Sensor for Non-Destructive and Quantitative Glucose Monitoring in Aqueous Solution", *Sensors*, Vol. 16, No. 10, pp. 1733–1–1733–7, 2016.

173. Hofmann, M., T. Fersch, R. Weigel, G. Fischer and D. Kissinger, "A novel approach to non-invasive blood glucose measurement based on RF transmission", *IEEE International Symposium on Medical Measurements and Applications*, pp. 39–42, 2011.

174. Harnsoongnoen, S. and A. Wanthong, "Real-time monitoring of sucrose, sorbitol, d -glucose and d -fructose concentration by electromagnetic sensing", *Food Chemistry*, Vol. 232, No. 1, pp. 566–570, 2017.

175. Juan, C. G., E. Bronchalo, B. Potelon, C. Quendo, E. Ávila-Navarro and J. M. Sabater-Navarro, "Concentration Measurement of Microliter-Volume Water–Glucose Solutions Using Q Factor of Microwave Sensors", *IEEE Transactions on Instrumentation and Measurement*, Vol. 68, No. 7, pp. 2621–2634, 2019.

176. Verma, A., S. Bhushan, P. N. Tripathi, M. Goswami and B. R. Singh, "A defected ground split ring resonator for an ultra-fast, selective sensing of glucose content in blood plasma", *Journal of Electromagnetic Waves and Applications*, Vol. 31, No. 10, pp. 1049–1061, 2017.

177. He, X., X. Hao, S. Yan, F. Wu and J. Jiang, "Biosensing using an asymmetric split-ring resonator at microwave frequency", *Integrated Ferroelectrics*, Vol. 172, No. 1, pp. 142–146, 2016.

178. Sharafadinzadeh, N., M. Abdolrazzaghi and M. Daneshmand, "Highly sensitive microwave split ring resonator sensor using gap extension for glucose sensing", *IEEE MTT-S International Microwave Workshop Series on Advanced Materials and Processes for RF and THz Applications (IMWS-AMP)*, pp. 1–3, 2017.

179. Harnsoongnoen, S. and A. Wanthong, "Coplanar Waveguide Transmission Line Loaded With Electric-LC Resonator for Determination of Glucose Concentration Sensing", *IEEE Sensors Journal*, Vol. 17, No. 6, pp. 1635–1640, 2017.

180. Oloyo, A. A. and Z. Hu, "A highly sensitive microwave resonator for non-invasive blood glucose level detection", *12th European Conference on Antennas and Propagation (EuCAP)*, pp. 1–5, 2018.

181. Baghelani, M., Z. Abbasi, M. Daneshmand and P. E. Light, "Non-invasive continuous-time glucose monitoring system using a chipless printable sensor based

on split ring microwave resonators", *Scientific Reports*, Vol. 10, No. 12980, pp. 1–15, 2020.

182. Adhikari, K. K., Z. Chuluunbaatar, H. Park, Y. Jung, G. Cho, Y. H. Jo, S. S. Kim and N. Y. Kim, "Flexible screen printed biosensor with high-Q microwave resonator for rapid and sensitive detection of glucose", *IEEE MTT-S International Microwave Workshop Series on RF and Wireless Technologies for Biomedical and Healthcare Applications (IMWS-Bio)*, pp. 1–3, 2014.

183. Zhou, H., C. Yang, D. Hu, D. Li, X. Hui, Y. Yi and X. M., "Integrating Metamaterial and Microchannel onto Flexible Paper as Miniaturized Biochemical Sensing Platform", *20th International Conference on Solid-State Sensors, Actuators and Microsystems Eurosensors XXXIII (Transducers Eurosensors XXXIII)*, pp. 677–680, 2019.

184. Dhakal, R., E. Kim, Y.-H. Jo, S.-S. Kim and N.-Y. Kim, "Characterization of micro-resonator based on enhanced metal insulator semiconductor capacitor for glucose recognition", *Medical Engineering & Physics*, Vol. 41, No. 1, pp. 55 – 62, 2017.

185. Sauviac, B., C. Simovski and S. Tretyakov, "Double Split-Ring Resonators: Analytical Modeling and Numerical Simulations", *Electromagnetics*, Vol. 24, No. 5, pp. 317–338, 2004.

186. Shamonin, M., E. Shamonina, V. Kalinin and L. Solymar, "Resonant frequencies of a split-ring resonator: Analytical solutions and numerical simulations", *Microwave and Optical Technology Letters*, Vol. 44, No. 2, pp. 133–136, 2005.

187. Bilotti, F., A. Toscano, L. Vegni, K. Aydin, K. B. Alici and E. Ozbay, "Equivalent-Circuit Models for the Design of Metamaterials Based on Artificial Magnetic Inclusions", *IEEE Transactions on Microwave Theory and Techniques*, Vol. 55, No. 12, pp. 2865–2873, 2007.

188. Zhurbenko, V., T. Jensen, V. Krozer and P. Meincke, "Analytical model of planar double split ring resonator", *SBMO/IEEE MTT-S International Microwave and Optoelectronics Conference*, pp. 753–756, 2007.

189. Wang, J., S. Qu, Z. Xu, H. Ma, Y. Yang and C. Gu, "A Controllable Magnetic Metamaterial: Split-Ring Resonator With Rotated Inner Ring", *IEEE Transactions on Antennas and Propagation*, Vol. 56, No. 7, pp. 2018–2022, 2008.

190. Naoui, S., L. Lassaad and A. Gharsallah, "Equivalent Circuit Model of Double Split Ring Resonators", *International Journal of Microwave and Optical Technology*, Vol. 11, No. 1, pp. 1–6, 2016.

191. Chen, H., L. Ran, J. Huangfu, T. M. Grzegorczyk and J. A. Kong, "Equivalent circuit model for left-handed metamaterials", *Journal of Applied Physics*, Vol. 100, No. 2, pp. 024915–1–024915–6, 2006.

192. Pekçokgüler, N., G. Dündar, H. Torun and A. D. Yalçınkaya, "A novel equivalent circuit model for split ring resonator with an application of low phase noise reference oscillator", *Integration*, Vol. 61, No. 1, pp. 160 – 166, 2018.

193. Albishi, A. M., *Ultrasensitive Microwave Near-Field Sensors For Detection, Imaging, and Material Characterization*, Ph.D. Thesis, Electrical and Computer Engineering, University of Waterloo, 2018.

194. Nilsson, J. and S. Riedel, *Electric Circuits*, Prentice Hall PTR, 2011.

195. Delgado, V., O. Sydoruk, E. Tatartschuk, R. Marqués, M. Freire and L. Jelinek, "Analytical circuit model for split ring resonators in the far infrared and optical frequency range", *Metamaterials*, Vol. 3, No. 2, pp. 57 – 62, 2009.

196. Kusakci, E., *Bioapplications of Integrated MEMS Catheter Tracking System for MRI and Split Ring Resonator Based Glucose Sensor*, Master's Thesis, Electrical and Electronics Engineering, Boğaziçi University, 2013.

197. Pozar, D., *Microwave Engineering, 4th Edition*, Wiley, 2011.

198. Abduljabbar, A. A., *Compact Microwave Microfluidic Sensors and Applicator*, Ph.D. Thesis, Engineering, Cardiff University, 2016.

199. Hamzah, H. M., *Microwave Microfluidic Resonant Sensors and Applicators*, Ph.D. Thesis, Engineering, Cardiff University, 2017.

200. Ebrahimi, A., W. Withayachumnankul, S. F. Al-Sarawi and D. Abbott, "Microwave microfluidic sensor for determination of glucose concentration in water", *IEEE 15th Mediterranean Microwave Symposium (MMS)*, pp. 1–3, 2015.

201. Al-Naib, I. A. I., C. Jansen and M. Koch, "Thin-film sensing with planar asymmetric metamaterial resonators", *Applied Physics Letters*, Vol. 93, No. 8, p. 083507, 2008.

202. Debus, C. and P. H. Bolivar, "Frequency selective surfaces for high sensitivity terahertz sensing", *Applied Physics Letters*, Vol. 91, No. 18, pp. 184102–1–184102–3, 2007.

203. Camli, B., E. Kusakci, B. Lafci, S. Salman, H. Torun and A. D. Yalcinkaya, "Cost-Effective, Microstrip Antenna Driven Ring Resonator Microwave Biosensor for Biospecific Detection of Glucose", *IEEE Journal of Selected Topics in Quantum Electronics*, Vol. 23, No. 2, pp. 404–409, 2017.

204. Kaatze, U., "Complex permittivity of water as a function of frequency and temperature", *Journal of Chemical & Engineering Data*, Vol. 34, No. 4, pp. 371–374, 1989.

205. Smulders, P. F. M., M. G. Buysse and M. D. Huang, "Dielectric Properties of Glucose Solutions in the 0.5–67 GHz Range", *Microwave and Optical Technology Letters*, Vol. 55, No. 8, pp. 1916–1917, 2013.

206. Gavish, N. and K. Promislow, "Dependence of the dielectric constant of electrolyte solutions on ionic concentration: A microfield approach", *Physical Review E*, Vol. 94, No. 1, pp. 012611–1–012611–7, 2016.

207. Purich, D., *Enzyme Kinetics: Catalysis & Control : a Reference of Theory and Best-practice Methods*, Elsevier, 2010.

208. Camli, B., E. Kuşakcı, B. Lafci, S. Salman, H. Torun and A. Yalcinkaya, "A Microwave Ring Resonator Based Glucose Sensor", *Procedia Engineering*, Vol. 168, No. 1, pp. 465–468, 2016.

209. Jang, C., J.-K. Park, H.-J. Lee, G.-H. Yun and J.-G. Yook, "Temperature-Corrected Fluidic Glucose Sensor Based on Microwave Resonator", *Sensors*, Vol. 18, No. 11, pp. 3850–1–3850–12, 2018.

210. Sedra, A. and K. Smith, *Microelectronic Circuits*, Oxford University Press, 2015.

211. Choi, H., J. Naylon, S. Luzio, J. Beutler, J. Birchall, C. Martin and A. Porch, "Design and In Vitro Interference Test of Microwave Noninvasive Blood Glucose Monitoring Sensor", *IEEE Transactions on Microwave Theory and Techniques*, Vol. 63, No. 10, pp. 3016–3025, 2015.

212. Camli, B., H. Torun, G. Dundar and A. Yalcinkaya, "Reference-Incorporating Microwave Resonator-Based Sensors for Biological Sensing Applications", *Proceedings*, Vol. 1, No. 4, pp. 542–1–542–4, 2017.

213. Vélez, P., L. Su, K. Grenier, J. Mata-Contreras, D. Dubuc and F. Martín, "Microwave Microfluidic Sensor Based on a Microstrip Splitter/Combiner Configuration and Split Ring Resonators (SRRs) for Dielectric Characterization of Liquids", *IEEE Sensors Journal*, Vol. 17, No. 20, pp. 6589–6598, 2017.

214. Ebrahimi, A., J. Scott and K. Ghorbani, "Differential Sensors Using Microstrip Lines Loaded With Two Split-Ring Resonators", *IEEE Sensors Journal*, Vol. 18,

No. 14, pp. 5786–5793, 2018.

215. Zhou, H., D. Hu, C. Yang, C. Chen, J. Ji, M. Chen, Y. Chen, Y. Yang and X. Mu, "Multi-Band Sensing for Dielectric Property of Chemicals Using Metamaterial Integrated Microfluidic Sensor", *Scientific Reports*, Vol. 8, No. 14801, pp. 1–11, 2018.

216. Kiani, S., P. Rezaei and M. Navaei, "Dual-sensing and dual-frequency microwave SRR sensor for liquid samples permittivity detection", *Measurement*, Vol. 160, No. 107805, pp. 1–8, 2020.

217. Mostafalu, P., M. Akbari, K. A. Alberti, Q. Xu, A. Khademhosseini and S. R. Sonkusale, "A toolkit of thread-based microfluidics, sensors, and electronics for 3D tissue embedding for medical diagnostics", *Microsystems &Amp; Nanoengineering*, Vol. 2, No. 16039, pp. 1–10, 2016.

218. Kenry, J. C. Yeo and C. T. Lim, "Emerging flexible and wearable physical sensing platforms for healthcare and biomedical applications", *Microsystems &Amp; Nanoengineering*, Vol. 2, No. 16043, pp. 1–19, 2016.

219. Chen, J., H. Guo, J. Zheng, Y. Huang, G. Liu, C. Hu and Z. L. Wang, "Self-Powered Triboelectric Micro Liquid/Gas Flow Sensor for Microfluidics", *ACS Nano*, Vol. 10, No. 8, pp. 8104–8112, 2016.

220. Altinagac, E., S. Taskin and H. Kizil, "Single cell array impedance analysis in a microfluidic device", *Journal of Physics: Conference Series*, Vol. 757, No. 012010, pp. 1–6, 2016.

221. Luka, G., A. Ahmadi, H. Najjaran, E. Alocilja, M. DeRosa, K. Wolthers, A. Malki, H. Aziz, A. Althani and M. Hoorfar, "Microfluidics Integrated Biosensors: A Leading Technology towards Lab-on-a-Chip and Sensing Applications", *Sensors*, Vol. 15, No. 12, pp. 30011–30031, 2015.

222. Riahi, R., A. Tamayol, S. A. M. Shaegh, A. M. Ghaemmaghami, M. R. Dokmeci and A. Khademhosseini, "Microfluidics for advanced drug delivery systems", *Current Opinion in Chemical Engineering*, Vol. 7, No. 1, pp. 101 – 112, 2015.

223. Rackus, D. G., M. H. Shamsi and A. R. Wheeler, "Electrochemistry, biosensors and microfluidics: a convergence of fields", *Chemical Society Reviews*, Vol. 44, No. 15, pp. 5320–5340, 2015.

224. Yang, K., H. Peretz-Soroka, Y. Liu and F. Lin, "Novel developments in mobile sensing based on the integration of microfluidic devices and smartphones", *Lab Chip*, Vol. 16, No. 6, pp. 943–958, 2016.

225. Pires, N. M. M., T. Dong, U. Hanke and N. Hoivik, "Recent developments in optical detection technologies in lab-on-a-chip devices for biosensing applications", *Sensors (Basel, Switzerland)*, Vol. 14, No. 8, pp. 15458–15479, 2014.

226. Son, M., D. Kim, H. J. Ko, S. Hong and T. H. Park, "A portable and multiplexed bioelectronic sensor using human olfactory and taste receptors", *Biosensors and Bioelectronics*, Vol. 87, No. 1, pp. 901 – 907, 2017.

227. Zhang, W., S. Guo, W. S. Pereira Carvalho, Y. Jiang and M. J. Serpe, "Portable point-of-care diagnostic devices", *Analytical Methods*, Vol. 8, No. 44, pp. 7847–7867, 2016.

228. Altintas, Z., M. Akgun, G. Kokturk and Y. Uludag, "A fully automated microfluidic-based electrochemical sensor for real-time bacteria detection", *Biosensors and Bioelectronics*, Vol. 100, No. 1, pp. 541 – 548, 2018.

229. Lee, G., J. Lee, J. Kim, H. S. Choi, J. Kim, S. Lee and H. Lee, "Single Microfluidic Electrochemical Sensor System for Simultaneous Multi-Pulmonary Hypertension Biomarker Analyses", *Scientific Reports*, Vol. 7, No. 7545, pp. 1–8, 2017.

230. Martín, A., J. Kim, J. F. Kurniawan, J. R. Sempionatto, J. R. Moreto, G. Tang,

A. S. Campbell, A. Shin, M. Y. Lee, X. Liu and J. Wang, "Epidermal Microfluidic Electrochemical Detection System: Enhanced Sweat Sampling and Metabolite Detection", *ACS Sensors*, Vol. 2, No. 12, pp. 1860–1868, 2017.

231. Shin, S. R., Y. S. Zhang, D.-J. Kim, A. Manbohi, H. Avci, A. Silvestri, J. Aleman, N. Hu, T. Kilic, W. Keung, M. Righi, P. Assawes, H. A. Alhadrami, R. A. Li, M. R. Dokmeci and A. Khademhosseini, "Aptamer-Based Microfluidic Electrochemical Biosensor for Monitoring Cell-Secreted Trace Cardiac Biomarkers", *Analytical Chemistry*, Vol. 88, No. 20, pp. 10019–10027, 2016.

232. Yang, H. and M. A. M. Gijs, "Micro-optics for microfluidic analytical applications", *Chemical Society Reviews*, Vol. 47, No. 4, pp. 1391–1458, 2018.

233. Tahirbegi, I. B., J. Ehgartner, P. Sulzer, S. Zieger, A. Kasjanow, M. Paradiso, M. Strobl, D. Bouwes and T. Mayr, "Fast pesticide detection inside microfluidic device with integrated optical pH, oxygen sensors and algal fluorescence", *Biosensors and Bioelectronics*, Vol. 88, No. 1, pp. 188 – 195, 2017.

234. Weng, X., G. Gaur and S. Neethirajan, "Rapid Detection of Food Allergens by Microfluidics ELISA-Based Optical Sensor", *Biosensors*, Vol. 6, No. 2, pp. 24–1–24–10, 2016.

235. Yin, M.-J., B. Huang, S. Gao, A. P. Zhang and X. Ye, "Optical fiber LPG biosensor integrated microfluidic chip for ultrasensitive glucose detection", *Biomedical Optics Express*, Vol. 7, No. 5, pp. 2067–2077, 2016.

236. Burger, R., L. Amato and A. Boisen, "Detection methods for centrifugal microfluidic platforms", *Biosensors and Bioelectronics*, Vol. 76, No. 1, pp. 54 – 67, 2016.

237. RoyChoudhury, S., V. Rawat, A. H. Jalal, S. Kale and S. Bhansali, "Recent advances in metamaterial split-ring-resonator circuits as biosensors and therapeutic agents", *Biosensors and Bioelectronics*, Vol. 86, No. 1, pp. 595 – 608, 2016.

238. Kling, A., C. Chatelle, L. Armbrecht, E. Qelibari, J. Kieninger, C. Dincer, W. Weber and G. Urban, "Multianalyte Antibiotic Detection on an Electrochemical Microfluidic Platform", *Analytical Chemistry*, Vol. 88, No. 20, pp. 10036–10043, 2016.

239. Mason, A., O. Korostynska, M. Ortoneda-Pedrola, A. Shaw and A. Al-Shamma'a, "A resonant co-planar sensor at microwave frequencies for biomedical applications", *Sensors and Actuators A: Physical*, Vol. 202, No. 1, pp. 170 – 175, 2013.

240. Mondal, D., N. Tiwari and M. J. Akhtar, "Microwave Assisted Non-Invasive Microfluidic Biosensor for Monitoring Glucose Concentration", *IEEE Sensors*, 2018.

241. Ebrahimi, A., J. Scott and K. Ghorbani, "Microwave reflective biosensor for glucose level detection in aqueous solutions", *Sensors and Actuators A: Physical*, Vol. 301, No. 111662, pp. 1–8, 2020.

242. Vélez, P., J. Muñoz, J. Mata-Contreras, D. Dubuc, K. Grenier and F. Martín, "Measuring Glucose Content in Aqueous Solutions by means of Split Ring Resonator (SRR) Loaded Transmission Lines", *12th International Congress on Artificial Materials for Novel Wave Phenomena (Metamaterials)*, pp. 418–420, 2018.

243. Gan, H., W. Zhao, Q. Liu, D. Wang, L. Dong, G. Wang and W. Yin, "Differential Microwave Microfluidic Sensor Based on Microstrip Complementary Split-Ring Resonator (MCSRR) Structure", *IEEE Sensors Journal*, Vol. 20, No. 11, pp. 5876–5884, 2020.

244. Camli, B., E. Altinagac, H. Kizil, H. Torun, G. Dundar and A. D. Yalcinkaya, "Gold-on-glass microwave split-ring resonators with PDMS microchannels for differential measurement in microfluidic sensing", *Biomicrofluidics*, Vol. 14, No. 5, pp. 054102–1–054102–9, 2020.

245. Ansari, A. and P. I. Imoukhuede, "Plenty more room on the glass bottom: Sur-

face functionalization and nanobiotechnology for cell isolation", *Nano Research*, Vol. 11, No. 10, pp. 5107–5129, 2018.

246. Engel, S., E.-C. Fritz and B. J. Ravoo, "New trends in the functionalization of metallic gold: from organosulfur ligands to N-heterocyclic carbenes", *Chemical Society Reviews*, Vol. 46, No. 8, pp. 2057–2075, 2017.

247. Zhou, T., Y. Zhu, X. Li, X. Liu, K. W. Yeung, S. Wu, X. Wang, Z. Cui, X. Yang and P. K. Chu, "Surface functionalization of biomaterials by radical polymerization", *Progress in Materials Science*, Vol. 83, No. 1, pp. 191 – 235, 2016.

248. Kumar, S., W. Ahlawat, R. Kumar and N. Dilbaghi, "Graphene, carbon nanotubes, zinc oxide and gold as elite nanomaterials for fabrication of biosensors for healthcare", *Biosensors and Bioelectronics*, Vol. 70, No. 1, pp. 498 – 503, 2015.

249. García, H., C. G. Juan, E. Ávila-Navarro, E. Bronchalo and J. M. Sabater-Navarro, "Portable Device Based on Microwave Resonator for Noninvasive Blood Glucose Monitoring", *41st Annual International Conference of the IEEE Engineering in Medicine and Biology Society (EMBC)*, pp. 1115–1118, 2019.

250. Juan, C. G., H. García, E. Ávila-Navarro, E. Bronchalo, V. Galiano, Ó. Moreno, D. Orozco and J. M. Sabater-Navarro, "Feasibility study of portable microwave microstrip open-loop resonator for non-invasive blood glucose level sensing: proof of concept", *Medical & Biological Engineering & Computing*, Vol. 57, No. 11, pp. 2389–2405, 2019.

251. Dautta, M., M. Alshetaiwi, J. Escobar and P. Tseng, "Passive and wireless, implantable glucose sensing with phenylboronic acid hydrogel-interlayer RF resonators", *Biosensors and Bioelectronics*, Vol. 151, No. 112004, pp. 1–8, 2020.

252. Kumari, R., P. N. Patel and R. Yadav, "An ENG-Inspired Microwave Sensor and Functional Technique for Label-Free Detection of Aspergillus Niger", *IEEE*

Sensors Journal, Vol. 18, No. 10, pp. 3932–3939, 2018.